AD-A117 626 COLUMBIA RADIATION LAB NEW YORK F/G 20/3
RESEARCH INVESTIGATION DIRECTED TOWARD EXTENDING THE USEFUL RAN--ETC(U)
MAR 82 G W FLYNN DAAG29-79-C-0079
UNCLASSIFIED NL

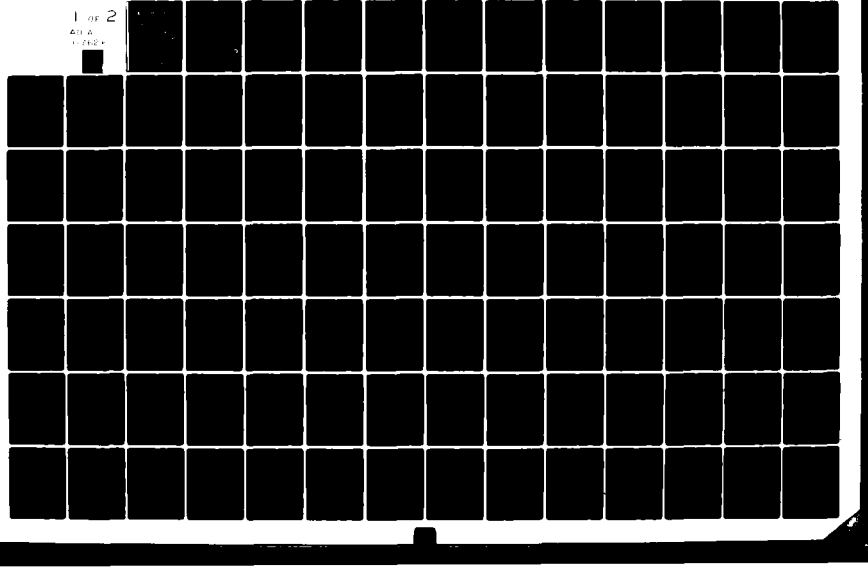

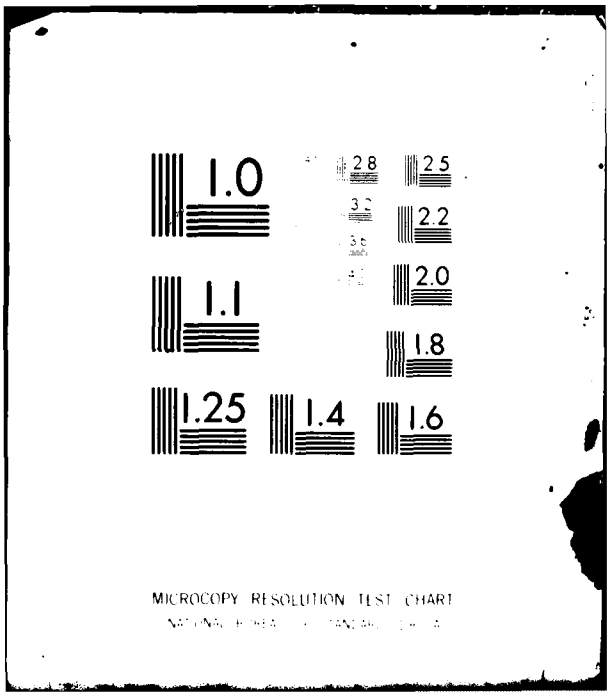
1.0
2.8
2.5
3.2
2.2
3.6
2.0
1.1
1.8
1.25
1.4
1.6
MICROCOPY RESOLUTION TEST CHART

(12)

COLUMBIA UNIVERSITY

DEPARTMENTS OF PHYSICS,
CHEMISTRY, ELECTRICAL ENGINEERING

PROGRESS REPORT NO. 32

April 1, 1981 - March 31, 1982

CONTRACT DAAG29-79-C-0079

APPROVED FOR PUBLIC RELEASE: DISTRIBUTION UNLIMITED

To:

THE JOINT SERVICES TECHNICAL ADVISORY COMMITTEE

REPRESENTING: THE U.S. ARMY ELECTRONICS COMMAND
THE U.S. ARMY RESEARCH OFFICE
THE OFFICE OF NAVAL RESEARCH
THE AIR FORCE OFFICE OF SCIENTIFIC RESEARCH

COLUMBIA RADIATION LABORATORY, NEW YORK, NEW YORK 10027

March 31, 1982

COLUMBIA RADIATION LABORATORY

RESEARCH INVESTIGATION DIRECTED TOWARD EXTENDING THE USEFUL RANGE OF THE ELECTROMAGNETIC SPECTRUM

Progress Report No. 32

April 1, 1981 through March 31, 1982

Contract DAAG29-79-C-0079

Object of the Research:

Basic research in the fields of quantum electronics; electromagnetic propagation, detection and sensing; and solid state electronics.

The research reported in this document was made possible through support extended the Columbia Radiation Laboratory, Columbia University, by the Joint Services Electronics Program (U. S. Army Electronics Command and U. S. Army Research Office, Office of Naval Research, and the Air Force Office of Scientific Research) under Contract DAAG29-79-C-0079.

Submitted by: G. W. Flynn, Director

Coordinated by: Vicki J. Zell, Administrative Assistant

COLUMBIA UNIVERSITY

Division of Government-Aided Research

New York, New York 10027

March 31, 1982

Approved for public release; distribution unlimited

The research reported in this document was made possible through support extended the Columbia Radiation Laboratory, Columbia University by the Joint Services Electronics Program (U. S. Army Electronics Command and U. S. Army Research Office, Office of Naval Research, and the Air Force Office of Scientific Research) under Contract DAAG29-79-C-0079.

Portions of this work were also supported by:

Air Force Office of Scientific Research

Grant AFOSR-81-0009-A

AFOSR/DARPA

F-49620-82-K-0008

Army Research Office

Grant DAAG29-82-K-0089

National Science Foundation

Grant NSF-ENG 78-19426

Grant NSF-ENG 78-26498

Grant NSF-ECS 80-06881

Grant NSF-DMR 80-06966

Grant NSF-CHE 80-23747

Grant NSF-CHE 81-21945

Grant NSF-BNS 80-21140

Office of Naval Research

Contract N00014-78-C-0517

Department of Energy

Contract DE-AS02-78-ER-S-04940

Contract DOE/SERI xz-ϕ-9226

Contract DOE/SERI xw-1-1272-1

Jet Propulsion Laboratory
California Institute of Technology

Contract 955335

Contract 955336

The support of these agencies is acknowledged in footnotes in the text.

REPORT DOCUMENTATION PAGE

READ INSTRUCTIONS BEFORE COMPLETING FORM

1. REPORT NUMBER: Progress Report No. 32	2. GOVT ACCESSION NO.: AD-A117626
3. RECIPIENT'S CATALOG NUMBER:	
4. TITLE (and Subtitle): RESEARCH INVESTIGATION DIRECTED TOWARD EXTENDING THE USEFUL RANGE OF THE ELECTROMAGNETIC SPECTRUM	5. TYPE OF REPORT & PERIOD COVERED: 1 April 1981 - 31 March 1982
	6. PERFORMING ORG. REPORT NUMBER: 32
7. AUTHOR(s): George W. Flynn	8. CONTRACT OR GRANT NUMBER(s): DAAG29-79-C-0079
9. PERFORMING ORGANIZATION NAME AND ADDRESS: Columbia Radiation Laboratory, Columbia University, New York, New York 10027	10. PROGRAM ELEMENT, PROJECT, TASK AREA & WORK UNIT NUMBERS:
11. CONTROLLING OFFICE NAME AND ADDRESS: Department of the Army, U. S. Army Research Office, Research Triangle Park, NC 27709	12. REPORT DATE: 31 March 1982
	13. NUMBER OF PAGES:
14. MONITORING AGENCY NAME & ADDRESS (if different from Controlling Office):	15. SECURITY CLASS. (of this report): Unclassified
	15a. DECLASSIFICATION/DOWNGRADING SCHEDULE:

16. DISTRIBUTION STATEMENT (of this Report)

Approved for public release; distribution unlimited

17. DISTRIBUTION STATEMENT (of the abstract entered in Block 20, if different from Report)

18. SUPPLEMENTARY NOTES

Portions of this work were also supported by the Air Force Office of Scientific Research, the Army Research Office, the National Science Foundation, the Office of Naval Research, the Department of Energy, AFOSR/DARPA, and JPL.

19. KEY WORDS (Continue on reverse side if necessary and identify by block number)

Grain boundary
Polycrystalline silicon
Transport
Poisson point process

20. ABSTRACT (Continue on reverse side if necessary and identify by block number)

We have made substantial progress in understanding the behavior of multiplied-Poisson processes, and in particular, an important special case of such processes, the shot-noise-driven doubly stochastic Poisson point process (SNDP). The SNDP turns out to provide an appropriate model for important effects inherent in the generation and detection of optical and ionizing radiation, including:

(1) the detection of scintillation photons produced by ionizing

radiation;
(ii) the generation of luminescence noise by ionizing radiation; and
(iii) cathodoluminescence emission.

The SNDP can be quite important in properly interpreting the behavior of optical detectors, fibers and electro-optic devices and in determining the performance of communications, surveillance, navigation, guidance and control systems incorporating these devices. The SNDP will also be useful for studying image intensification, cosmic-ray noise in electro-optic systems, and cosmic ray soft errors in electronics and computer systems.

Substantial progress has also been made toward the analysis and implementation of the first wideband incoherent frequency-shift keyed (FSK) fiber-optic communication link. Results were obtained in three specific areas: (i) optimal (single-threshold) processing and receiver design; (ii) new technique for system performance analysis; (iii) FSK system demonstration. In the area of receiver design, a simplified (single-threshold) processor was derived that is optimal for a broad variety of fiber-optic systems using PIN or avalanche photodiodes. A new technique was developed for calculating fiber-optic system performance using a normalizing transform. Whereas previously, Gaussian approximations were resorted to for such calculations, the new technique is as simple, but more accurate. Finally, a 10 Mbit/sec wideband FSK fiber-optic link was implemented with center wavelength 827 nm, using a direct detection avalanche photodiode receiver. The performance was shown to be 3-4.5 dB better than a comparable on-off keyed system. It is expected that the FSK fiber-optic link, when combined with wavelength multiplexing, will be important in high-data-rate, high-performance digital communications.

We have developed a general theoretical model of grain boundary (GB) recombination, carrier transport and electrostatics under assumptions of Gaussian energy distributions of GB interface states, and unequal capture cross-section of these GB states for electrons and holes in polycrystalline materials. Calculations have been performed of the recombination current density and the recombination velocity at grain boundaries in polycrystalline silicon for four different energy distributions. It appears that the experimental data of photoconductivity variation with light intensity are consistent with the multi-level trap distribution proposed although detailed correlation requires further studies.

We report here data of the capacitance-voltage and current-voltage measurements on cw laser processed Al-nSi diodes. The range of the laser power is between 12 and 20W. Significant changes in the ideality factor, reverse saturation current, thermal activation energy, doping concentration, and effective Schottky barrier height have been observed. These results appear to be consistent with the mechanisms of aluminum diffusion and defect generation with high-temperature stress under high-power laser irradiation.

The grain boundary recombination velocity of polycrystalline Si is separated from bulk effects and its value is determined with practically no assumption of numerical values for any parameter other than the minority barrier diffusion coefficient. The method used utilizes photoconductance measurements taken by the scanning laser spot technique. It is found that,

Block 20 continued - Abstract

for the illumination levels used, there is a transition from low level to high-level injection of minority carriers, and this transition is used to estimate the quasi-Fermi level separation. The recombination velocity S, ranging in value from 5000 to 17000 cm/sec. is thus presented both as a function of the illumination level as well as of the quasi-Fermi level separation. It is found that S increases monotonically with illumination and does not saturate, even at the high light concentrations used.

A physical theory using a charge scattering model is proposed to interpret the experimental data of grain boundary transport in polycrystalline semiconductors. The calculated result explains the need of an attenuation factor as an added coefficient in the thermionic emission current.

The behavior of Al-nSi diodes heat treatment above the eutectic temperature (600°C) is studied by varying the annealing time and cooling rate. We have used the capacitance-voltage characteristic as a measure of the influence of the doping density and thickness of the recrystallized silicon layer at the interface. Poisson's equation is solved to obtain the C-V characteristic and to relate it to the effective barrier height. We find that the barrier height is independent of the annealing time, but it is a function of the cooling rate. It appears that the diffusion of alluminum into silicon does not play a significant role, but fast quenching tends to prevent aluminum from precipitation, so that the recrystallized silicon layer is highly doped.

A new laboratory for studying novel processing and diagnostic techniques for microelectronics materials has been established. One major research area of this laboratory is the application of laser surface chemistry to microfabrication. In conjunction with this experimental research, a theoretical study has shown the importance of surface composition and morphology in controlling laser-initiated photochemistry.

We have determined the relaxation dynamics of electronically excited bromine molecules imbedded in rare gas matrices of Ar, Kr, and Xe at temperatures ranging from 10 - 40°K. A restriced relaxation mechanism leads to emission for all electronic states (B, A, and A') energetically accessible to the laser photons used for excitation. Preliminary results for iodine molecules indicate that emission is only observed from the A electronically excited state. The relaxation mechanism for iodine will provide information useful in determining the upper limits of efficiency for chemical iodine lasers.

The vibrational relaxation of oxalyl fluoride has been studied and found to be very rapid. The presence of a low-lying torsional frequency in this molecule enhances the relaxation efficiency by orders of magnitude over rigid molecules of roughly the same size. Vibrational relaxation of OCS in He has also been investigated to determine if an unusual cyclic relaxation path occurs in this molecule. Definitive evidence for this process is still lacking.

Block 20 continued - Abstract

Photofragmentation of HBr in the presence of CO_2 and CO has been investigated. Vibrational excitation of CO_2 and CO by fast H atoms produced in the photodissociation of the diatomic has been observed. In CO_2 collisions with fast hydrogen atoms produce predominantly bend/stretch excitation while in CO very high levels of rotational excitation are observed (ΔJ of approximately 20). Photofragmentation of triazine $(HCN)_3$ has also been studied. This molecule cleanly produces three HCN molecules when exposed to 193 nm excimer laser light. We have observed strong vibrational excitation of both the bend (ν_2) and C-H stretch (ν_3) modes of HCN produced via photodissociation. Population inversions may exist for these molecules.

A new capillary ion source has been constructed and coupled to a standard molecular beam/mass spectrometer system. Preliminary results with this device show that hot ions having a significant spread in ion energy are produced at discharge voltages of a few kilovolts. Emission spectra of the discharge indicate that substantial quantities of metastable neutrals are produced by this source in addition to fast ions.

The origin and dynamics of an anomalous dual fluorescence in molecules such as p-dimethylamino benzonitrile have been investigated using picosecond laser sources. The key issues of the relationship between the ultraviolet and visible emissions and the role of the solvent in this photoinduced charge separation in molecules are elucidated.

We have found in our studies of small chain motions in molecules of the type anthracene-$(CH_2)_3$-N,N'-dimethyl andine, using picosecond laser methods that: (1) the dynamics of end to end reactive encounters are influenced by different starting ground state conformations, (2) the lifetime of chain relaxation scales as $(\text{viscosity})^{1/2}$ and (3) that a single chain relaxation mode, perhaps the large scale end to end relaxation mode, is dominant for the three methylene chain in the picosecond to nanosecond time domain.

We have used picosecond spectroscopy to study the pathway involved in the generation of singlet oxygen, $^1O_2$, from photoexcited anthracene endoperoxide. We have determined the dynamics and relative importance of the various channels for photofragmentation of these molecules.

A centralized laser pump facility was developed to allow a pair of YAG lasers to be simulataneously shared at three separate experimental stations. The Billiard Ball Echo Theory was invented to explain most optical coherent transient phenomena in an unconventional but simple way. New optical coherent effects were discovered which will be used to obtain physical data. A theoretical analysis of the combined effects of phase changing and velocity changing collisions in gases was completed. Measurements were made to determine the relative orientation of the principle axes of the ground and excited state nuclear hyperfine hamiltonians of Pr^{3+} in LaF_3.

Block 19 continued - Key Words

Shot-noise-driven doubly stochastic Poisson point process (SNDP)
Scintillation photons
Luminescence noise
Ionizing radiation
Cathodoluminescence emission
Frequency-shift keyed (FSK)
Avalanche photodiode
cw laser
quasi-Fermi level separation
Charge scattering
Photon counting
Thermionic emission
Laser surface chemistry
Microfabrication
Morphology
Bromine molecule
Ar
Kr
Xe
Iodine molecule
Vibrational relaxation
Oxalyl fluoride
Torsional frequency
Photofragmentation
Vibrational excitation
Photofragmentation of triazine $(HCN)_3$
YAG lasers
Capillaritron
The Billiard Ball Echo Theory
Optical coherent transient phenomena
Carbenes
Magnetometers
Picosecond laser
Photodissociation
Energy relaxation
Photon echo

TABLE OF CONTENTS

PUBLICATIONS AND REPORTS

Publications

M. K. Crawford, Y. Wang and K. B. Eisenthal, "Effects of Conformation and Solvent Polarity on Intramolecular Charge-Transfer: A Picosecond Laser Study," Chemical Physics Letters, 79, 529 (1981). (NSF, AFOSR and JSEP - work unit 8)

Ying Wang, M. McAuliffe, F. Novak, and K. B. Eisenthal, "Picosecond Dynamics of Twisted Internal Charge Transfer Phenomena," The Journal of Physical Chemistry, 85, 3736 (1981). (NSF, AFOSR and JSEP - work units 8,9)

S. Y. Hou, C. G. Dupuy, M. J. McAuliffe, D. A. Hrovat, and K. B. Eisenthal, "Picosecond Laser Study of the Adiabatic Photodissociation of an Endoperoxide," Journal of the J. Am. Chem. Soc., 103, 3982 (1981). (NSF, AFOSR and JSEP - work units 8,9)

G. W. Flynn, "Collision-Induced Energy Flow Between Vibrational Modes of Small Polyatomic Molecules," Chemical Research 14, 334 (1981). (NSF, DOE and JSEP - work units 4,5)

K. Chiang, E. A. Whittaker, and S. R. Hartmann, "Photon Echo Nuclear Double Resonance in $LaF_3:Pr^{3+}$," Phys. Rev. B 23, 6142 (1981). (NSF and JSEP - work unit 11)

T. W. Mossberg and S. R. Hartmann, "Coherent Transients Theorem: A Comment," Phys. Rev. A 24, 2247 (1981). (ONR and JSEP - work unit 10)

R. Kachru, T. H. Chen, and S. R. Hartmann, and P. R. Berman, "Measurement of a Total Atomic-Radiator-Perturber Scattering Cross Section," Phys. Rev. Lett. 47 902 (1981). (ONR and JSEP - work unit 10)

W. Hwang, P. Panayotatos, E. Poon and H. C. Card, "Carrier Transport and Recombination Processes at Grain Boundaries in Polycrystalline Silicon under Optical Illumination," Proceed. 15th IEEE Photovoltaic Specialists Conference, 871-876, (1981). (DOE)

F. S. Yang, E. Poon, C. M. Wu, W. Hwang, and H. C. Card, "Majority Carrier Current Characteristics in Large-Grain Polycrystalline Silicon Schottky Barrier Solar Cells," IEEE Trans. Electron Devices ED-28, 1131 (1981). (JSEP - work units 15-17 and DOE)

P. R. Prucnal, W. Hwang, and H. C. Card, "Statistical Fluctuations of Dopant Impurities in Ion-Implanted Bipolar Transistor Structures and the Minimum Device Dimensions for VLSI System Reliability," Computer and Info. Abs., 26 Issue 8/9, #267787, p. CA19. e. (1981). (JSEP - work units 13,15)

Paul R. Prucnal, "Single-Threshold Processing for Orthogonal Likelihood-Ratio Detection with Application to FSK Fiber-Optic Communications," IEEE Tran. Comm. COM-29, 743 (1981). (JSEP - work units 13,15 and NSF)

P. R. Prucnal and Bahaa E. A. Saleh, "Transformation of Image-Signal-Dependent Noise into Image-Signal-Independent Noise," Opt. Lett. 6,316 (1981). (NSF and JSEP - work unit 13)

M. C. Teich and B. E. A. Saleh, "Fluctuation Properties of Multiplied-Poisson Light: Measurement of the Photon-Counting Distribution for Radioluminescence Radiation from Glass," Phys. Rev. A24, 1651-1654 (1981). (JSEP - work unit 13)

B. E. A. Saleh, J. T. Tavolacci, and M. C. Teich, "Discrimination of Shot-Noise-Driven Poisson Processes by External Dead Time: Application to Radioluminescence from Glass," IEEE J. Quantum Electron. QE-17, 2341-2350 (1981). (NSF, JPL and JSEP - work unit 14)

M. C. Teich, "Role of the Doubly Stochastic Neyman Type-A and Thomas Counting Distributions in Photon Detection," Appl. Opt. 20, 2457 (1981). (NSF, JPL and JSEP - work unit 13)

M. C. Teich and B. E. A. Saleh, "Interevent-Time Statistics for Shot-Noise-Driven Self-Exciting Point Processes in Photon Detection," J. Opt. Soc. Am. 71, 771-776 (1981). (NSF and JSEP - work unit 14)

M. C. Teich and G. Lachs, "A Neural-Counting Model Incorporating Refractoriness and Spread of Excitation: Application to Intensity Discrimination and Loudness Estimation for Variable-Bandwidth Noise Stimuli," J. Acoust. Soc. Am. 69, S104 (1981). (NSF)

M. C. Teich, "Infrared Heterodyne Detection, "Current Contents: Engineering, Technology, & Applied Sciences (Citation Classic) 12 (#35), 16 (1981). (JSEP - work unit 12)

M. C. Teich and B. E. A. Saleh, "Counting Statistics for the Photoelectric Detection of Light in the Presence of Ionizing Radiation," J. Opt. Soc. Am. 71, 1583 (1981). (JSEP - work unit 13 and NSF)

M. C. Teich, "Fluctuation Properties of Multiplied Poisson Light," in Proc. NSF Grantee-User Meeting, edited by D. L. Snyder (Washington University, St. Louis, 1981), Optical Communication Systems, pp. 110-111. (NSF and JSEP - work unit 13)

E. S. Yang and J. M. Brownlow, "Thermal Release of Trapped Electrons and Phosphorescent Decay in Zinc Silicon Phosphors," J. Appl. Phys. 52, 4753 (1981). (JSEP - work unit 15)

E. S. Yang, "Oscillators," in McGraw-Hill Encyclopedia of Science and Technology, 5th edition (to appear).

C. M. Wu and E. S. Yang, "Dependence of Rectification Properties of AL-nS: Contacts on Thermal Annealing and Quenching," J. Appl. Phys. 52, 7287 (1981). (DOE and JSEP - work unit 15)

C. M. Wu and E. S. Yang, "A Low-Temperature Fabrication Process of Poly-Silicon-Silicon P^+-n Junction Diode," Appl. Phys. Lett. 38, 813 (1981). (NSF, DOE and JSEP - work unit 15)

C. M. Wu and E. S. Yang, "Investigation of High-Temperature Annealing and Quenching Effects on Al-nSi Diodes by C-V and I-V Measurements," J. Appl. Phys. 52, 4700 (1981). (DOE/SERI and JSEP - work unit 17)

E. S. Yang, D. B. Dove, M. Shafer, and I. F. Chang, "Electron Trap in $AlPO_4$ Substituted Zinc Silicate Phosphors," J. Electronic Materials, 10, 423 (1981). (IBM Research)

C. M. Wu, E. S. Yang, T. O. Sedgwick, and R. T. Hodgson, "Dependence of Electrical Characteristics on Laser Power in cw Laser Processed Al-nSi Diodes," J. Appl. Phys. 52, 7287 (1981). (IBM Research and JSEP - work units 16, 17)

Y. Wang, E. V. Sitzmann, F. Novak, D. Dupuy, and K. B. Eisenthal, "Reactions of Excited Triplet Diphenylcarbene Studied With Picosecond Lasers," to be published in Journal of the American Chemical Society (1982). (NSF, AFOSR and JSEP - work units 8,9)

Y. Wang, M. K. Crawford, and K. B. Eisenthal, "Picosecond Laser Studies of Intramolecular Excited State Charge Transfer Dynamics and Small Chain Relaxation," to be published in Journal of the American Chemical Society (1982). (NSF, AFOSR and JSEP - work units 8,9)

Ying Wang and K. B. Eisenthal, "Picosecond Laser Studies of Ultrafast Processes in Chemistry," to be published in Journal of Chemical Education (1982). (NSF, AFOSR and JSEP - work units 8,9)

R. K. Bohn, K. H. Casleton, Y. V. C. Rao, and G. W. Flynn, "Vibrational Energy Transfer in Laser-Excited COF_2, Infrared Fluorescence from the Intermediate Mode ν_4," J. of Physical Chemistry 86, 736 (1982). (NSF, DOE and JSEP - work units 4,5)

Paul Beeken, Mary Mandich, and George Flynn, "Photochemical Dynamics of $^{79}Br_2$ in Xe Matrices," to be published in J. Chem. Phys. (1982). (NSF, DOE and JSEP - work unit 6)

Mary Mandich, Paul Beeken, and George Flynn, "Emission Spectra and Relaxation Dynamics of Excited $^{79}Br_2$ in Ar and Kr Matrices," to be published in J. Chem. Phys. (1982). (NSF, DOE and JSEP - work unit 6)

T. Allick and G. W. Flynn, "Laser Excited Infrared Fluorescence in Oxalyl Fluoride: Rapid Intermode Equilibration," to be published in J. Phys. Chem. (1982). (NSF, DOE and JSEP - work units 4,5)

E. A. Whittaker and S. R. Hartmann, "Hyperfine Structure of the $^1D_2 - {}^3H_4$ Levels of Pr^{3+}:LaF_3 with the use of Photon Echo Modulation Spectroscopy," to be published in Phys. Rev. B (1982). (NSF and JSEP - work unit 11)

R. Beach, S. R. Hartmann, and R. Friedberg, "The Billiard Ball Echo Model," Phys. Rev. A 25, 2658 (1982). (ONR and JSEP - work unit 10)

K. P. Leung, T. W. Mossberg, and S. R. Hartmann, "Noble-gas-induced Collisional Broadening of the $6P_{1/2}$-$6P_{3/2}$ Transition of Tl Measured by Raman Echoes," Phys. Rev. A 25, 3097 (1982). (ONR and JSEP - work unit 10)

R. Kachru, T. J. Chen, T. W. Mossberg, and S. R. Hartmann, "Relative Noble-gas-induced Broadening of the D lines of Atomic Lithium," Phys. Rev. A 25, 1546 (1982). (ONR and JSEP - work unit 10)

K. P. Leung, T. W. Mossberg, and S. R. Hartmann, "Observation and Density Dependence of the Raman Echo in Atomic Thallium Vapor," to be published in Optics Communication (1982). (ONR and JSEP - work unit 10)

P. R. Berman, T. W. Mossberg, and S. R. Hartmann, "Collision Kernels and Laser Spectroscopy," to be published in Phys. Rev. A (1982). (ONR and JSEP - work unit 10)

T. W. Mossberg, R. Kachru, T. J. Chen, S. R. Hartmann, and P. R. Berman, "Noble Gas Induced Relaxation of the Li 3S-3P Transition Spanning the Short Term Impact Regime to the Log Term Assymptotic Regime," Published in the Laser Spectroscopic Conference, Jasper Canada (1982). (ONR and JSEP - work unit 10)

R. Beach, S. R. Hartmann, and R. Friedberg, "Billiard Ball Echo Model," Published in the Preceeding Laser Conference, New Orleans (1981). (ONR and JSEP - work unit 10)

P. Panayotatos, E. S. Yang, and W. Hwang, "Determination of the Grain Boundary Recombination Velocity in Polycrystalline Silicon as a Function of Illumination," to be published in Solid State Electronics (1982). (DOE and JSEP-work units 15,16,17)

E. Poon and W. Hwang, "Phenomenological Model of Grain Boundary Trapping States in Polycrystalline Silicon under Optical Illumination," to be published in Solid State Electronics (1982). (DOE and JSEP-work units 15,16,17)

R. T. Young, G. E. Jellison, and W. Hwang, "Carrier Transport Properties at Grain Boundaries in Polycrystalline Si," Bulletin of the American Physical Society, 27, 208 (1982). (DOE).

D. J. Ehrlich, R. M. Osgood, and T. F. Deutsch, "Photodeposition of Metal Films with Ultraviolet Laser Light," J. Vac. Science Tech. 20, 738 (1982). (AFOSR and DARPA)

D. J. Ehrlich and R. M. Osgood, Jr., "Optically-Induced Microstructures in Laser Photodeposited Metal Films," to be published in Opt. Lett. (1982). (DARPA and Dept. of Army)

R. M. Osgood, Jr., A. Sanchez-Rubio, D. J. Ehrlich, and V. Daneu, "Localized Laser Etching of Compound Semiconductors in Aqueous Solution," Appl. Phys. Lett. 40, 391 (1982). (DARPA, AFOSR and Dept. of Army)

C. J. Chen and R. M. Osgood, Jr., "Surface Enhancement of Interface Photochemical Reactions," to be published in Chem. Phys. Lett. (1982). (JSEP - work unit 5)

D. J. Ehrlich and R. M. Osgood, Jr., "Laser Microchemistry, Local Nucleation Mechanisms for Photodeposition," to be published in Thin Solid Films (1982). (DARPA and AFOSR)

Paul R. Prucnal and Bahaa E. A. Saleh, "Evaluation of Fiber-Optic Error Rates Using a Normalizing Transform," to appear in J. Opt. Soc. Am. 72, 410 (1982). (NSF and JSEP - work unit 13)

Paul R. Prucnal and Howard C. Card, "Effects on VLSI Yield of Doubly-Stochastic Impurity Distribution," to be published in IEEE. Reliability (1982). (JSEP - work unit 13)

Paul R. Prucnal and M. C. Teich, "Multiplication Noise in the Human Visual System at Threshold: 2. Probit Estimation of Parameters," Biol. Cybern. 43, 87 (1982). (NSF)

Bahaa E. A. Saleh and Malvin Teich, "Multiplied-Poisson Noise in Pulse, Particle, and Photon Detection," Proceedings of the IEEE 70, 229 (1982). (NSF and JSEP - work units 13,14)

Giovanni Vannucci and Malvin Carl Teich, "Dead-time-modified Mean and Variance for Doubly Stochastic Poisson Processes," J. of Opt. Soc. (1982) submitted for publication. (NSF and JSEP - work unit 14)

Malvin Carl Teich and Giovanni Vannucci, "Observation of Dead-time-modified Photocounting Distributions for Modulated Laser Radiation," J. of Opt. Soc. (1982) submitted for publication (NSF and JSEP - work unit 14)

Kuniaki Matsuo, Bahaa E, A. Saleh, and Malvin Carl Teich, "Cascaded Poisson Processes," J. of Math. Physics scheduled to appear December, 1982. (NSF and JSEP - work unit 13)

M. C. Teich and B. E. A. Saleh, "The Effects of Random Deletion and additive Noise on Bunched and Antibunched Photon-Counting Statistics," Opt. Lett. scheduled to appear August, 1982. (NSF and JSEP - work units 12,14)

Bahaa E. A. Saleh and Malvin Carl Teich, "Statistical Properties of a Nonstationary Neyman-Scott Cluster Process," IEEE Transactions Inform Theory (1982) submitted for publication (JSEP - work unit 13)

C. M. Wu and E. S. Yang, "Physical Basis of Scattering Potential at Grain Boundary of Polycrystalline Semiconductors," Appl. Phys. Lett. 40, 49 (1982). (DOE/SERI and JSEP - work unit 16)

E. S. Yang, "Structures and Performance of Polycrystalline Thin-Film Solar Cells," to be published in Thin Solid Films (1982). (DOE/SERI)

I. F. Chang, J. J. Cuomo, and E. S. Yang, "Fabrication of Thin-Film Zinc Silicate Phosphors," IBM Technical Disclosure Bulletin, to be published. (IBM Research)

C. A. Chang and E. S. Yang, "Multi-Layered Integrated Structurers," to be published in IBM Technical Disclosure (1982). (IBM Research)

Papers by CRL Staff Members Presented at Scientific Meetings

K. Eisenthal, "Direct Experimental Studies of Picosecond Molecular Processes in Condensed Phases", U. S. - France Binational Meeting on Lasers in Chemistry, Talloires, France, June 1981.

K. Eisenthal, "Applications of Picosecond Lasers to Chemistry", International Conference of Luminescence, Berlin, West Germany, July 1981.

K. Eisenthal, "Photofragmentaion, Photoionization and Charge Transfer in Gases and Liquids", International Union of Pure and Applied Chemistry, Vancouver, Canada, August 1981.

K. Eisenthal, "Picosecond Studies of Electon Transfer, Photofragmentation and Energy Relaxation", Symposium on Interactions Between Light and Matter, American Chemical Society National Meeting, New York, August 1981.

K. Eisenthal, "Picosecond Laser Spectroscopy", Chemical Education Symposium on Lasers, American Chemical Society National Meeting, New York, August 1981.

K. Eisenthal, "Picosecond Laser Studies in Chemistry", Western Spectroscopy Association Twenty-Ninth Annual Conference, Asilomar, California, January 1982.

S. -Y. Hou, C. G. Dupuy, M. J. McAuliffe, and K. Eisenthal, "Picosecond Studies of Anomalous Dual Fluorescences, The Role of Charge Transfer Interactions", American Chemical Society National Meeting, New York, August 1981.

S.-Y. Hou, C. G. Dupuy, M. J. McAuliffe, and K. Eisenthal, "Laser Generation of $^1O_2$ Fragment on Photodissociation of Endoperoxides", American Chemical Society National Meeting, New York, August 1981.

S. Hartmann, "Billiard Ball Echo Model", Gorden Conference on Nuclear Magnetic Research, Wolfboro, New Hampshire, June 15-19, 1981.

S. Hartmann, "Billiard Ball Echo Model", Gorden Conference on Atomic Physics, Wolfboro, New Hampshire, July 6-10, 1981.

S. Hartmann, "Billiard Ball Echo Model", Gorden Conference on Non-linear Optics, Wolfboro, New Hampshire, August 3-7, 1981.

S. Hartmann, "Billiard Ball Echo Model", Laser '81, New Orleans, Louisiana, December 16-18, 1981.

S. Hartmann, "Billiard Ball Echo Model", American Chemical Society National Meeting, Las Vegas, Nevada, March 29, 1982.

S. Hartmann, "Billiard Ball Echo Model", Laser Spectroscopy Conference, Jasper, Canada, June 1982.

W. Hwang, P. Panayotatos, E. Poon and H. C. Card, "Carrier Transport and Recombination Processes at Grain Boundaries in Polycrystalline Silicon under Optical Illumination", 15th IEEE Photovoltaic Specialists Conference, Kissimmee, Florida, May 1981.

E. S. Yang and W. Hwang, "Fundamental Studies of MS and MIS Solar Cells on Polycrystalline Silicon", The Polycrystalline Silicon Solar Cells DOE/SERI Subcontracts' Review Meeting, Alexandria, Va., June 1981.

P. Panayotatos, E. S. Yang and W. Hwang, "Determination of Grain Boundary Recombination Velocity in Polycrystalline Silicon as a Function of Illumination from Photoconductance Measurements", Gordon Research Conference on Thin Films and Solid Surfaces, New London, NH, July 1981.

P. Panayotatos, J. S. Song, E. S. Yang and W. Hwang, "Measurement of Diffusion Length and Grain Boundary Recombination Velocity in Solar-Graded Polycrystalline Silicon", 1981 Annual Meeting of Materials Research Society, Symposium B, Grain Boundaries in Semiconductors, Boston, Mass., November 1981.

E. S. Yang and W. Hwang, "Fundamental Studies of Polycrystalline Silicon for Photovoltaic Applications", The Polycrytalline Silicon Solar Cells DOE/SERI Subcontracts' Review Meeting, Washington, D. C., December 1981.

R. T. Young, G. E. Jellison and W. Hwang, "Carrier Transport Properties at Grain Boundaries in Polycrystalline Si", The March Meeting of The American Physical Society, Dallas, Texas, 8-12 March (1982).

P. Prucnal, "Wideband FSK Fiber-Optic Communication Experiment", Conference on Lasers and Electrooptics, Phoenix, Arizona, April 1982.

P. Prucnal, "Evaluation of Fiber-Optic Error Rates Using a Normalizing Transform." Optical Society of America Annual Meeting, Orlando, Florida, October 1981.

M. Teich and G. Lachs, "A Neural-Counting Model Incorporating Refractoriness and Spread of Excitation: Application to Intensity Discrimination and Loudness Estimation for Variable-Bandwidth Noise Stimuli," Meeting of the Acoustical Society of America, Ottawa, Canada, May 1981.

M. Teich, "Fluctuation Properties of Multiplied Poisson Light," Joint Meeting of the NSF Grantee-User Group in Optical Communication Systems and the Department of Commerce Optical Communication Task Force, St. Louis, Missouri, June 1981.

M. Teich and B. E. A. Saleh, "Counting Statistics for the Photoelectric Detection of Light in the Presence of Ionizing Radiation," Annual Meeting of the Optical Society of America, Kissimmee, Florida, October 1981.

E. S. Yang, "Al-nSi Diodes for Photovoltaic Applications", EXXON Research Center Linden, N. J., June 1981.

E. S. Yang, "Recent Advances in Photovoltaic Devices," Society of Physics Student Lecture, Columbia University, February 22, 1982.

Lectures

K. Eisenthal, "Studies of Chemical Reactions and Energy Relaxation with Picosecond Lasers", Department of Chemistry, Harvard University, May 14, 1981.

K. Eisenthal, "Picosecond Time Resolved Studies of Molecular Relaxation and Chemical Processes", Nuclear Research Center, Strasbourg, France, June 17, 1981.

K. Eisenthal, "Electron Transfer and Photofragmentation Studies", Laboratory of Quantum Optics, Palaiseau, France, June 18, 1981.

K. Eisenthal, "Picosecond Studies of Electron Solvation in Liquids", Nuclear Studies Center (CEA), Saclay, France, June 19, 1981.

K. Eisenthal, "Picosecond Laser Studies in Condensed Phases", Department of Physics, University of Bordeaux, Bordeaux, France, June 22, 1981.

K. Eisenthal, "Picosecond Carbon Studies of Electron Transfer and Photofragmentation in Molecules", The University of Texas at Austin, November 19, 1981.

K. Eisenthal, "Picosecond Carbon Studies of Electron Transfer and Photofragmentation in Molecules", The University of Houston, November 20, 1981.

K. Eisenthal, "Picosecond Chemistry", IBM Lecture, Yorktown Heights, N.Y., April 20, 1982.

K. Eisenthal, "Studies of Ultra Fast Phenomena in Chemistry With Picosecond Lasers", Wesleyan University Seminar, April 30, 1982.

G. Flynn, "Lasers in Chemical Dynamics: A Decade of Revolution", State University of New York at New Paltz, Frontiers in Chemistry Series, April 1981.

G. Flynn, "Vibrational Energy Transfer in Small Molecules", Symposium on Laser Chemistry, Joint Central-Great Lakes Regional ACS Meeting, Dayton, Ohio, May 1981.

G. Flynn, "Vibrational Energy Transfer in Fluorine Compounds", Lasers in Flourine Chemistry Symposium, Am. Chem. Soc. Mtg. New York, N.Y., August 1981.

G. Flynn, "Photofragmentation and Energy Transfer in Low Pressure Gases and Low Temperature Matrices", Lasers in Chemistry Symposium IUPAC Meeting, Vancouver, B. C., Canada, August 1981.

G. Flynn, "Photofragmentation and Energy Transfer in Low Pressure Gases and Low Temperature Matrices", Pure Chemistry Award Symposium A. C. S. Meeting, Las Vegas, Nevada, March 1982.

G. Flynn, "Photofragmentation in Low Pressure Gases and Low Temperature Matrices", University of Texas, Austin, Texas, April 28, 1982.

G. Flynn, "Photofragmentation in Low Pressure Gases and Low Temperature Matrices", University of Houston, Houston, Texas, April 1982.

G. Flynn, "Lasers in Chemical Dynamics: A Decade of Revolution", Frontiers in Chemistry Series Case-Western Reserve University, Cleveland, Ohio, April 1982.

G. Flynn, "The Maser The Laser and The Columbia Radiation Laboratory: An Historical Perspective", Columbia College Dean's Day,. Columbia University, New York, N. Y., April 1982.

S. Hartmann, "Billiard Ball Echo Model", University of British Columbia, British Columbia, Canada, October 1, 1981.

S. Hartmann, "Billiard Ball Echo Model", Brooklyn Polytechnical Inst., New York, N.Y., October 15, 1981.

S. Hartmann, "Billiard Ball Echo Model", Columbia University, New York, N.Y., October 16, 1981.

S. Hartmann, "Billiard Ball Echo Model", University of Connecticut, Storrs, Connecticut, October 30, 1981.

S. Hartmann, "Billiard Ball Echo Model", Naval Research Laboratory, Washington, DC , November 6, 1981.

S. Hartmann, "Billiard Ball Echo Model", College of William and Mary, Williamsburg, Virginia, November 20, 1981.

S. Hartmann, "Billiard Ball Echo Model", University of Toronto, Toronto, Canada, November 24, 1981.

S. Hartmann, "Billiard Ball Echo Model", Bell Labs, Holmdale, NJ , November 30, 1981.

S. Hartmann, "Billiard Ball Echo Model", Exxon Research Laboratory, Linden, NJ, December 7, 1981.

S. Hartmann, "Billiard Ball Echo Model", Massachusetts Institute of Technology, Cambridge, Massachusetts, May 4, 1982.

R. Osgood, "Laser Photochemical Etching", IBM Thomas Watson Lab., Yorktown, N. Y., January 1982.

R. Osgood, "Laser Direct Writing", NATO Adm. Research Institution, Microelectronics, Les Deux Alpes, France , March 1982.

M. Teich, "Multiplication and Refractoriness in Visual Information Processing", Harvard/MIT Division of Health Sciences and Technology, Cambridge, Massachusetts, October 1981.

M. Teich, "Neural Counting in Intensity Discrimination and Loudness Estimation", Fechner Day '81 Celebration Lecture at Harvard University, Cambridge, Massachusetts, October 1981.

M. Teich, "Infrared Heterodyne Detection: Theme and Variations", Riverside Research Institute, New York, New York, November 1981.

M. Teich, "Cascaded Poisson Processes in Photon Detection", University of Rochester Department of Physics and Astronomy, Rochester, New York, November 1981.

M. Teich, "Multi-Frequency Heterodyne Detection", Night-Vision and Electro-Optics Laboratory, Ft. Belvoir, Virginia, January 1982.

M. Teich, "Multiplied-Poisson Noise in Optics", University of Central Florida, Orlando, Florida, February 1982.

M. Teich, "How Few Photons Can the Human Eye Perceive?", University of Pennsylvania Department of Bioengineering, Philadelphia, Pennsylvania, March 1982.

E. Yang and C. M. Wu, "Coulombic Scattering at the Grain Boundary of Polycrystalline Semiconductors", Gordon Conference on Thin-Film and Solid Surfaces, Colby-Sawyer College, July 13-17, 1981.

E. Yang, P. Panayotatos, and W. Hwang, "Determination of Diffusion Length and Recombination Velocity in Polycrystalline Semiconductors by Scanning Laser-spot Photoconductivity", Gordon Conference on Thin-Film and Solid Surface, Colby-Sawyer College, July 13-17, 1981.

E. Yang, "Structures and Performance of Polycrystalline Thin-Film Solar Cells", Material Research Society Meeting - Thin-Film Symposium, Boston, November 17-19, 1981.

E. Yang, P. Panayotatos, J. S. Song and W. Hwang, "Measurement of Diffusion Length and Grain-Boundary Recombination Velocity in Solar-grade Polycrystalline Silicon", Material Research Society Meeting-Semiconductor Grain Boundary Symposium Boston, November 16-19, 1981.

Resonance Seminars

Meetings are held periodically at Columbia University, New York, New York during the academic year and are open to all members of the New York Scientific community. Guest speakers are invited to discuss work in the general area of the research in the Columbia Radiation Laboratory.

Herbert Strauss, University of California, Berkeley, "Ultrafast Rates and Phase Transitions by Vibrational Spectroscopy," September 23, 1981.

Peter Sorokin, I. B. M. Research Laboratories, "Time Resolved Infrared Laser Spectroscopy," October 29, 1981.

Aaron Wyner, Bell Laboratory, Murry Hill, NJ, "Information Theory - Optical Communications," November 20, 1981.

Arthur Gossard, Bell Laboratories, "Multi-Layer Semiconductor Structures by Molecular Beam Epitaxy," December 8, 1981.

Tom Manuccia, Naval Research Laboratory, "Circumventing the Wavelength-Spatial Barrier - A CARS (i.e. Raman Laser) Microscope," December 16, 1981.

B. Picinbono, Laboratoire des Signaux et Systemes Ecole Superieure d'Electricite, "On Canonical Representation of Signals by Instantaneous Amplitude and Phase," March 22, 1982.

E. Evleth, Centre de Mécanique Ondulatoire Appliquée, "Small Molecule Rydberg Photochemistry," March 26, 1982.

Ahmed Zewail, California Institute of Technology, "Coherent Picosecond Excitation of Large Molecules in Supersonic Jets," April 9, 1982.

Don Silversmith, MIT Lincoln Laboratory, "Physics and Device Implications of Silicon-on-Insulator (SOI)Substrates," April 28, 1982.

Gary Bjorklund, I. B. M. San Jose Research Laboratory, "Frequency Domain Optical Memories Based on Photochemical Hole Burning," May 6, 1982.

I. QUANTUM DETECTION AND SENSING OF RADIATION

A. WAVE AND PARTICLE NOISE IN OPTICAL DETECTION AND COMMUNICATIONS*

(M. C. Teich, P. R. Prucnal)

(Principal Investigator: M. C. Teich (212) 280-3117)
(JSEP work units 12, 13 and 14, 1979-1982)

We have made substantial progress in understanding the behavior of multiplied-Poisson processes, as indicated below.

For a Poisson primary process generating a Poisson number of secondaries for each primary, we arrive at an important special case, the shot-noise-driven doubly stochastic Poisson point process (SNDP), as illustrated in Fig. 1. The sum of the functions associated with the primary events constitutes a filtered Poisson point process, or shot noise (Fig. 1b). Since the primary events are stationary, this will also be a stationary stochastic process. The subsidiary events now form a doubly stochastic Poisson point process whose stochastic rate is the shot noise $\lambda(t)$; this provides the rationale for the name SNDP. The structure of the model is schematically illustrated in the block diagram of Fig. 2, which clearly shows its multiplicative Poisson nature. Physical systems that are describable by an SNDP model will exhibit a physical structure characterized by these three cascaded blocks.

Figure 2. Model for generation of the SNDP process.

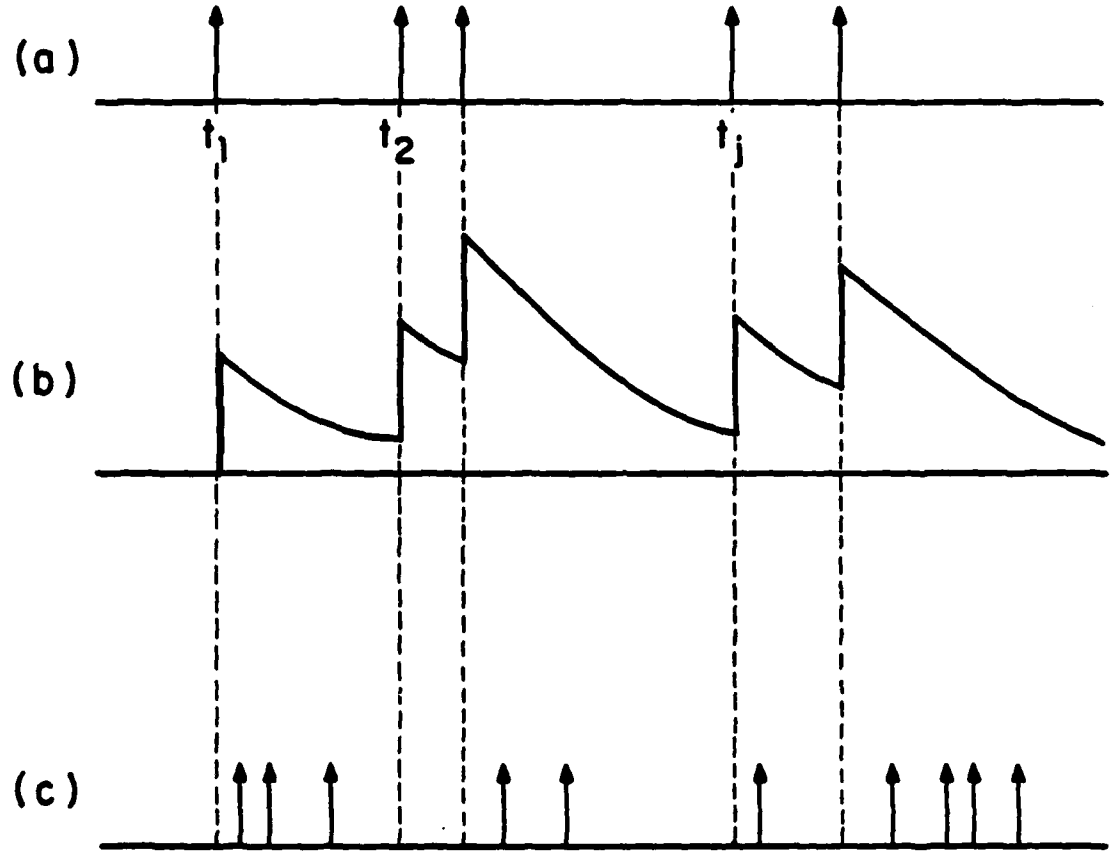

Figure 1. Production of SNDP events. (a) primary Poisson events; (b) filtered Poisson events (shot noise); (c) subsidiary doubly stochastic Poisson events whose rate is shot noise.

The SNDP model turns out to provide an appropriate description for a variety of important effects involving multiplication. These effects are often inherent in the generation and detection of optical and ionizing radiation. This multiplication noise can be quite important in properly interpreting the behavior of individual electro-optic devices and in determining the performance of communication, surveillance, navigation, guidance, and control systems incorporating these devices.

We have carried out a number of studies to ascertain the importance of multiplication noise.[1]-[5] We have explicitly demonstrated the applicability of the SNDP model for describing the following processes: (i) the detection of scintillation photons produced by ionizing radiation, e.g., high-energy electrons or nuclear particles; (ii) the generation of luminescence noise, by ionizing radiation, in optical detectors, optical fibers, and electro-optic components; and (iii) cathodoluminescence emission. We pointed out that the SNDP model will also be useful for studying other important effects, such as image intensification, cosmic-ray noise in electro-optic systems, and cosmic-ray soft errors in electronics and computer systems. In all of these cases, there is a multiplication process involved, in which a primary event produces a random number of secondary events, with a certain time course. The SNDP may be useful in other electronics applications as well, e.g., for determining scaling limitations and reliability factors in submicron structures and VLSI systems resulting from statistical effects. If dopant impurities cluster to an appreciable degree, as has been reported,[6] this can be accommodated in the framework of a spatial multiplicative noise description. The doubly stochastic Thomas distribution[1] might provide a first approximation to such behavior, when there is such clustering and when there is a simultaneous uncertainty in the impurity profile. We now proceed to discuss multiplication noise in more detail for the three processes cited above.

(i) Scintillation Photon Counting

The detection of ionizing radiation is often accomplished through a radiation-matter interaction in which a single high-energy particle produces a shower of lower energy particles. A case in point is the scintillation detector which is a combination of a scintillation crystal (e.g., NaI:Tl, plastic) with a photomultiplier tube. Conditions for the validity of the SNDP in describing scintillation detection are that the incident primary ionizing particles (e.g., electrons, gammas, protons) be represented as a homogeneous Poisson point process, and that each primary event have associated with it an impulse response function h(t) that governs the rate of production of Poisson optical photons.

A model for the physical process is illustrated in Fig. 3. It is seen to be identical in form to the block diagram presented in Fig. 2, so that the resulting photon emissions form an SNDP. The function h(t) will often be able to be roughly represented by a decaying exponential so that the counting and time statistics can be calculated explicitly. The description is completely characterized by the driving rate μ and the impulse-response function h(t), and therefore, in this case, by three parameters: μ, the rate of the primary process; α, the multiplication parameter; and τ_p, the lifetime of the process of secondary event generation. If we perform photon counting, we must add T, the counting time. In the limit of counting times long in comparison with the exponential decay time, the counting distribution will reduce to the Neyman Type-A for arbitrary h(t). It is usually assumed in the literature, generally tacitly, that scintillation photon counting statistics are described by the fixed multiplicative Poisson distribution; this provides an appropriate approximation only for $T >> \tau_c$ and $\alpha >> 1$, however.[1]

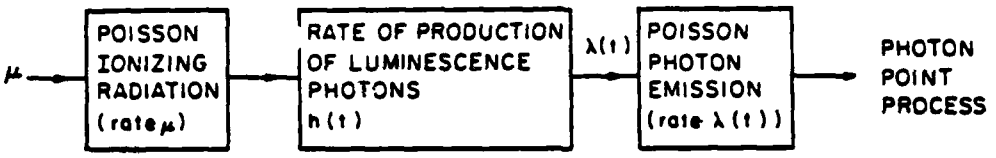

Figure 3. Model for the photon point process generated by scintillation radiation, cathodoluminescence, and photoluminescence. Observe the relation to Fig. 2 which is the mathematical model studied here.

We have demonstrated that the experimental counting distribution for radioluminsecence photons produced in glass can be represented in terms of the Neyman Type-A.[2] That this is plausible can be understood from the following argument. Consider a stream of Poisson-distributed β^- rays irradiating a glass sample. If each high-energy electron produces a Poisson distributed number of luminescence photons with a maximum time delay that is short in comparison with the counting time ($\tau_c << T$), the overall photon count will reflect both sources of *independent Poisson randomness*, leading to the Neyman Type-A photon-counting distribution.

A series of such experiments was carried out.[2] β^- particles from a ^{90}Sr-^{90}Y equilibrium-mixture source irradiated the Corning 7056 glass faceplate of an EMR type 541N-01 photomultiplier tube from a distance of about 11.5 cm. The maximum β^- energies were 0.54 and 2.23 MeV for the ^{90}Sr and ^{90}Y, respectively, and the β^- flux was $\sim 8.2 \times 10^3$ $cm^{-2}s^{-1}$. External light was excluded. The photomultiplier anode pulses were passed through a discriminator and standardized. Unavoidable system dead time was $\sim$60 ns. The standardized pulses were counted during consecutive fixed counting intervals (T = 40 μs) and the counts were recorded. The experiment was performed repeatedly to obtain good statistical accuracy, and a histogram representing the relative frequency of

the counts was constructed. The total duration of a run was about 4 min. In the particular experiment we illustrated, the observed mean count was 85.89 (this number was substantially higher than the mean dark count which could therefore be neglected) and the observed count variance was 429.58. The data are shown as the dots in Fig. 4. The solid curve represents the Neyman Type-A theoretical counting distribution with the count mean and variance fixed at the experimental values. It is clearly in accord with the data. The experimental multiplication parameter $\alpha = 4.0$. A Poisson distribution with mean 85.89 (indicated by arrow) is plotted as the dashed curve in Fig. 4; clearly it bears no relation to the data.

Because the primary process in this case consisted of high-energy charged particles (electrons), Čerenkov radiation could have been produced in addition to luminescence radiation. However, even if a large number of photoelectrons were generated by the Čerenkov photons arising from a single particle, they would nevertheless appear as a single (large) photoelectron pulse since the Čerenkov radiation emission time is much shorter than the transit time in the photomultiplier tube. The appropriate counting distribution has been worked out for this case as well and it is the Thomas distribution, which is very similar in character to the Neyman Type-A distribution, and to the fixed multiplicative Poisson distribution for large multiplication parameter.[1]

(ii) Luminescence Noise in Electro-Optic Devices

Consider an application in which we wish to observe photon arrivals by using a photomultiplier tube or solid-state detector in an ionizing radiation environment. Examples might be in surveillance, high-altitude astronomy, the guidance system of a spacecraft, or in the aftermath of a nuclear detonation. In these cases, the description provided above may be characteristic of the

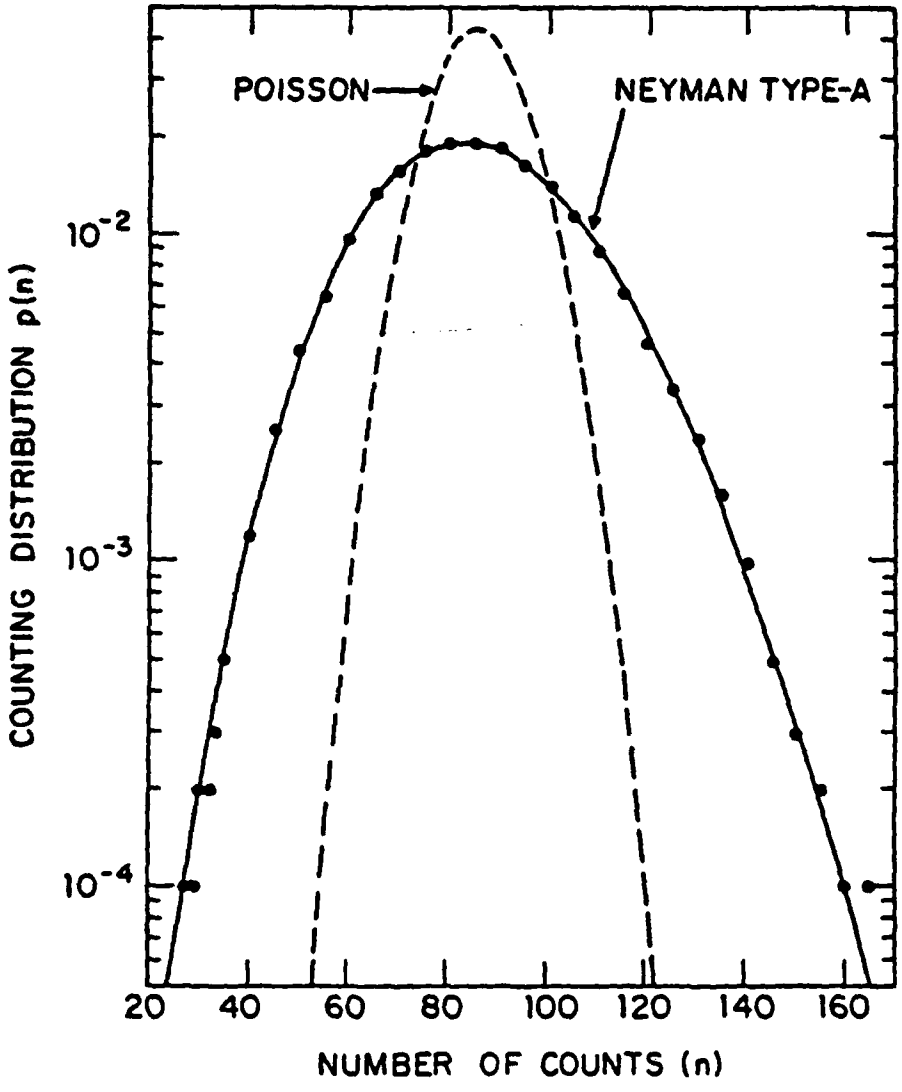

Figure 4. Photon counting distribution p(n) vs number of photon counts n. Data (dots) represent radioluminescence photon registrations from the glass faceplate of a photomultiplier tube, induced by ^{90}Sr-^{90}Y β^- rays. The counting time T = 400 μs. The experimental count mean and variance are 85.89 and 429.58, respectively. The solid curve represents the Neyman Type-A theoretical counting distribution with the same values of count mean and variance (α = 4.0). The Poisson distribution with mean 85.89 (indicated by arrow) is shown as the dashed curve.

noise rather than of the signal. Several authors have discussed sources of noise in photomultiplier tubes in the ionizing radiation environment of space. Such noise may arise from several mechanisms such as luminescence and Čerenkov radiation in the photomultiplier window; secondary electron emission from the window, photocathode, and dynodes; Bremsstrahlung, in turn, causing such secondary electron emission; cosmic-ray bursts; and, of course, thermionic emission dark current. These effects clearly degrade both the dynamic range and the photometric accuracy of low-light-level measurements, and therefore must be properly modeled. It is evident from the experimental results reported in the previous subsection that the SNDP provides a sound point of departure for modeling a number of these sources of noise (luminescence will be the dominant source of noise in many applications). Similar effects will occur in solid-state devices.

Photomultiplier tubes are often preferred to solid-state detectors in such applications precisely because of their relative radiation hardness. The radiation hardness of optical fibers,[7] in particular, and of optical systems more generally, has received substantial attention recently. Aside from their many other advantages,[8] optical fiber and signal processing systems have the additional allure of immunity to electromagnetic pulse (EMP) interference.[9],[10] As is clear from our earlier discussion, an additional factor that must be considered in using electro-optic systems in ionizing-radiation environments is the induced multiplicative luminescence noise.

(iii) Cathodoluminescence Noise

Cathodoluminescence is an important process in which a beam of accelerated electrons incident on a luminescent material (e.g., a phosphor) induces the emission of light.[11],[12] It is the process responsible for the radar, television monitor, and oscilloscope images. Conditions for the validity of the SNDP in describing cathodoluminescence emission are that the electron beam reaching the sample be represented as a homogeneous Poisson point process, and that each primary event have associated with it an impulse response function $h(t)$ that governs the rate of production of Poisson optical photons. Cathodoluminescence may therefore be represented by the physical model in Fig. 3 if we simply replace the block labeled "Poisson ionizing radiation" by a block entitled "Poisson electron beam."

The counting and time statistics can then be obtained by using techniques to be outlined in the next section. The description is completely characterized by μ and $h(t)$ and, again, in the limit of counting times long in comparison with the time scale of $h(t)$, the counting distribution will reduce to the Neyman Type-A for arbitrary $h(t)$.

If the function $h(t)$ is a decaying single-time-constant exponential, each electron entering the sample induces an exponentially decaying flux of luminescence photons. In this special case, the results will be the same as those derived by van Rijswijk[13],[14] via an entirely different method. It appears that van Rijswijk's result can be used only for luminescence that decays precisely exponentially whereas our general result will be valid for arbitrary $h(t)$. In particular, we can easily account for the finite "decay" (rise) time of the luminescence emission.

The statistics for the time to the first cathodoluminescent photon arrival

were experimentally measured by van Rijswijk[14] for a $YVO_4:Eu^{3+}$ phosphor and, more recently, by Timmermans and Zijlstra[15] for ZnS:Ag. In Fig. 5 we present the normalized forward recurrence time data (dots) for YVO_4: Eu^{3+} obtained by van Rijswijk[14] with an incident electron energy of 10.2 keV, The mean photon counting rate was $2.54 \times 10^4 s^{-1}$ and the mean dark counting rate was $1.28 \times 10^3 s^{-1}$. The solid curve is a plot of the expected theoretical forward recurrence time probability density $P_1(\tau)$ for an exponentially decaying shot-noise pulse, with $\bar{\tau} = 39.7\ \mu s$, $\alpha = 9.6$, and $\tau_c = 0.5$ ms. The effects of dark noise were not negligible in this case, and were accounted for in the solid curve. The experimental data clearly deviate from the straight-line behavior representing the exponential interval distribution characteristic of a Poisson process, and so does the theoretical result. Clearly, cathodoluminescence photons are not Poisson distributed.

Intensity fluctuations for cathodoluminescence were first investigated by means of the spectral properties of excess noise in the photomultiplier anode current.[16],[17] The theoretical expression for the spectrum in the general case (viz., for arbitrary h(t) and arbitrary T) can be derived using techniques we propose to develop. The result for an exponentially decaying shot-noise pulse, in a form appropriate when measurements are made by a real-time spectrum analyzer, turns out to be Lorentzian, in agreement with previously derived results.

Recent excess noise measurements were performed by van Rijswijk[14] for $YVO_4:Eu^{3+}$ and by Timmermans and Zijlstra[15] for ZnS:Ag. In Fig. 6 we present the ZnS:Ag experimental relative excess noise as a function of frequency (dots) obtained by Timmermans and Zijlstra. The solid curve is a Lorentzian which clearly provides an excellent fit to the data, lending confirmation to the exponential decay shape and the luminescent center lifetime. Use of the SNDP

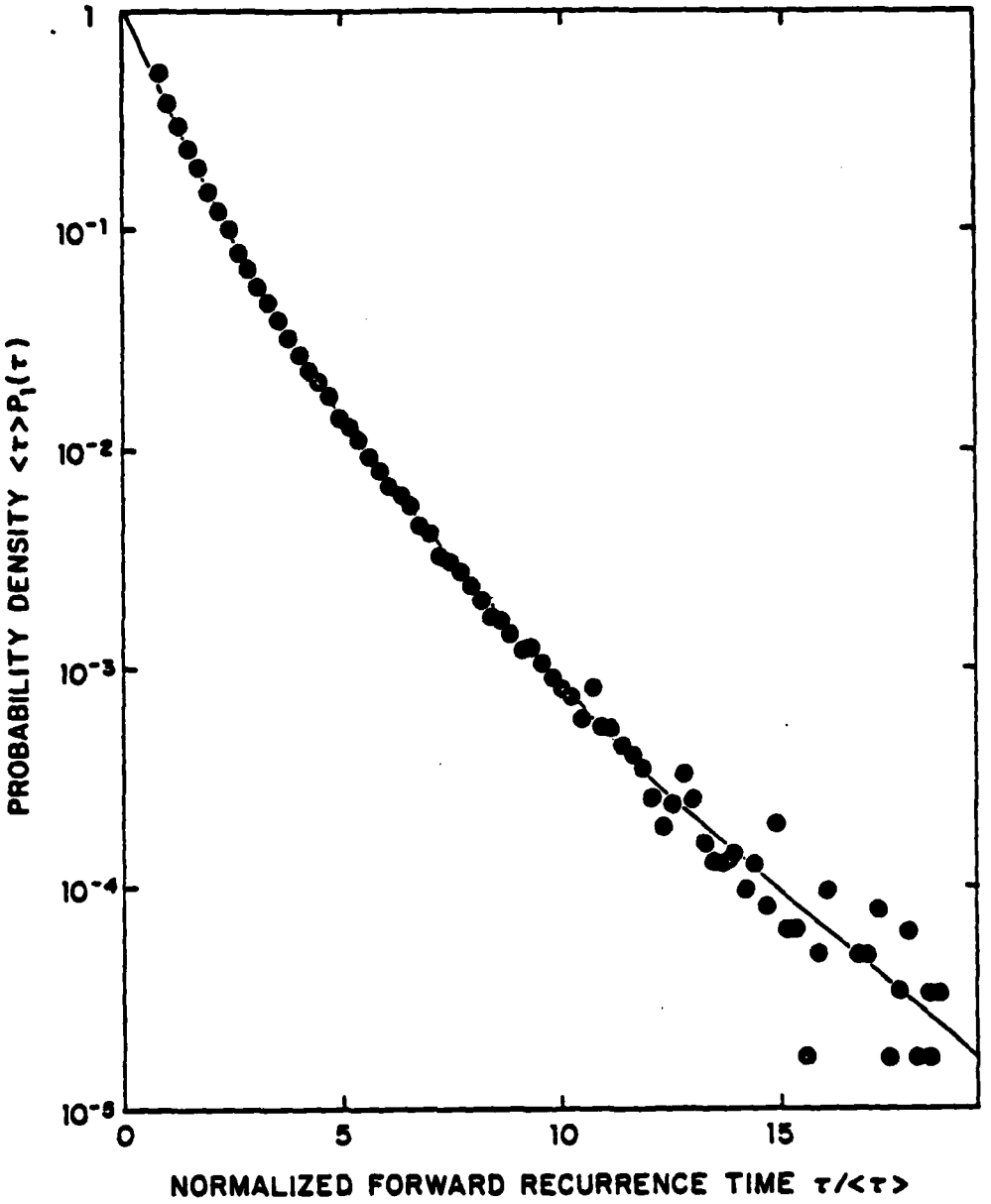

Figure 5. Dots represent the relative frequency of the time to the first cathodoluminescent photoelectron event for a $YVO_4:Eu^{3+}$ phosphor with the exciting electron energy fixed at 10.2 keV. The mean photon counting rate was $2.54 \times 10^4 s^{-1}$ and the mean dark counting rate was $1.28 \times 10^3 s^{-1}$. The solid curve is a plot of the SNDP theoretical probability density function $\langle\tau\rangle P_1(\tau)$ vs the normalized forward recurrence time $\tau/\langle\tau\rangle$ for an exponentially decaying shot-noise pulse, with $\bar{\tau}$ = 39.7 μs, α = 9.6, and τ_c = 0.5 ms. Dark noise has been accounted for in the theoretical curve. Data adapted from Fig. 6 of the paper by van Rijswijk.[14] The data demonstrate that cathodoluminescence photons are clearly not Poisson distributed.

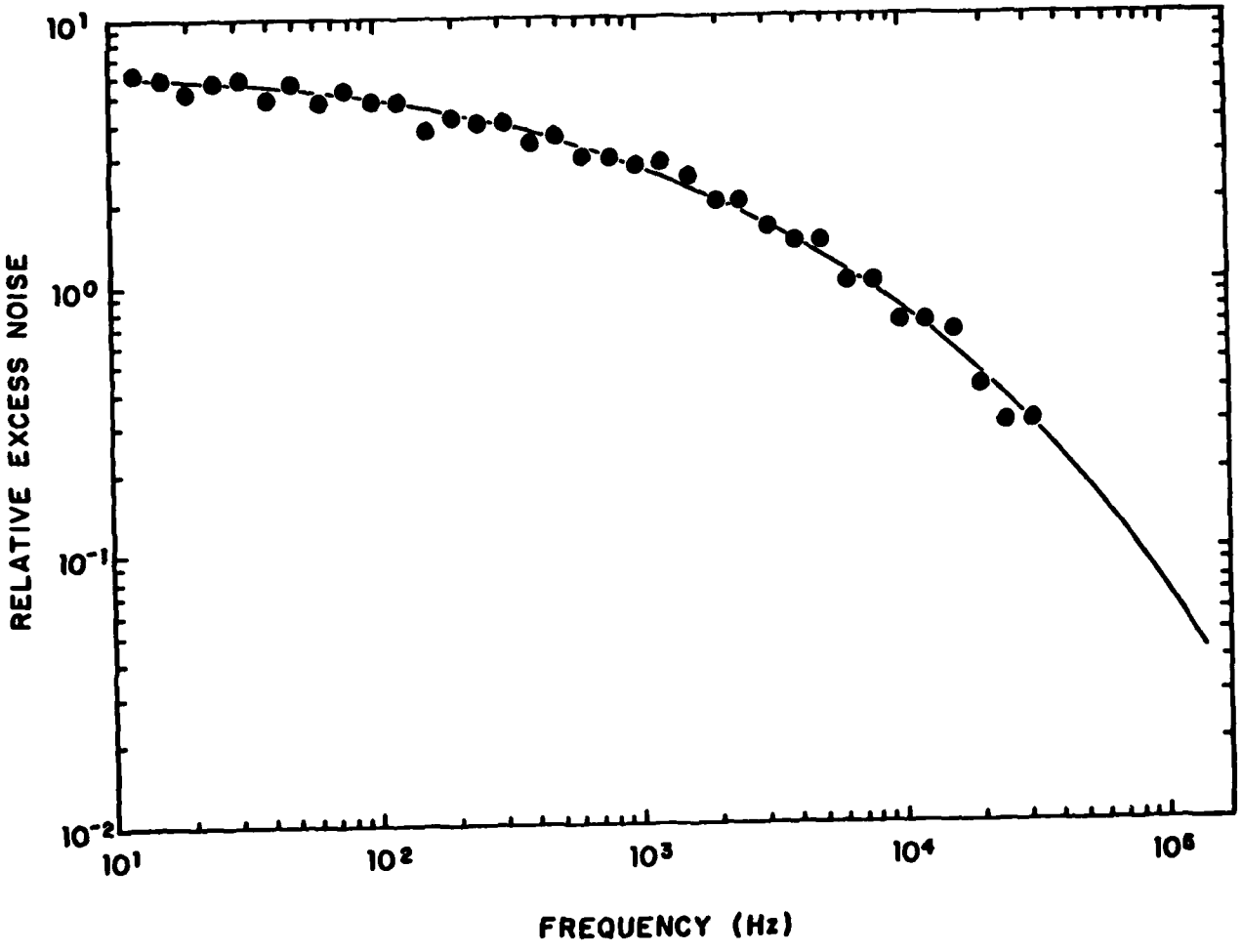

Figure 6. Dots represent the experimental relative excess noise in the photomultiplier anode current for cathodoluminescence from ZnS:Ag. The solid curve is a Lorentzian. Figure adapted from Fig. 3 of the paper by Timmermans and Zijlstra.[15]

would permit us to obtain the excess noise for an arbitrary impulse response function.

Substantial progress has also been made toward the implementation and analysis of a frequency-shift keyed (FSK) fiber-optic communication link. Work accomplished in the areas of optimal (single-threshold) processing schemes, a new technique for computing performance, and the demonstration of a wideband FSK fiber-optic link are summarized below.

(1) Single-Threshold Detection for an FSK Fiber-Optic System.

It is well known that optimal processing in photocounting optical communications systems consists of the likelihood ratio test (LRT) applied to an observed quantity at the detector output. In practice, however, the LRT may be difficult or impossible to implement. We have derived a remarkably simple optical processor that replaces the complicated LRT for a broad class of systems.

The results were applied to an FSK photocounting fiber-optic communication system in which the noise was considered to be of the Poisson or Poisson-avalanche types (corresponding to a PIN or avalanche photodiode detector). For the PIN detector, single-threshold processing was shown to be optimal for several decision rules. For the avalanche photodiode, it was shown that single-threshold processing did not necessarily apply. Examples of avalanche photodiode receivers were single-threshold processing was not optical were presented. Other cases for which the noise contained a point of inflection were also investigated, such as the Polya density under certain conditions, the distribution of photocounts from a sinusoidally modulated single-mode laser, and the Cauchy density.

(2) Probability of Error for an FSK Fiber-Optics System

It has become the habit of those engaged in photocounting optical receiver design who are unable to compute bit-error rates exactly to resort to Gaussian approximations, series expansions, and special bounds. These techniques all trade off between simplicity and accuracy.

A new technique for evaluating system performance was developed which is as simple as the Gaussian approximation, yet is more accurate. This technique is based upon a point transformation, "the normalizing transform", which is applied to the noisy receiver output, and renders its statistics more nearly Gaussian. The resulting output is then more accurately approximated by conventional Gaussian techniques.

The form of the normalizing transform was determined for a number of probability density functions, including the Poisson, binomial, negative-binomial, lognormal, and non-central chi-squared. In particular, the normalizing transform for the Poisson was a simple square-root point transformation. The form of the normalizing transform was also determined for a broad class of receiver outputs x where the variance var x is a known function of the mean $\langle x \rangle$

$$\text{var } x = D^2 (\langle x \rangle). \tag{1}$$

We have shown that the normalizing transform solution for this case is

$$g(x) = \int (1/D(x))dx \tag{2}$$

This resulting family of random variables g(x) was nearly normally distributed even though the untransformed family x might exhibit excessive skewness.

The normalizing transform technique was used to evaluate the performance of fiber-optic systems with avalanche photodiode receivers. The output voltage of a typical binary digital receiver employing an avalanche photodiode was

represented by a filtered randomly multiplied Poisson process.

It was found in many examples that the normalizing transform provided an approximation that was as good, or better than the Gaussian approximation for evaluating system performance, with little additional computation. The improvement was more pronounced when the pdf was skewed and exhibited a strong signal-dependence. The improvement was less pronounced in limits where the pdf approached Gaussian and was relatively signal-independent.

(3) Wideband FSK Fiber-Optic Experiment

A series of experiments have been performed in which a digital fiber-optic communication link has been implemented using wideband frequency modulation. System performance was measured and compared to a system using on-off keyed modulation.

By now the merits of frequency modulation in radio communication are widely recognized. For digital FM (frequency-shift keying or FSK), when compared to on-off keying (OOK) on a peak-power basis, the SNR is increased in 3 dB for both coherent and noncoherent detection. For FSK, optimal processing is straightforward to implement. In contrast, OOK requires knowledge of all key system parameters to set an optimal threshold. These parameters may be impossible to measure exactly and may change with time causing severe degradation of OOK performance.

The advantages of FM in optical communication are even more striking, since optical bandwidth is plentiful at the present time, and the potential bandwidth expansion is enormous. However, all attempts to utilize FM in optical communications have been thwarted by the lack of tunable sources.[18] Various subcarrier FM intensity modulation schemes have been resorted to.[19],[20] These subcarrier FM.IM schemes are inherently limited by the excursion of the intermediate frequency carrier (e.g., 25±5 MHz) and therefore do not exploit

the advantages of wideband optical FM.

Recent developments in frequency tunable lasers have now made FM optical communications viable.[21]-[23] Olsson and Tang have demonstrated electronic tuning, at 100 MHz, of a room-temperature cw laser over a 5 nm spectral range.[24] Gigabit data rates can be obtained with a double-wavelength mode-locked laser.[22],[24]

This paper reports the first experimental demonstration of a wideband FSK optical fiber communication system. The center wavelength was 827 nm with an excursion of 3 nm. Pseudorandom data was transmitted at a rate of 10 Mbits/sec. A block diagram of the FSK system is shown in Fig. 7. A comparable OOK system is implemented by removing one of the lasers and removing the narrowband filter.

Shown in Fig. 8 is the bit-error rate versus total optical attenuation for FSK and OOK. The curves represent the theoretical results obtained using the appropriate estimates of system parameters. The theoretical optical loss is given in dB on the upper scale. The dots are experimental data obtained using the systems described in the previous section. The experimental optical loss is given in dB on the lower scale. Approximately 12.9 dB attenuation is introduced in the connectors, couplers and focussing elements of this system. The total optical loss also includes 3.3 dB from the spool of graded index fiber, plus 36.3 - 41.8 dB introduced using neutral density filters. This attenuation is equivalent to 13.2 - 15 km of fiber with 3 dB/km loss. Negligible inter-symbol interference will occur over these distances at the bit rates used in our system. As seen in Fig. 8, the experimental results are in good agreement with the theory in terms of the slope and relative position of the data points. A 3 dB improvement in sensitivity of FSK over OOK is exhibited over 6 orders of magnitude of bit-error rates. The experimental losses are approximately 4.2 dB higher than predicted by theory, as seen by the difference between the experimental

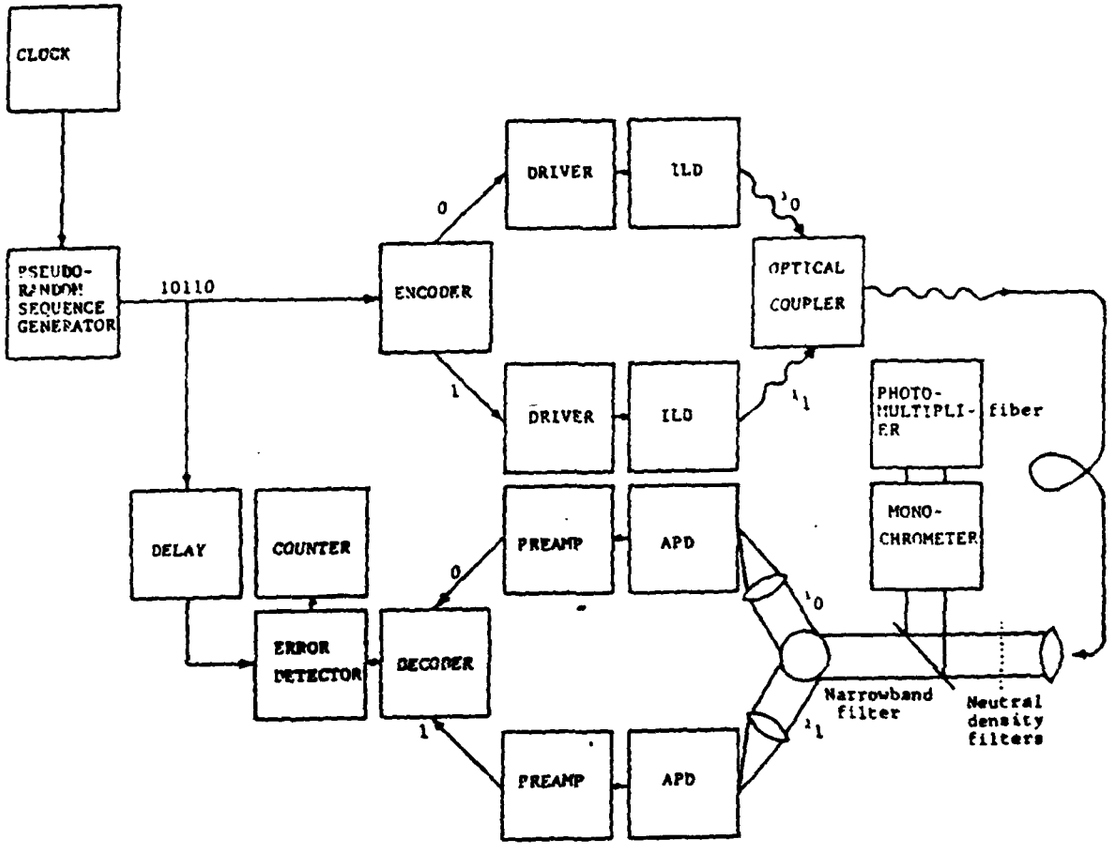

Figure 7. Block diagram of FSK fiber-optic experiment.

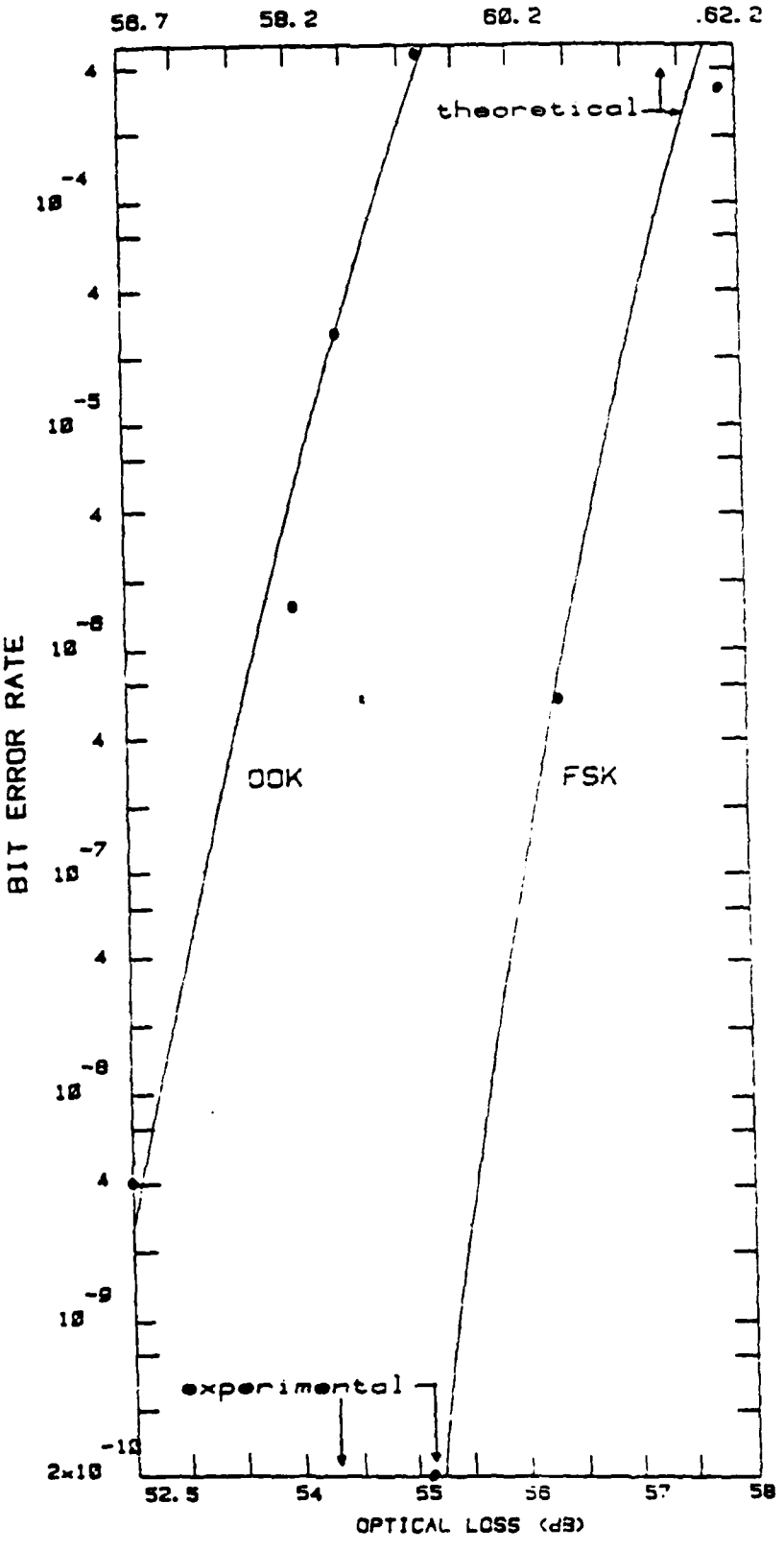

Figure 8. Bit-error rate versus total optical attenuation for FSK and OOK.

(lower) and theoretical (upper) scales in Fig. 8. This is accounted for, in part, by the fact that average rather than actual estimates of device parameters were used in the theoretical calculations.

In summary, the superior noise immunity of wideband frequency-modulation was demonstrated in a fiber-optic communication system. If suitable tunable lasers are used, FSK can provide a high-performance alternative to conventional OOK for fiber-optic transmission.

*This research was also supported by the National Science Foundation under Grants NSF-ENG78-26498 and NSF-ECS-8006881.

(1) M. C. Teich, Appl. Opt. 20, 2457 (1981).

(2) M. C. Teich and B. E. A. Saleh, Phys. Rev. A 24, 1651(1981).

(3) M. C. Teich and B. E. A. Saleh, J. Opt. Soc. Am. 71, 771 (1981).

(4) B. Saleh, J. T. Tavolacci, and M. C. Teich, J. IEEE J. Quant-Electron. QE-17, 2341 (1981).

(5) B. Saleh and M. C. Teich, Proc. IEEE 70, 229 (1982).

(6) L. V. Berman, E. V. Soloveva, M. G. Milvidsky, L. N. Nazhivina, and L. D. Sabanova, Fiz. Tekh. Poluprovodn. 13, 659 (1979) [Trans.: Sov. Phys. - Semicond. 13, 388 (1979)].

(7) G. H. Siegel, Jr. and E. J. Friebele, IOOC Conf. Digest, San Francisco, April 1981.

(8) C. L. Cuccia, Military Electron./Countermeas. 7(#4), 58 (1981).

(9) C. L. Longmire, IEEE Trans. Electromag. Compat. EMC-20, 3 (1978).

(10) E. J. Lerner, Spectrum. 5, 41 (1981).

(11) H. W. Leverenz, Introduction to Luminescence of Solids, Wiley, New York, 1970.

(12) S. Larach and A. E. Hardy, Proc. IEEE 61, 915 (1973).

(13) F. C. van Rijswijk, Physica, 82B, 193 (1976).

(14) F. C. van Rijswijk, Physica, 82B, 205 (1976).

(15) J. Timmermans amd R. J. J. Zijlstra, in Noise in Physical Systems, D. Wolf, ed. Springer-Verlag, Berlin/Heidelberg/New York, 1978.

(16) T. M. Chen and A. van der Ziel, IEEE Trans. Electron. Devices ED-12, 489 (1965).

(17) H. M. Fijnaut and R. J. J. Zijlstra, J. Phys. D. Appl. Phys. 3, 45 (1970).

(18) T. A. Nussmeier, F. E. Goodwin , and J. E. Zavin, IEEE J. Quant. Elec. QE-10, 230 (1974).

(19) A. Albanese and H. Lensing, Proc. ICC79 (IEEE Publication 79, Boston, 1979), I.1.7.

(20) G. M. Borsuk and W. J. Thaler, IEEE Trans. Sonics and Ultrasonics SU-17, 207 (1970).

(21) C. L. Tang, V. G. Kreismanis, and J. M. Ballantyne, Appl. Phys. Lett. 40, 113 (1977).

(22) S. Blit, A. Olsson, and C. L. Tang, Opt. Lett. 4, 245 (1179).

(23) J. M. Osterwalter and B. J. Rickett, IEEE J. Quant. Elec. QE-16, 250 (1970).

(24) A. Olsson and C. L. Tang, IEEE J. Quant. Elec. QE-15, 1085 (1979).

II. PHYSICAL AND PHOTOCHEMICAL PROPERTIES OF ELECTRONIC MATERIALS

A. PHENOMENOLOGICAL MODEL OF GRAIN-BOUNDARY TRAPPING STATES IN POLYCRYSTALLINE SILICON UNDER OPTICAL ILLUMINATION *

(E. Poon, W. Hwang and E. S. Yang)
(JSEP work units 16 and 17, 1979-82)
(Principal Investigator: W. Hwang (212) 280-3115)

Electronic transport properties of polycrystalline silicon have been receiving much attention because of their applicability to VLSI bipolar and MOS integrated circuits and their potential for low-cost terrestrial solar energy applications.[1],[2] Photovoltaic devices fabricated on polycrystalline silicon films have been studied by many investigators.[3],[4] It appears that the grain boundary (GB) interface states play a dominant role in determining the electronic and photovoltaic properties of polycrystalline silicon by acting as traps and recombination centers. However, the fundamental understanding of these GB states is still not clear and substantial research effort in this direction is required. In this work, we develop a new theoretical model of the grain boundary recombination, charge carrier transport and electrostatics under the assumptions of Gaussian energy distributions of interface states, and unequal capture cross-sections for electrons and holes. We also demonstrate that the Gaussian energy distributions can be reduced to other distributions as special cases, in particular to exponential energy distribution, uniform distributions and discrete energy levels. Carrier generation is expected to introduce another degree of freedom and provide valuable additional insight into the optical dependence of the electrostatic effects of grain boundary interface states.

The energy band diagram of a polycrystalline semiconductor in the dark and under illuminated conditions in the neighborhood of two grain boundaries is shown in Fig. 1. At the grain boundary plane are localized interface

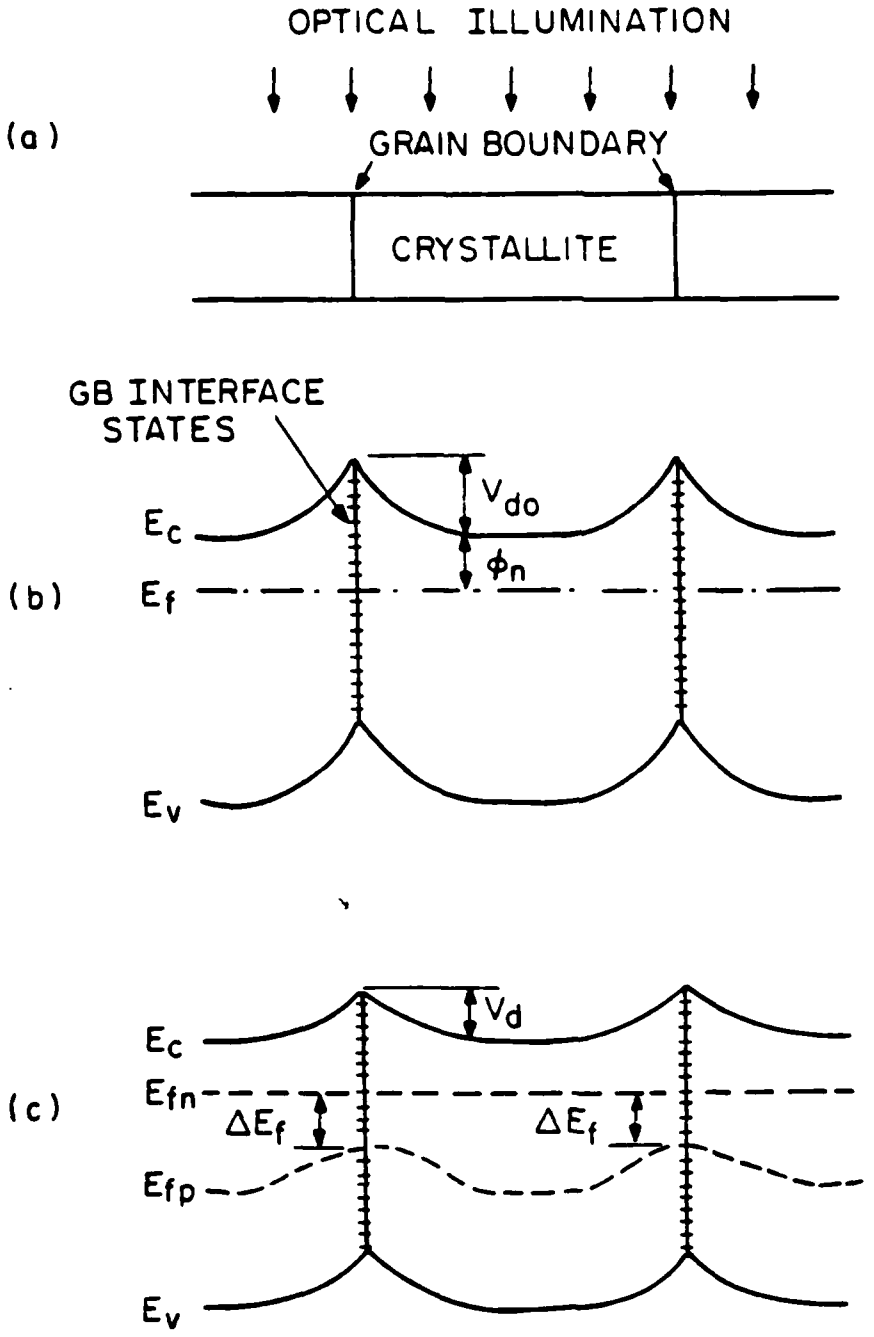

Fig. 1. Schematic representations of energy diagrams in the neighborhood of grain boundaries in a polycrystalline semiconductor. (a) One-dimensional grain structure. (b) In the dark. (c) Under optical illumination.

states, which in general are statistically distributed in energy over the energy gap. These states have a distribution determined by the nature of the disorder in the silicon bond structure such as dangling bonds, and by the local electronic potential fluctuations producing stress fields in the regions of structural irregularities. They may also arise from chemical impurities between adjacent grains. Together dangling bonds and local structural strain can produce an inhomogeneous broadening of the discrete levels in the gap if their effects are sufficiently severe. As a feasible approximation of the energy spectra for these localized states, Gaussian energy distributions are proposed. These states are classified into two types, "donor-like" and "acceptor-like" interface states. The energy distribution of the resultant donor-like and acceptor-like states $h_{tD}(E)$ and $h_{tA}(E)$ are expressed by the formula[15,16]

$$h_{tA}(E) = \frac{H_{tA}}{\sqrt{(2\pi)}S_A} \exp\left[-\frac{(E-E_{tA})^2}{2S_A^2}\right] \qquad (1)$$

and

$$h_{tD}(E) = \frac{H_{tD}}{\sqrt{(2\pi)}S_D} \exp\left[-\frac{(E-E_{tD})^2}{2S_D^2}\right] \qquad (2)$$

where H_{tA} and H_{tD} are the total number of the localized states per unit area, S_A and S_D are distribution parameters and E_{tA} and E_{tD} are the mean-values of the acceptor-like and donor-like distributions, respectively.

Figure 1(b) shows the band diagram in the absence of illumination. The GB diffusion potential barrier height, V_{dO}, can be calculated by equating the depletion-region charge accumulated in the interface states. The numerical value of V_{dO} have been calculated for both uniform and nonuniform energy

distributions of interface states by several workers.[2],[5],[7]

The presence of optical illimination, as shown in Fig. 1(c), separates the quasi-Fermi levels $E_{fn}(0)$ and $E_{fp}(0)$ for electrons and holes, and diffusion potential V_d decreases from its dark value V_{d0}. Between $E_{fn}(0)$ and $E_{fp}(0)$ the GB interface states act as recombination centers and the occupancy of the recombination center is determined by the relative magnitude of capture cross-sections and by the relative concentration of electrons and holes at GB, according to Shockly-Read-Hall (SRH) statistics.[2] The recombination centers at the GB are either neutral or charged depending on whether they are occupied donor-like or acceptor-like states, or whether they are empty acceptor-like or donor-like states. In the steady state a flux of electrons and an equal flux of holes of the GB is sustained by the photogeneration of these carriers in the neighborhood of the GB. Thus flux is equal to the steady state recombination rate at the grain boundary.

The carrier transport in polycrystalline semiconductors is dominated by the thermionic emission of majority carrier over the GB diffusion potential barrier. The conductivity of polycrystalline films is given by Eq. (9) for $V < \frac{kT}{q}$ [5],[8],[11]

$$\sigma = \frac{q^2 dN_d}{(2\pi m^* kT)^{1/2}} \exp\left(-\frac{qV_{do}}{kT}\right) . \qquad (3)$$

The optical illumination modifies the GB potential barrier V_d, as discussed above, and V_d decreases from its dark value V_{do}. Hence the enhancement of conductivity due to the optical illumination (photoconductivity) is given by

$$\sigma_{ph} = \frac{q^2 d\ N_d}{(2\pi m^* kT)^{1/2}} \exp\left(-\frac{qV_{do}}{kT}\right) \exp\left(\frac{q\Delta V_d}{kT}\right) \qquad (4)$$

where $V_d = V_{do} - \Delta V_d$, and it is assumed that $\sigma_{ph} >> \sigma_{dark}$. Equation (4) can also be rewritten as

$$\sigma_{ph} = q N_d \mu_{eff} \tag{5}$$

where

$$\mu_{eff} = \frac{qd}{(2\pi m^* kT)^{1/2}} \exp(-\frac{qV_{do}}{kT}) \exp(\frac{q\Delta V_d}{kT}) \tag{6}$$

In these expressions, μ_{eff} is the effective majority carrier mobility which reflects the optical modulation of the GB potential barrier. μ_{eff} depends exponentially on ΔV_d which in turn is controlled by the optical illumination. In other words, the photoconductivity in polycrystalline semiconductors can be a "majority" carrier effect due to optical mobility modulation which differs in principle from that of crystalline semiconductors.

The density and distribution of the GB trapping states strongly depend on the polycrystalline samples preparation, passivation and annealing processes. The typical experimental results of the GB trapping states observed in polysilicon are summarized in Table 1. As mentioned earlier, the Gaussian distribution is capable of representing different types of distributions when suitable conditions are imposed on it. With the approximation S_D, $S_A << kT$, the GB interface state distributions given by Eqns. (1) and (2) become confined to two discrete energy levels (or two δ-function distributions in energy). With the approximation $E_{tD} = E_v = 0$, $E_{tA} = E_c = E_g$ and S_A, $S_D > kT$, Eqns. (1) and (2) approach two exponential distributions in which the densities of acceptor-like and donor-like states decrease exponentially into the energy gap from the conduction band edge and the valence band edge, respectivelv. In fact, in this case the distribution becomes a U-shaped distribution.[12] For S_D, $S_A >> kT$, Eqns. (1) and (2) approach two uniform distributions.

Table 1

The various GB trapping states observed in polysilicons

GB TRAPPING STATES	SAMPLES	EXPERIMENTAL TECHNIQUES	REFERENCES
SINGLE DISCRETE LEVEL (δ-SHAPED)	CVD POLY-Si FILMS	RESISTIVITY, HALL MOBILITY	SETO (1975)[10] BACCARANI ET AL (1978)[8] LU ET AL (1980)[13]
EXPONENTIAL DISTRIBUTION	BICRYSTALS POLY-Si (NTD)	RESISTIVITY, I-V DECOVOLUTION, C-V RECOVERY MEASUREMENTS,	SEAGER ET AL (1979)[4]
U-SHAPED DISTRIBUTION (TWO EXP. DIST.)	CVD POLY-Si FILMS	PHOTOCONDUCTIVITY, ADMITTANCE MEASUREMENTS.	HIRAE ET AL (1980)[12]
UNIFORM DISTRIBUTION	POLY-Si	SCHOTTKY BARRIER I-V	CARD AND YANG (1977)[2] YANG ET AL (1981)[6] PIKE AND SEAGER (1979)[3]
GAUSSIAN DISTRIBUTION(S)	BICRYSTALS (P-TYPE) WACKER POLY-Si	DLTS, CONDUCTANCE SCANNING LASER SPOT (SLS).	CHENG ET AL (1981)[14] HWANG ET AL (1981)[15]

The following major conclusions can be drawn from the work reported herein. Photoelectronic processes at grain boundaries (GBs) in polycrystalline semiconductors have been studied theoretically and experimentally. A generalized Gaussian distribution of GB interface states has been proposed, which can be specialized by suitable conditions to express other distributions as well. The photoconductivity in polycrystalline silicon is observed to be strongly dependent on the optical illumination intensity, showing a pronounced increase with intensity which we believe to be correlated with a decrease in GB diffusion potential. It is concluded that the photoconductivity in polysilicon is the result of a "majority" carrier mobility modulation effect and hence differs in principle from photoconductivity mechanisms of crystalline semiconductors.

*This research was also supported by the Department of Energy under Contract DOE/SERI #xw-1-1272-1.

(1) L. L. Kazmerski (Ed.), Polycrystalline and Amorphou Thin Films and Devices. Academic Press, New York (1980).

(2) H. C. Card and E. S. Yang, IEEE Trans. ED-24, 397 (1977).

(3) G. E. Pike and C. H. Seager, J. Appl. Phys. 50, 3414 (1979).

(4) C. H. Seager, G. E. Pike and S. Ginley, Phys. Rev. Lett. 43, 532 (1979).

(5) W. Hwang, E. S. Yang, H. C. Card and C. M. Wu, Proc. 14th IEEE Photo. Spec. Conf., p. 404 (1980).

(6) E. S. Yang, E. Poon, C. M. Wu, W. Hwang and H. C. Card, IEEE Trans. ED-28, 1131 (1981).

(7) J. B. Milstein, Y. W. Tsuo, R. W. Hardy and T. Surek, Proc. 15th IEEE Photo. Spec. Conf., p. 1399 (1981).

(8) G. Baccarini, B. Ricco and G. Spadini, J. Appl. Phys. 49, 5565 (1978).

(9) H. C. Card and W. Hwang, IEEE Proc. I. Solid-St. Electron. Dev. 127, 161 (1980).

(10) J. Y. W. Seto, J. Appl. Phys. 46, 5247 (1975).

(11) G. J. Korsch and R. S. Muller, Solid-St. Electron 21, 1045 (1978).

(12) S. Hirae, M. Hirose and Y. Osaka, J. Appl. Phys. 51, 1043 (1980).

(13) N. C. C. Lu, L. Getzberg and J. D. Meindl, IEEE Electron Dev. Lett. EDL-1, 38 (1980).

(14) L. J. Cheng and C. M. Shyn, Proc. 4th Int. Symp. on Silicon Materials Science and Tech. (1981). (to be published)

(15) W. Hwang, P. Panayotatos, E. Poon and H. C. Card, Proc. 15th IEEE Photo. Spec. Conf., p. 871 (1981).

(16) K. C. Kao and W. Hwang, Electrical Transport in Solids. Pergamon Press, Oxford (1981).

B. LASER PROCESSED SCHOTTKY BARRIERS*

(C. M. Wu, E. S. Yang, T. O. Sedgwick,† R. T. Hodgson†)
(JSEP work units 16 and 17, 1979-82)
(Principal Investigator: E. S. Yang (212) 280-3120)

Recently, we have reported a thin-film structure using polycrystalline silicon as the energy absorbing layer to form an Al-nSi Schottky barrier.[1] In contrast with the p-n junction structure without the capped layer reported by Parks and Rose,[2] the required laser power in our experiment is substantially lower and our diodes have low turn-on voltage, indicating they are similar to a Schottky barrier rather than p-n junction. In our experiments, both a Nd-YAG pulse laser and a cw argon laser have been used. Because the argon laser scanning system is more flexible and the result is readily reproducible, we have used it to investigate the electrical behavior of diodes as a function of the laser power. This paper reports the results of our study.

Aluminum dots with a thickness of 2000 Å and an area of 1.13 mm^2 were deposited on (111)n/n^+ silicon wafers. The epitaxial layer's resistivity is 7 Ωcm ($N_d = 7 \times 10^{14}$ cm^{-3}) and its thickness is 15 μm. These dots were covered with an E-beam evaporated polysilicon film of approximately 100 Å thick. In the backside of the wafer, gold was evaporated to provide a good ohmic contact. Subsequently, the devices were subjected to laser irradiation. A cw argon laser (4880 and 5145 Å), operated at a power level between 12 and 22 W, is focused to a spot size of 50 μ. The spacing between adjacent scanning lines is 20 μm, so that complete coverage of the surface by the laser beam is ensured.

The substrate temperature was set at 350°C (the minimum temperature in the experimental setup), and the stepping motor movement (with a speed of 2 cm/sec) gives rise to overlapping spots of laser irradiation. The average power reaching the target is (6-10) x 10^5 W/cm^2 [(3.5) x 10^3 J/cm^2].

Laser-irradiated dots have the traces of the laser beam, showing that the surface has been melted and then solidified. The surface morphology was reported previously.[1] When the sample is laser irradiated with a power higher than 20 W, the evaporated silicon film shows ripping between the aluminum dots. In the areas with aluminum, less energy is absorbed and no significant damage is observed. The ripping of silicon film around the periphery of aluminum dots causes a large leakage current and unstable I-V characteristics. Therefore, we will only show the results of the dots prepared by power levels below 20 W.

The room-temperature current-voltage (I-V) curves of the dots processed with various laser powers are shown in Figs. 1 and 2. At high forward bias, the dots display different ideality factors which may be used to identify the various conduction mechanisms. The dots of 12 W has an I-V curve similar to diodes prepared by thermal annealing[3],[4] and the ideal factor is substantially less than two. The other diodes show higher saturation current and larger ideality factor. The reverse-biased current appears to be a generation current, and it increases as the irradiation power is raised. The kink in the reverse current of the 20-W diode is not understood, but it is likely to be caused by leakage paths through the diode periphery. From the generation current component, the lifetime of minority carrier in the 16-W diode is estimated to be 200 nsec which corresponds to a trapping-center density of 5×10^{14} cm^{-3}.

The temperature effect of the I-V characteristics is investigated between 200° and $300^{\circ}K$. The reverse saturation current J_0 is found by extrapolating the forward current at high bias (> 0.5 V) to the current axis. By plotting J_0 versus 1/T, we deduce the activation energy from the slope, and the result is shown in Fig. 3. The activation energy of the 12-W diode is 0.807 eV and its current is dominated by the thermionic emission across a barrier.

A value of activation energy equal to half of the forbidden gap is found on the 16-W diode, indicating the current is dominated by the space-charge layer

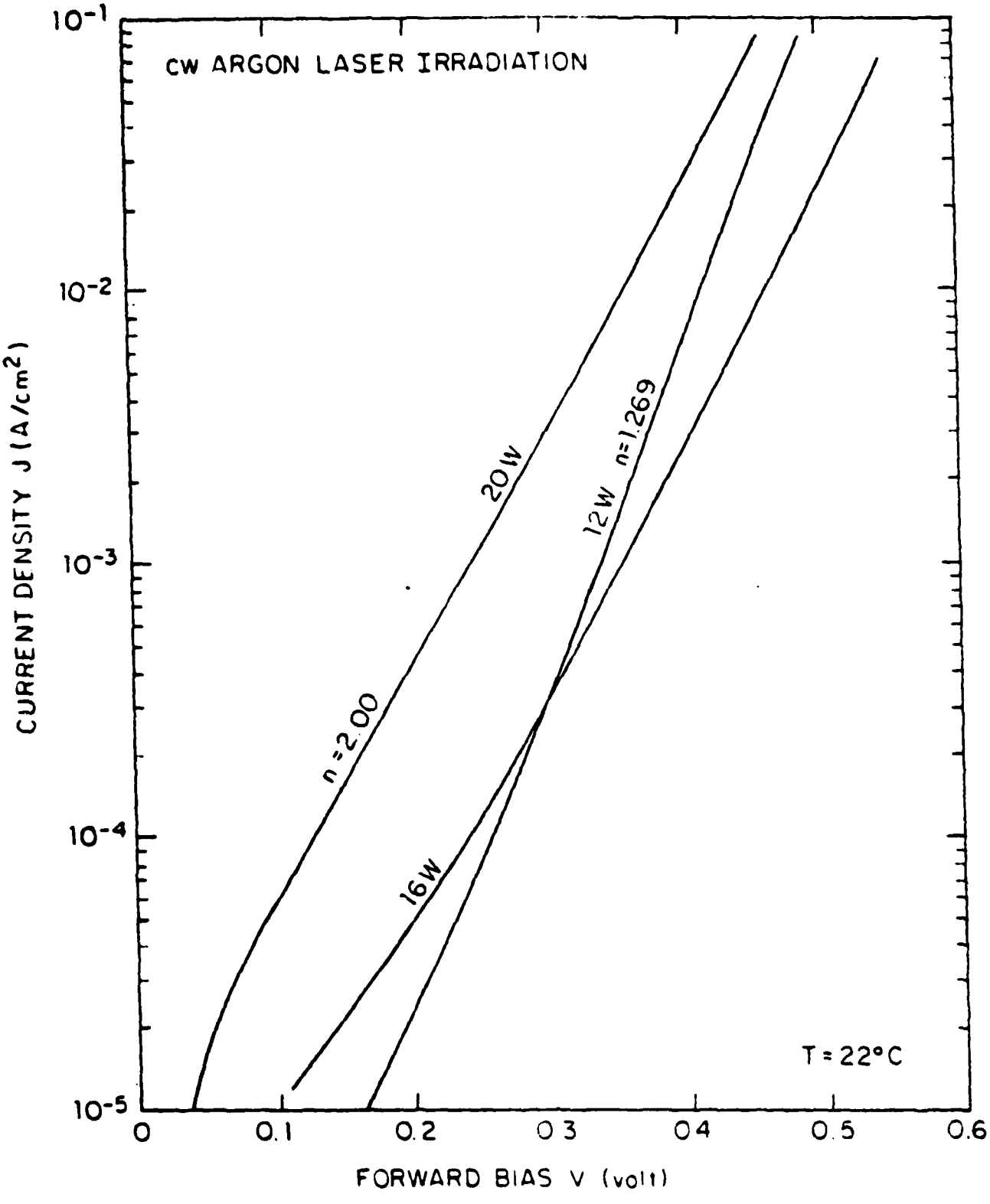

Figure 1. The forward I-V characteristics of the diodes irradiated by 12W, 16W, 20W.

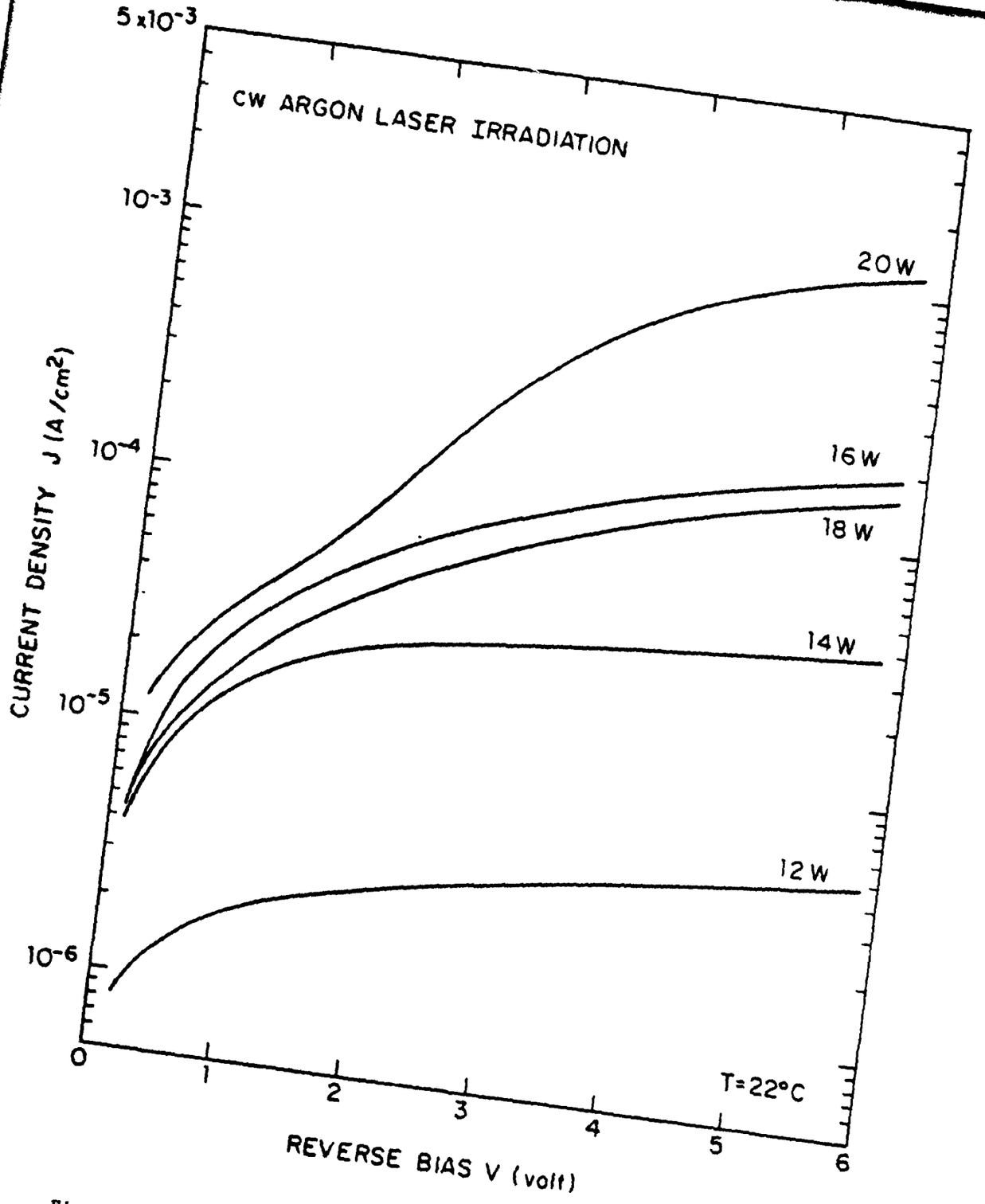

Figure 2. Reverse I-V characteristics of the diodes irradiated by 12, 16, and 20W.

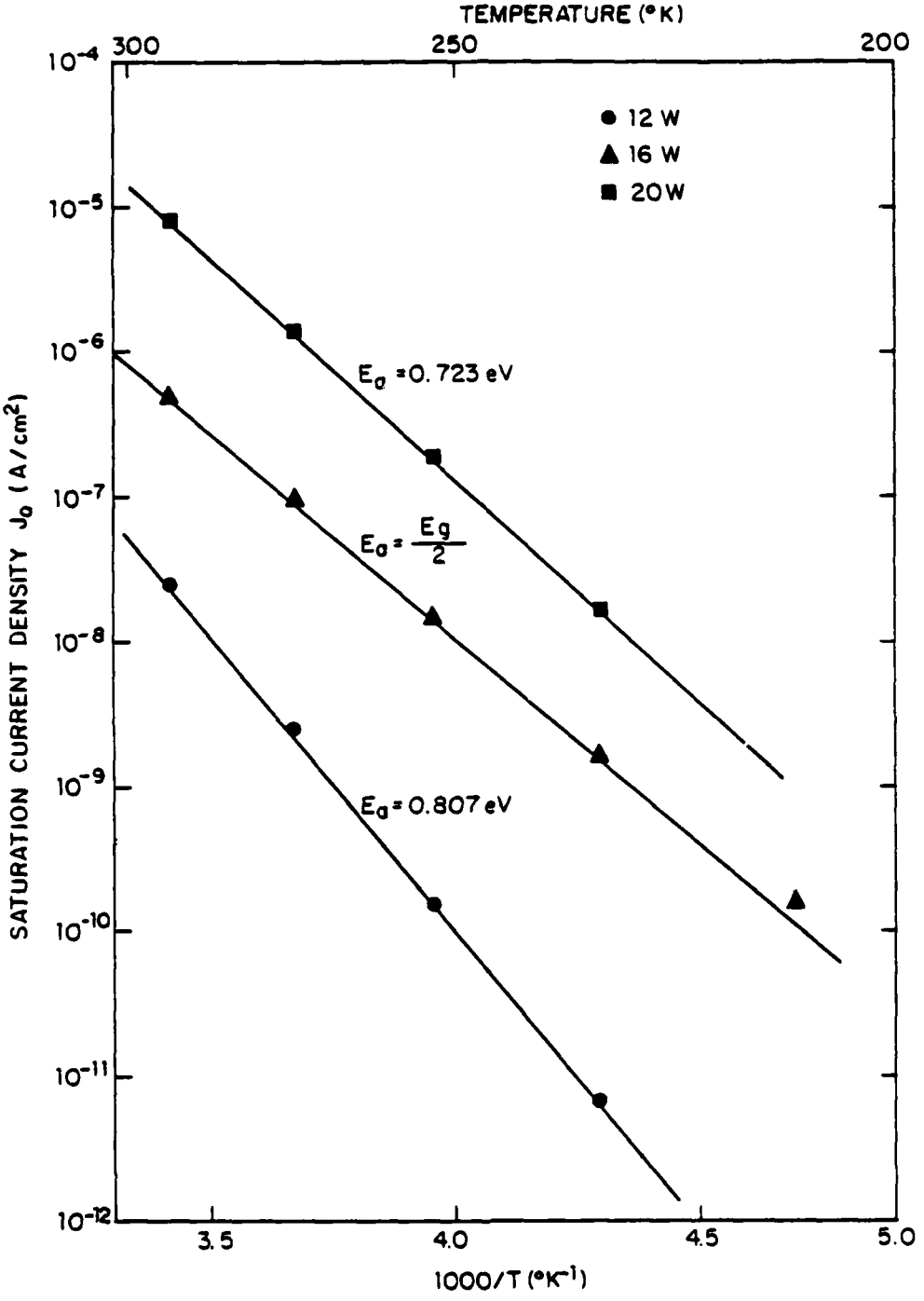

Figure 3. Saturation current density vs the inverse of the temperature. The diodes are separately irradiated by 12, 16, and 20W.

recombination process. The 16-W diode has a higher value of J_0 than that of the 12-W diode because its ideality factor is equal to two; however, the forward current of the former is lower than that of the latter at the high-bias regime. With over 16 W of laser irradiation, the diode current has an opposite tendency; i.e., the larger laser power causes a higher forward current because both recombination and thermionic emission are increased. A detailed discussion will be presented in the next section.

In the C-V measurements, we find that the plots of $1/C^2$ versus the bias voltage are all straight line except for the 20-W diode. From the C-V data, we obtain the value of the intersection voltage ϕ_{int}, the doping density N_d, and the Fermi potential V_n which are listed in Table I. These parameters for the 20-W diode are estimated by using the C-V data at the regime of small reverse bias (< 1 V). It is evident that the laser power of 12 W does not change the substrate doping density. In other words, the irradiation power is consumed in the process of melting the aluminum and the interface region. The contact barrier is formed by recrystallizing a p^+ layer between aluminum and the silicon substrate.[3] However, the measured substrate doping is changed when the laser power is higher than 14 W. The measured doping density is lower than the original doping when the laser power is between 12 and 16 W, and it increases when the laser power is higher than 16 W.

When the surface layer of silicon under the aluminum is irradiated and its temperature is near the melting point of silicon (1410°C), the aluminum atoms may easily diffuse into the silicon substrate. Because of a very short heating period (∿ 2.5 msec), the aluminum atoms will remain in a shallow region. At the temperature of 1400°C, the diffusivity of aluminum in silicon is 2×10^{-10} cm^2/sec. Thus the thickness of the aluminum doped silicon layer is approximately 70 Å. If a higher power or longer dwell time is applied, the substrate will stay at high temperature longer presumably allowing more aluminum

Table I

The deduced values from the C-V data at T = 295°K.

cw laser power (W)	12	14	16	18	20
N_d (10^{14} cm^{-3})	6.9	5.13	4.43	10.2	11.6
ϕ_{int}(V)	0.523	0.562	0.567	0.554	0.543
V_n(V)	0.270	0.277	0.281	0.261	0.257

diffusion. The aluminum-diffused layer forms a negative space-charge region which enhances the contact barrier of the aluminum on the n-type silicon substrate. The n-type Schottky diode with a shallow p layer between metal and semiconductor has been studied by Shannon[5] and Van der Ziel.[6] Recently, we have presented both theoretical and experimental works on the thermally-treated Al-nSi diodes.[3],[4] Assuming a uniform doping in both p- and n-type region, N_a and N_d, the capacitance per unit area is given by

$$1/c^2 = \frac{2}{q\varepsilon N_d} (\phi_{int} - V), \tag{1}$$

$$\phi_{int} = \phi_{Bn_0} - V_n - V_T + \frac{q(N_a + N_d)}{2\varepsilon} t^2, \tag{2}$$

where q is the electron charge, ε is the dielectric constant of silicon, V_n is the Fermi potential in the n side, t is the thickness of p^+ layer, V_T is the thermal voltage, and ϕ_{Bn_0} is the barrier height determined by the difference of the metal work function and the electron affinity of the semiconductor. ϕ_{Bn_0} was experimentally found to be 0.075 eV.[4] ϕ_{int} is the intersection voltage by extrapolating the $1/C^2$ curve to the voltage axis.

The barrier height at zero bias can be deduced by using

$$\phi_{Bn} \approx \phi_{int} + V_T + V_n = \phi_{Bn_0} + \frac{q(N_a + N_d)}{2\varepsilon} t^2 \quad . \tag{3}$$

Therefore the C-V data yield both the doping density and the barrier height at zero bias. From the value of the doping density, we obtain the Fermi potential at room temperature and then calculate the barrier height using Eq. (3). The result is shown in Fig. 4. It should be noted that Eq. (3) is valid only if N_a is much larger than N_d.[4] The barrier height of the diode after laser irradiation increases with the laser power. However, the barrier height reaches a maximum value of 0.87 eV when the laser power is 16 W ($\approx 4 \times 10^5$ J/cm^2) and it then decreases with increasing power. Examining Eq. (3), we find that the barrier height strongly depends on the doping of p^+-layer N_a and the thickness t. If the p^+ layer is mainly due to the precipitation of silicon from the Al-Si solution formed by the laser irradiation, the thickness t should increase monotonically with the irradiation. Thus the barrier height lowering when the power is beyond 16 W is due to the decrease of the impurity density N_a. Under a higher-power laser irradiation, the silicon surface region is possibly melted such that the final solidified silicon layer on the surface does not have the same quality as before. Apparently, the precipitated silicon contains donor-like imperfection centers[7] which compensate the effect of ionized aluminum atoms and causes the reduction of the barrier height.

From C-V data, it is found that the substrate doping N_d is first reduced because of the aluminum diffusion. Subsequently, N_d reaches a value higher than the original epitaxial doping density (7×10^{14} cm^{-3}). To get a clearer picutre, we consider these data together with the generation current of the diode under a reverse bias. The lifetime of minority carriers in the 16-W diode is estimated to be 200 nsec which corresponds to a trapping-center

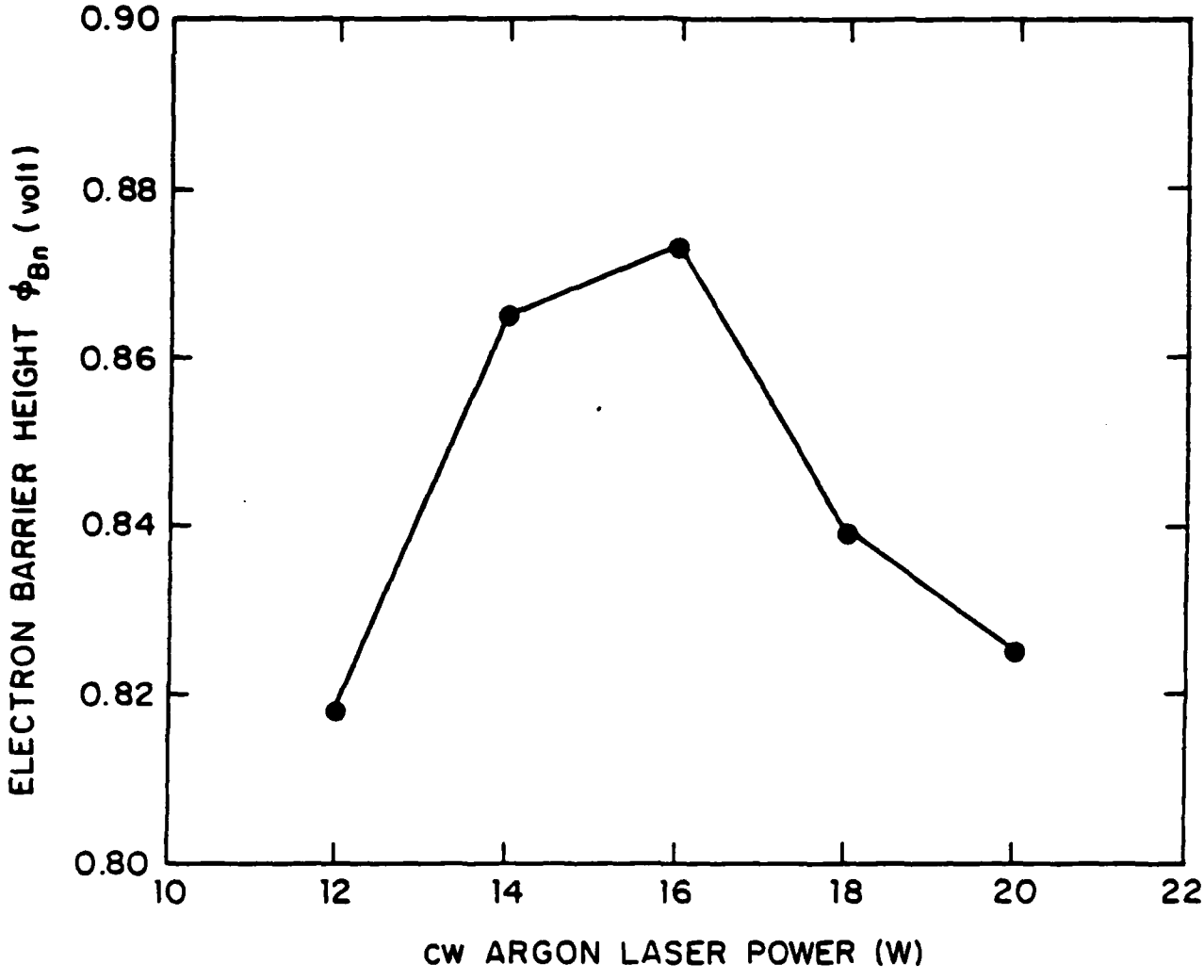

Figure 4. Barrier height vs the laser power after the diode is irradiated.

density of 5×10^{14} cm^{-3}, a value approaching the original doping density. When the laser irradiation power is increased, a large number of defects can be formed in the substrate to increase the generation current. Because the defects are donor-like,[7] the effective substrate doping density becomes higher than the original value. A thorough understanding of this phenomenon requires a detailed measurement of the traps which is being investigated.

Since the recombination current is a non-negligible term in the I-V characteristics, if the diode is irradiated by high power, the forward current is the sum of the thermionic emission and recombination currents. At room temperature or below, the ideality factor is equal to two and the recombination current dominates the forward current. But at higher temperatures the thermionic emission dominates such that the ideality factor decreases. This is consistent with the fact that the activation energy of the 20-W diode under forward bias has a value of 0.723 eV, which is between the barrier height and half of the forbidden gap.

†IBM T. J. Watson Research Center, Yorktown Heights, N. Y. 10598

*This research was also supported by the National Science Foundation under Grant NSF-ENG-78-19426.

(1) E. S. Yang, C. M. Wu, H. J. Vollmer, T. O. Sedgwick, and R. T. Hodgson, Appl. Phys. Lett. 37, 462 (1980).

(2) H. G. Parks and K. Rose, Laser and E-Beam Processing of Materials, edited by C. W. White and P. S. Peercy (Academic, New York, 1980), p.549.

(3) C. M. Wu and E. S. Yang, J. Appl. Phys. 51, 5889 (1980).

(4) C. M. Wu and E. S. Yang, J. Appl. Phys. 52(7), 4700 (1981).

(5) J. M. Shannon, Solid-State Electron. 19, 537 (1976).

(6) A. Van der Zeil, Solid-State Electron. 20, 269 (1977).

(7) J. L. Benton, C. J. Doherty, S. D. Ferrusm, L. C. Kimerling, H. J. Leamy, and G. K. Celler, Laser and E-Beam Processing of Materials, edited by C. W. White and P. S Peercy (Academic, New York, 1980), p. 430.

C. SCANNING LASER-SPOT PHOTOCONDUCTIVITY*

(P. Panayotatos, E. S. Yang, W. Hwang)
(JSEP work units 16 and 17, 1979-82)
(Principal Investigator: E. S. Yang (212) 280-3120)

In this work a scanning laser spot technique[1]-[3] has been used for the extraction of information about the grain boundary (GB) recombination kinetics. From the experimental measurements, the value of the GB recombination velocity can be determined using practically no assumption of parameter values. At the same time, the laser spot provides the illumination level to which the GB is subjected and modifies both the electrostatics and the kinetics there. The intensity of the laser was therefore varied, spanning more than two orders of magnitude, so that a quantitative relationship between illumination and recombination velocity could be extracted. Also described is a method based on the transition from low-to high-level injection of minority carriers for the estimation of the quasi-Fermi level separation corresponding to each illumination level, again without assumption of numerical values for any parameters other than the minority carrier diffusion coefficient.

The scanning light spot technique is a powerful experimental method for the extraction of information about the electrostatics and the recombination kinetics at the GB. A derivation of the correlation between the macroscopic parameters and the fundamental properties of the GB is given in Ref. (3). Briefly, under the assumption stated above, i.e. the length of the two depletion regions is much smaller than the grain size and for low-level injection and for a voltage drop $V < kT/q$ at the GB, the thermionic emission equation

$$J = A^{*}T^{2} \exp\left(-\frac{E_f + qV_D}{kT}\right)\frac{V}{kT} \qquad (1)$$

is used[3] to correlate the measured photovoltage with the intrinsic parameters. The modified form for the photoconductance is given by

$$\Delta G = bg_L \frac{L_n}{2D_n} \left(\frac{1}{1 + S_n \frac{L_n}{2D_n}} \right) e^{-x/L_n} \qquad (2)$$

where x is the distance of the light spot from the GB. b depends on several experimental parameters as well as on the dark GB diffusion potential but its value does not enter into our numerical calculation. Equation (2) predicts a linear log ΔG vs x relationship for as long as S_n remains constant. Furthermore L_n and D_n always appear as a ratio which will remain constant even if L_n changes as condition change from low- to high-level injection of minority carriers.

The samples of Wacker polycrystalline silicon were cut into 2 mm x 10 mm slabs and chemically etched to a mirror-like surface. Au ohmic contacts were then vacuum deposited at the ends of the (p-type) semiconductor slab, and the sample was mounted on an x-y translation stage (see insert, Fig. 1). The experimental set-up consisted mainly of a 5 mW He-Ne laser whose beam was chopped and then focused on sample to a 10 μm dia. spot. By using a lock-in amplifier and a reference signal from the copper, a signal proportional to the change of the sample conductance was measured and plotted vs position of the laser spot on the sample. A tungsten lamp was used for visual observation of the grain boundaries under consideration, as well as for focusing the laser spot. The schematic for the experimental set-up is shown in the insert of Fig. 1.[4]

Scanning of the sample with the laser spot produced conductance vs position curves typically as those of Fig. 1, where it was verified by visual observation that the peaks (largest increases in conductance) coincided with the points where the laser spot fell exactly on a grain boundary. Not all grain boundaries gave rise to such peaks, in agreement with earlier observations.[3] The magnitude of the largest peak also varied markedly from sample to sample.

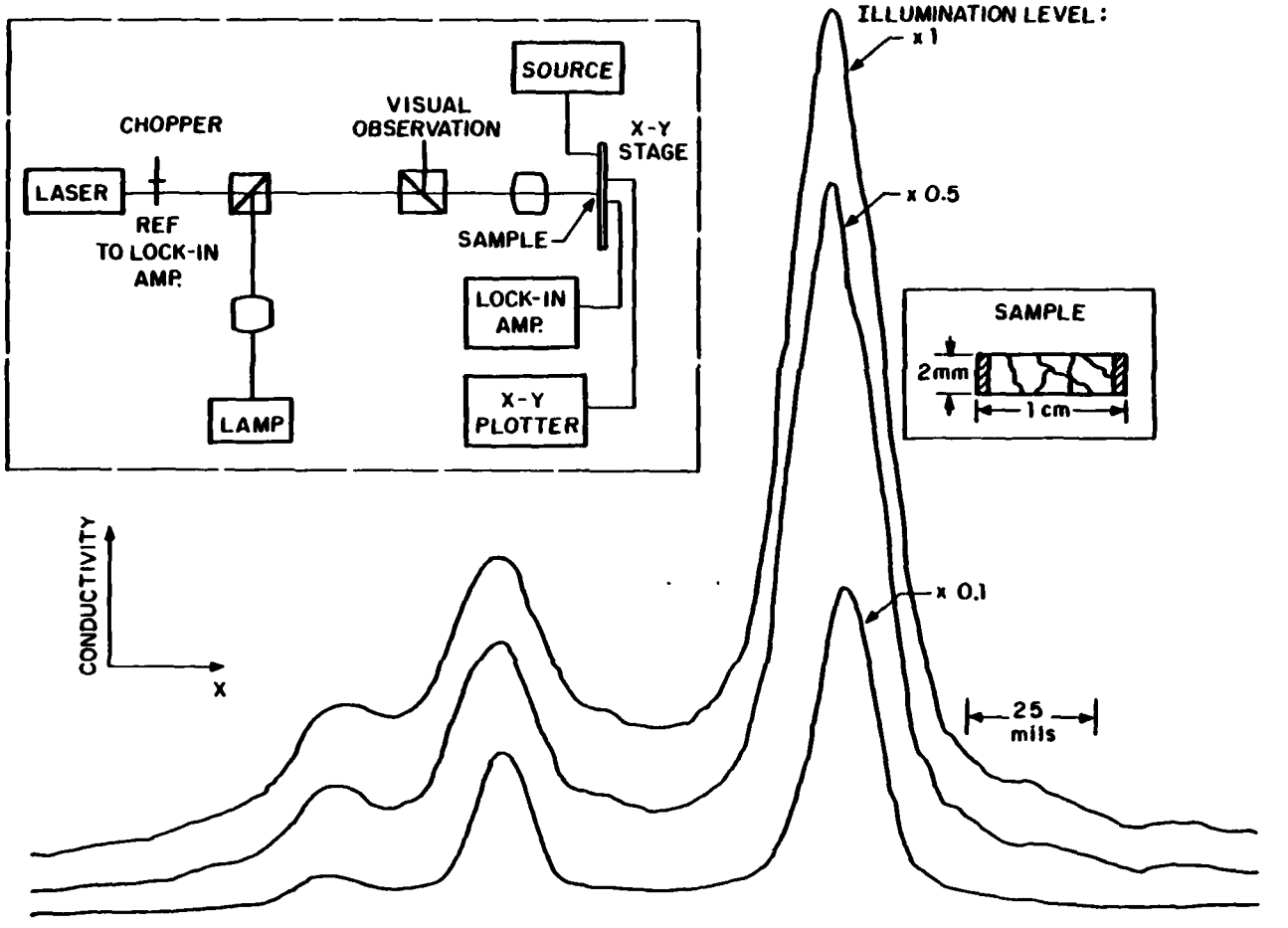

Figure 1. Plot of the illumination induced change in the conductance versus position of the laser spot on a Wacker polycrystalline Si sample in an extended scan. Peaks correspond to the laser spot crossing electrically active grain boundaries. Inserts show sample dimensions (shaded areas are Au ohmic contacts) and the experiment set-up.

The grain boundary that produced the largest such change in sample conductance was thus singled out.

The change of sample conductance vs position of the laser spot in the neighborhood of the grain boundary was recorded for ten different illumination levels chosen by the introduction of filters in the path of the laser beam, the highest level corresponding to 0.12 mW of light energy falling on the sample. More than two orders of magnitude in illumination level were thus covered and plots such as those of Fig. 2 were obtained. Care was taken to keep any effect of the DC biasing voltage across the grain boundary negligible so that any possible symmetry in the grain boundary electrostatics was not disturbed and that the assumptions necessary for the derivation of Eqn. (2) are correct.[3] The ratio of the dark sample resistance to a series resistance was such that the voltage across the whole sample was of the order of kT/q. That this was indeed the case and that the grain boundary under consideration did not present any assymetry was verified by comparing the plots of laser spot scans for both polarities of the DC bias. Curves A' in Fig. 2 represents such a response.

It is immediately apparent that there is a suppression of the change of conductance when the laser spot is very close or exactly on the grain boundary. This suppression is more pronounced for higher illumination levels (see curves A, B, C and compare to curve D in Fig. 2. It is assumed that this suppression is due to the radical increase of the grain boundary recombination velocity S_n that takes place when the laser spot is within one diffusion length away from the grain boundary. The above allows the effect of the grain boundary to be separated from any bulk effects. Wacker material is especially suited for such measurements. The diffusion lengths in Wacker are about one order of magnitude larger than the diameter of the laser spot and the grains are of the order of mm so that they in turn are much larger than the diffusion length, allowing

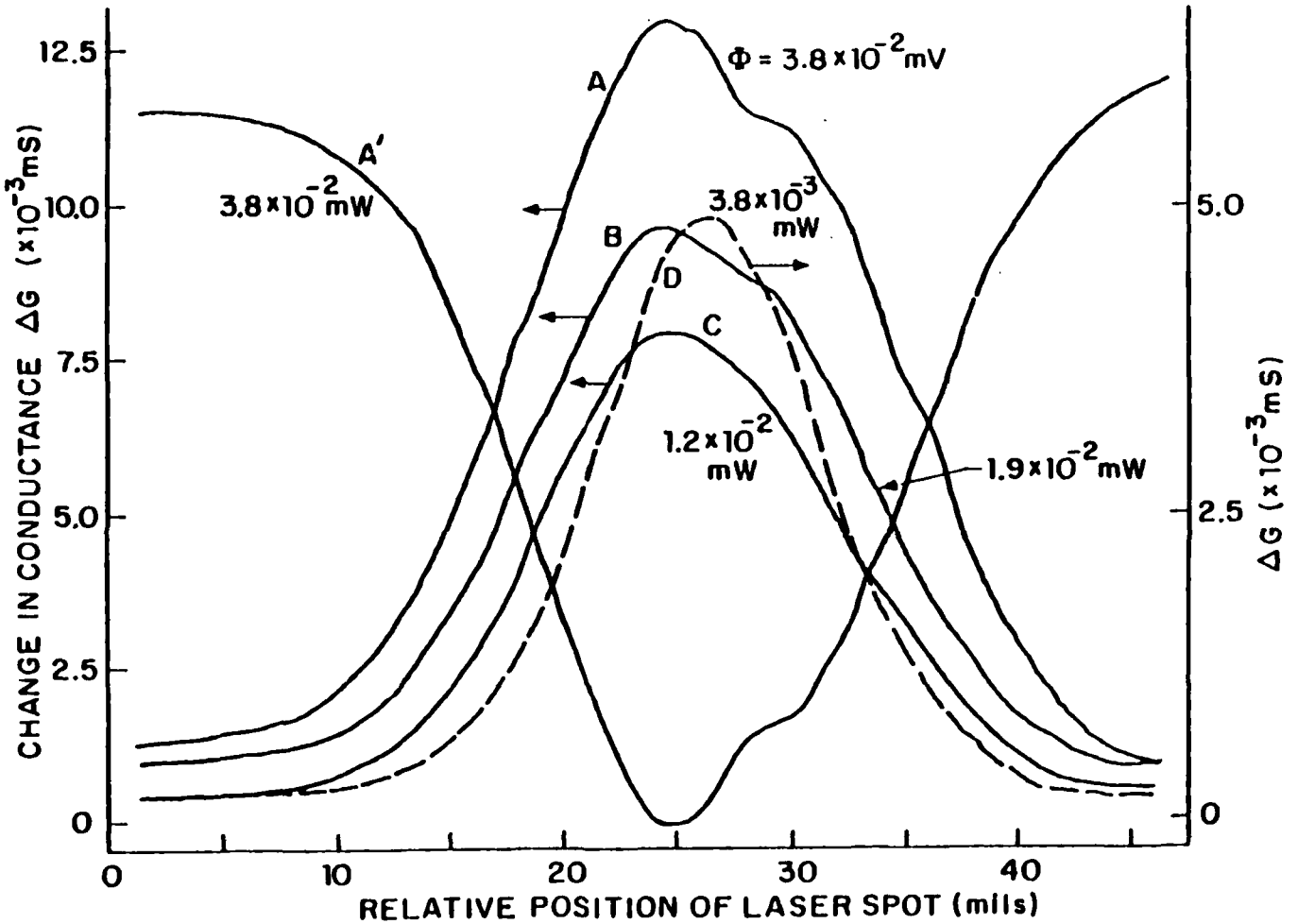

Figure 2. Laser spot scan in the neighborhood of the grain boundary for four different illumination levels. Note the suppression of the peak at higher illumination levels. Curve A' represents a scan identical to that of curve A except with the polarity of the external DC bias reversed.

rather extended scans around a particular grain boundary, with no interference from other grain boundaries. The suppression will not be apparent for materials where the diffusion lengths are comparable to the laser spot diameter[3] as was verified by unfocusing the laser beam and scanning the same area of the sample; much smoother curves were then observed.

We can, therefore, recognise two areas in the response: one with the laser spot very close or on the grain boundary, where grain boundary effects predominate and where there is a significant grain boundary recombination velocity, and another with the spot further away from the grain boundary where bulk effects are dominant and the effect of the recombination velocity is negligible so that the response should follow Eqn. (2) with S = 0, or

$$\Delta G = b \frac{L_n}{2D_n} \exp(-x/L_n). \qquad (3)$$

Indeed, for the latter region, a linear log ΔG vs x plot was obtained (see Fig. 3) from the slope of which the diffusion length L_n can be determined. The deviation from linearity for the values of x near the grain boundary indicates a nonconstant recombination velocity S which suppresses the photoconductance as represented by Eqn. (2). As the laser spot moves closer to the grain boundary, photogenerated carriers modify the carrier concentration at the grain boundary and therefore also the recombination velocity there.

The value of S can be determined from the plots of Fig. 3 in the following way: Extrapolating the lineary regions (bulk effect dominated part of the plot) to x = 0, which corresponds to the laser spot exactly on the grain boundary, determines what the value of ΔG would be if there were no interface recombination. In other words we measure $\Delta G^1(0) = bL_n/2D_n$. For $S \neq 0$, on the other hand, from Eqn. (6) we obtain that

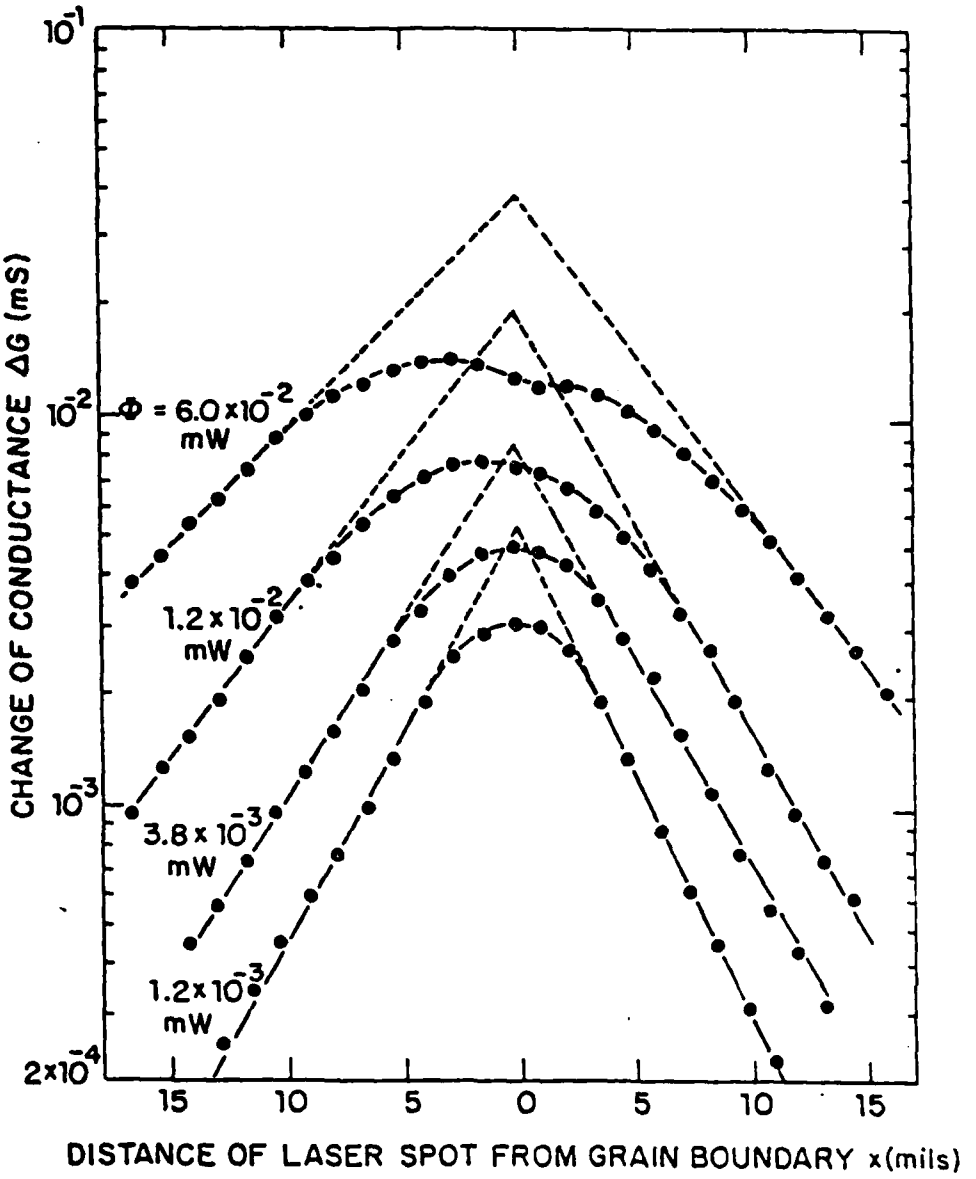

Figure 3. Plot of the logarithm of the photoconductance versus position of the laser spot for different illumination levels for a typical sample. Data have been taken from plots such as those of Figure 3. More than two orders of magnitude in illumination were covered. Not all illumination levels are shown here.

$$\Delta G(0) = b \frac{L_n}{2D_n} \frac{1}{1 + SL_n/2D_n}$$

so that the ratio of the observed value of the change in conductance ($\Delta G(0)$) to the value obtained by the extrapolation ($\Delta G''(0)$) has the value:

$$\frac{\Delta G(0)}{\Delta G''(0)} = \frac{1}{1 + SL_n/2D_n} \tag{4}$$

Equation (4) can therefore be used for the experimental determination of S independently of such parameters as Richardson's constant, interface state densities and distributions or values of illumination intensities. The recombination velocity can be thus directly plotted as a function of illumination. However, since the values of the diffusion lengths suggest a transition from low- to high-level minority carrier injection, an estimate can be made of the quasi-Fermi level separation ΔE_f. Thus S can be presented as a function of E_f as well as of illumination. In Fig. 4 we present the electron diffusion length L_n (obtained from the slopes of the linear segments of Fig. 3 as above) as a function of illumination. It is apparent that there is a transition from low- to high-level injection of minority carriers corresponding to the 1.2×10^{14} photons/sec level. The low level injection value of L_n is slightly larger than expected[5] rising to about twice its value at high illumination. Given that the minority carrier concentration n at this illumination level is about equal to the doping concentration ($N_A = 2.5 \times 10^{15}$ cm^{-3}) and electron concentration, the quasi-Fermi level separation ΔE_f can be calculated. S is presented as a function of ΔE_f as well as illumination in Fig. 5. S is shown to increase monotonically with illumination (or quasi-Fermi level separation) and is also shown not to saturate, even for the very large ΔE_f produced by the high illumination levels used.

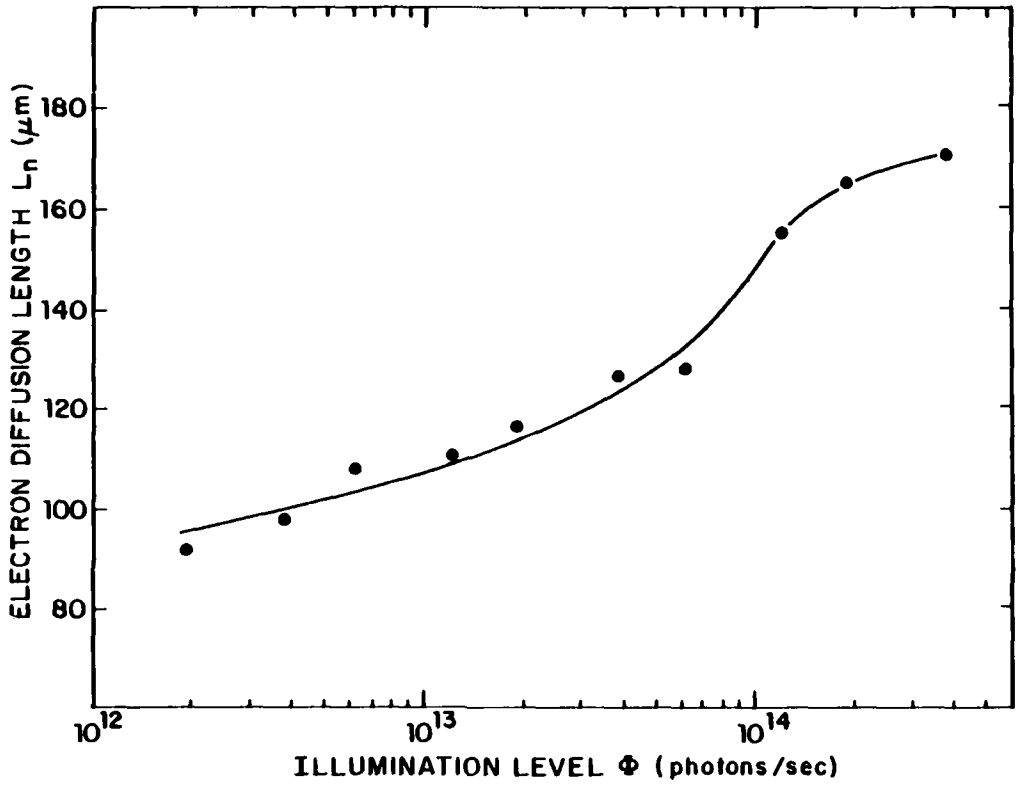

Figure 4. Plot of the electron diffusion length vs illumination level. L_n values are deduced from the slopes of the lines like those of Fig. 3.

Using the photoconductivity scanning technique, we have been able to measure the minority-carrier diffusion length within the grain and the recombination velocity at the grain boundary. The diffusion length is obtained from the slope of the semilog plot of the photoconductivity signal vs distance from the grain boundary. Extrapolation of the semilog plots allows us to determine the influence of the GB recombination, thus enables us to calculate the GB recombination velocity. This method is attractive in that it does not have to make a priori assumptions, is simple and self-contained. The numerical values we obtained are more than a factor of ten greater than Scholl's results[4] and an order of magnitude smaller than Seager's estimation.[6] An important consideration in our method is the spot size of the laser beam which should be small compared with the diffusion length. The diffusion length, in turn, should be much smaller than the grain size. It was found that the GB recombination velocity increases monotonically with illumination and does not saturate even at high intensity.

*This research was also supported by the Department of Energy under Contract SERI/DOE xw-1-1272-1.

(1) D. L. Lile and N. M. Davis, Solid-St. Electron. 18, 699 (1975).

(2) J. D. Zook, Appl. Phys. Lett. 37, 223 (1980).

(3) J. Martiner, A. Criado, and J. Pigueras, J. Appl. Phys. 52, 1301 (1981).

(4) F. W. Scholl, J. Appl. Phys. 52, 3439 (1981).

(5) W. A. Anderson and G. Rajeswaran, J. Appl. Phys. 52, 1597 (1981).

(6) C. H. Seager, J. Appl. Phys. 52, 3960 (1981).

D. COULOMBIC SCATTERING AT SEMICONDUCTOR GRAIN BOUNDARIES.*

(C. M. Wu, E. S. Yang)
(JSEP work units 16 and 17, 1979-82)
(Principal Investigator: E. S. Yang (212) 280-3120)

In the last few years, research activities have been extensive in polycrystalline semiconductors because of their importance in very large scale integrated structures as well as their potential in low cost photovoltaic applications. While the technology of polycrystalline materials is reasonably well established, the practical significance of grain boundaries as the dominating influence in the electronic properties of these semiconductors is recognized only recently. In general, a grain boundary GB has two different effects on the material. First, it has interfacial trapping states possibly resulting from mis-matched dangling bonds, impurity diffusion, and segregation, or defects. These states are minority-carrier sinks such that the overall minority-carrier lifetime and diffusion length are lowered. Second, a potential barrier, along with a depletion layer, is formed at the GB so that the majority-carrier current is impeded. The GB potential barrier reduces the mobility and increases the effective resistivity of the semiconductor. This is undesirable for most applications not only because of the higher resistance but also because of the difficulty in the reproducibility of the resistance value. This work addresses the second problem although the magnitude of the GB potential has obvious implications for minority-carrier recombination and transport.

A single energy-band diagram of the GB consisting of two back-to-back Schottky barriers is shown in Fig. 1. Most papers in the literature make use of this model in which the current is governed by the thermionic emission as expressed in the following form:[1]

$$J_{1\to 2} = A^* T^2 \exp[-q(\phi_B + V_n)/kT] \qquad (1)$$

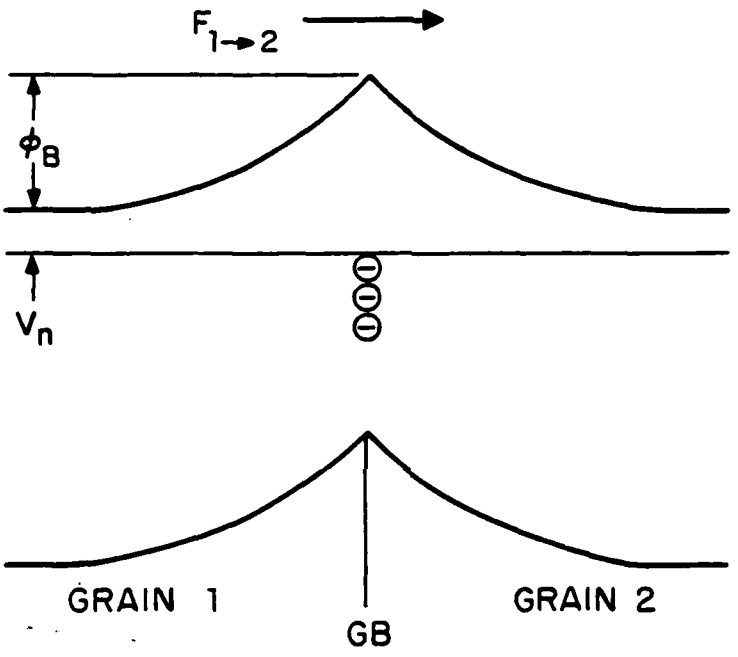

Figure 1. Band diagram of the grain boundary.

where A^* is Richardson's constant, ϕ_B is the barrier height measured from the conduction band, V_n is the Fermi potential, k is Boltzman's constant, q is the electronic charge, and T is the temperature in degree Kelvin. When the appropriate parameters are substituted in Eq. (1), however, the current is found to be significantly different from experimental data such that an attenuation factor is required in Eq. (1).[1] The current is reduced by this factor to provide more reasonable correlation. The experimentally determined value of the attenuation factor ranges from 0.06 to 0.2.[1]-[4] The large variation is probably due to the integrity of the GB interface as determined by the technology and processes. A model has been proposed by Lu et al.[5] to interpret this phenomenon by adding a scattering potential which gives better agreement between theory and experimental data. However, Lu et al. did not explain the origin of the scattering potential except that they did refer to the possiblity of phonon scattering.[6]

In this report, we show that a two-dimensional plane of fixed charge can contribute to significant scattering such that the majority-carrier transport is reduced. This Coulombic scattering is found to be much more important than phonon-assisted processes at room temperature.

The scattering of an electron in the Coulomb field of a charged center is described by using the Rutherford model. Let us assume that the GB surface is on the xy plane and the incident electron approaches the surface with a velocity ν and an angle θ. We can choose a system of coordinates such that the electron initially travels in the direction parallel to the xz plane as shown in Fig. 2. The initial velocity can be expressed as

$$\bar{\nu}_i = \nu(\sin\theta, 0, \cos\theta) \text{ in the xyz system.} \qquad (2)$$

For simplicity, an ionized charge is taken as located at the origin of the system. After scattering, the electron moves in a direction that depends upon not only the incident angle θ and the initial velocity but also on the distance of the incident path and the center of the ionized charge, b. The scattering angel θ is given by[7]

$$\cot\theta/2 = (4\pi\varepsilon m^*/q^2)\nu^2 b, \tag{3}$$

where ε is the semiconductor permittivity and m^* is the effective mass of electron. When we choose the x'y'z' system obtained by rotating the xyz system around the y axis, as shown in Fig. 2, such that the z' axis has the same direction as the initial velocity, the electron approaches the ionized charge and is headed toward the point (b $\cos\phi$, b $\sin\phi$, 0) on the x'y' plane. Thus, the position on the xy plane to which the electron points is (b $\cos\phi \sec\theta$, b $\sin\phi$, 0). If the collision is elastic, the final velocity is given by

$$\bar{\nu}_f = \nu(\sin\theta\cos\phi\cos\theta + \cos\theta\sin\theta, \sin\theta\sin\phi, \cos\theta\cos\theta - \sin\theta\cos\phi\sin\theta). \tag{4}$$

When the electron is scattered back from the xy plane, the z component of the final velocity must be less than zero. The cross section of the ionized charge can be deduced by the condition of $\nu_z < 0$. In other words,

$$\cot\theta < \cos\phi\tan\theta. \tag{5}$$

Substituting Eq. (3) into Eq. (5) and replacing $\cos\phi$ in terms of the variables in the xyz system, we obtain

$$(x^2 + y^2)^{1/2} < x\sin\theta + q^2/4\pi\varepsilon m^*\nu^2 \tag{6}$$

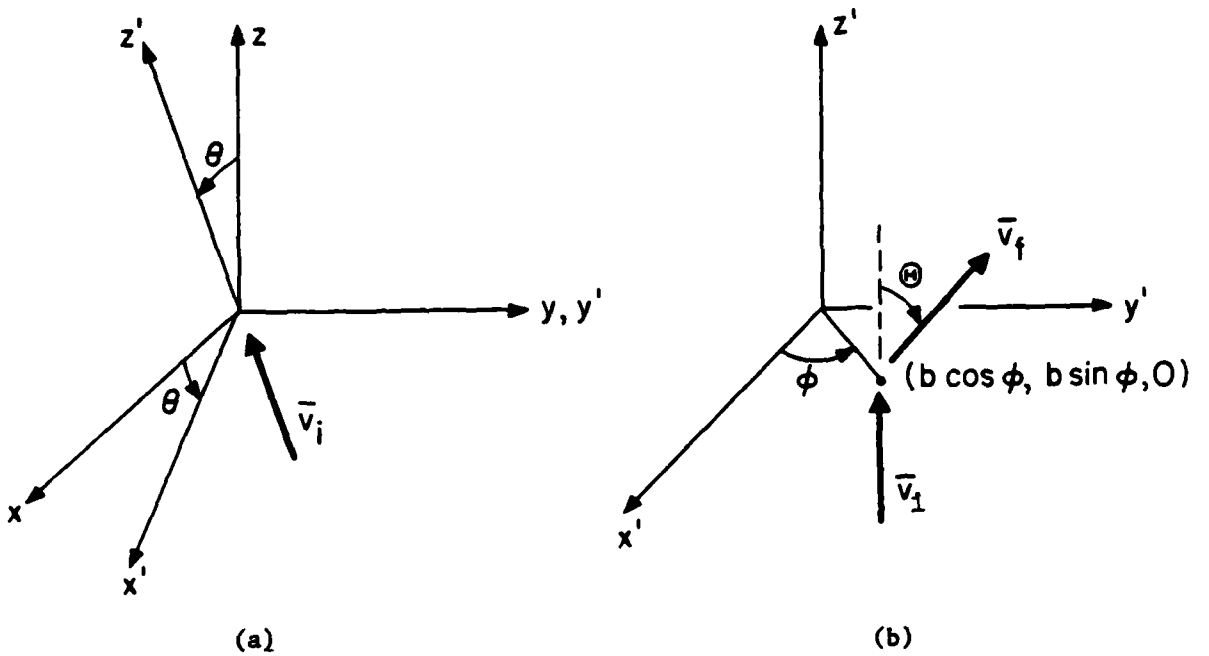

Figure 2. (a) x'y'z' system obtained by rotating the xyz system along the y axis such that the initial velocity is along the z' axis. (b) Schematic diagram of the relationship between the initial velocity and the final velocity due to the charge scattering.

Thus, the cross section is given by

$$\sigma(\theta,\nu) = \int_S dx\, dy, \tag{7}$$

where S is the area with a boundary determined by Eq. (6). After a two-dimension integration, the cross section is given by

$$\sigma(\theta,\nu) = (q^4/16\pi\varepsilon^2 m^{*2})\nu^{-4}\cos^{-3}\theta. \tag{8}$$

It is noticed that θ is the incident angle so that the cross section in Eq. (8) is different from the cross section in terms of the deflection angle θ in the calculation of the impurity scattering in the bulk single-crystal semiconductor.

Therefore, the transmission probability T of the electron across the grain boundary is a function of θ and ν. When the interface charge has a density of $N(cm^{-2})$, *T is given by*

$$\begin{aligned} T &= 0 && \text{if } \sigma_B \geq 1/N, \\ &= 1 - N\sigma_B && \sigma_B < 1/N. \end{aligned} \tag{9}$$

In obtaining the thermionic-emission current across the GB, it is necessary to consider this scattering effect due to the GB charge. By assuming that the GB surface is on the xy plane, the electron current from the first grain ($z < 0$) to the second grain ($z > 0$) is

$$\begin{aligned} J_{1\to 2} &= \frac{2q}{(2\pi)^3}\int\int\int dk^3 v_z \exp\left(-\frac{q(\phi_B + V_n)}{kT}\right) T(\theta,\nu), \\ &= \frac{2q}{(2\pi)^3}\frac{\pi}{m^*}\int dk\, k^3 \exp\left(-\frac{\pi^2 k^2}{2m^* kT}\right) \\ &\quad \times \int d\theta \sin\theta\cos\theta\; T(\theta,\nu), \end{aligned} \tag{10}$$

where $\hbar$ is $h/2\pi$ and h is the Planck's constant. The upper and lower bounds of the intergration are determined by $\sigma_B < 1/N$. When the electron trajectory is normal to the GB plane, i.e., $\theta = 0$, the cross section is

$$\sigma_B (\nu, \theta = 0) = (q^4/16\pi\epsilon^2 m^{*2})\nu^{-4}. \tag{11}$$

The transmission coefficient is zero when the electron energy is

$$E = 1/2\ m^*\nu^2 < q^2\sqrt{N}/8(\sqrt{\pi})\epsilon. \tag{12}$$

In other words, the electron cannot pass through the GB under the condition of Eq. (12). This situation is corresponding to a critical energy of $q\phi_{sc}$, that is defined as

$$\phi_{sc} = q\sqrt{N}/8(\sqrt{\pi})\epsilon \tag{13}$$

when the electron has a kinetic energy less than $q\phi_{sc}$, no thermionic emission can occur (i.e., we assume tunneling is negligible). On the GB surface, both positive and negative charges may cause the scattering of the approaching carrier. The maximum surface-state density of the silicon GB is 10^{15} cm^{-2} which is approximately equal to the number of surface atoms. Thus, the maximum scattering potential is 340 mV. The net GB interface charge density is likely to be in the order of 10^{12} cm^{-2}.

With the transmission coefficient given by (9), Eq. (10) may be simplified and we can obtain the thermionic emission current with a scattering factor η, which is given by

$$J_{1\to 2} = \eta A^* T^2 \exp[-q(\phi_B + V_n)/kT],$$

where

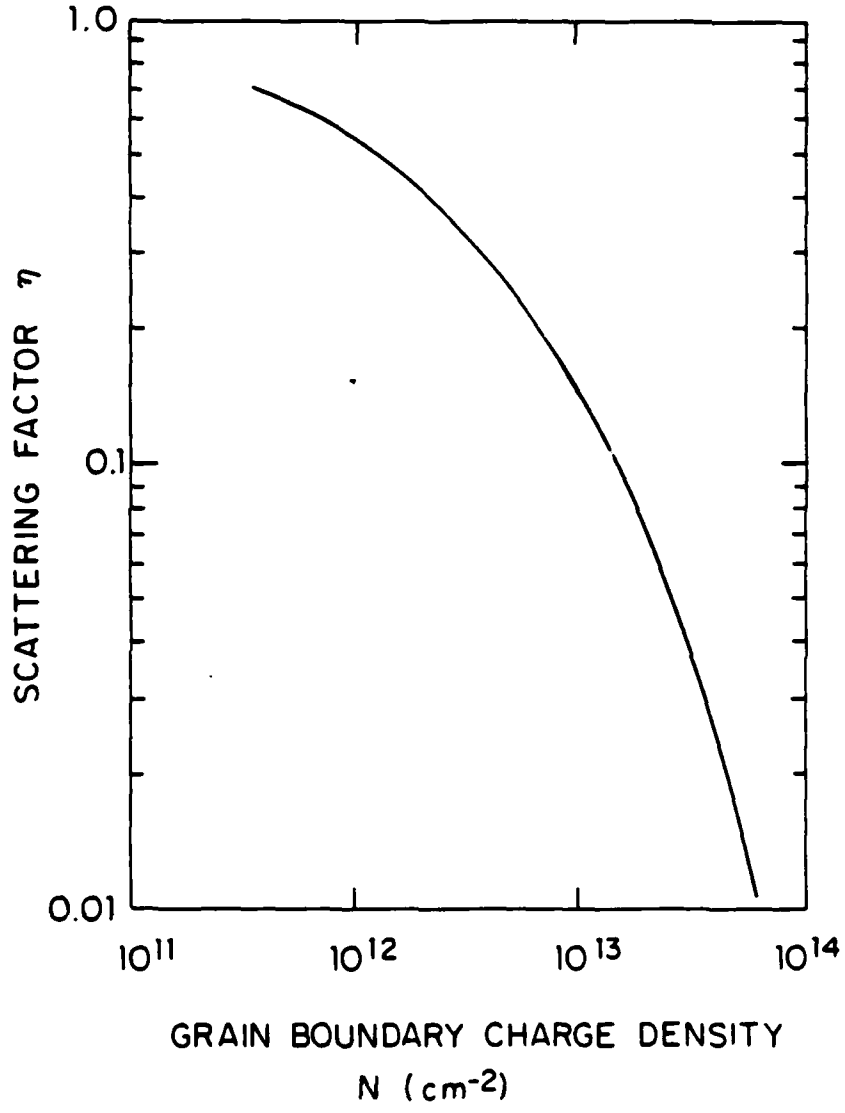

Figure 3. Scattering factor vs the interface charge density at 300°K.

$$\eta = \exp\left(-\frac{q\phi_{sc}}{kT}\right) \int_0^\infty ds \exp(-s)$$
$$\times \left[1-2\left(1+\frac{S}{q\phi_{sc}/kT}\right)^{-2} + \left(1+\frac{S}{q\phi_{sc}/kT}\right)^{-4}\right]. \quad (14)$$

In Fig. 3, we show η versus the charge density N at 300°K. Note that the attenuation of the thermionic emission strongly depends on the charge density.

For the charge density between 10^{12} and 10^{13} cm^{-2}, scattering factor is between 0.5 and 0.1. These values are a factor of 2 larger than reported experimental values. It is conceivable that there are both positive and negative charges at the GB such that they compensate each other. Although the resulted net charge is smaller the scattering calculation must include both types of charges. For this reason the model presented in this letter is reasonable.

The large fixed charge is not surprising in that they must exist to establish a large potential barrier at the grain boundary. Experimentally the potential barrier has been determined by conductance and capacitance measurements,[8]-[10] and a barrier height of approximately 1/2 eV at a doping level of 10^{15} is consistent with the results reported here. As for the origin of the fixed interface charge, it is likely that they are introduced by the material processing and discontinuity at the GB. In particular, impurity atoms have a tendency to congregate at the GB since they diffuse much faster along the planes of defects. In addition oxygen precipitation has also been found to enhance the electrical activity of the GB,[11] another probable origin of charged centers.

*This work is also supported by DOE/SERI Contract xz-ϕ-9226.

(1) E. S. Yang, E. Poon, C. M. Wu, H. C. Card, and W. Hwang, IEEE IEDM Tech. Digest 209 (1980).

(2) J. Y. W. Seto. J. Appl. Phys. 46, 5247 (1975).

(3) M. M. Mandurah, K. C. Saraswat, and T. I. Kamins, J. Electrochem. Soc. 126, 1019 (1979).

(4) N. C. C. Lu, L. Gerzberg, and J. D. Meindl, IEEE Electron Dev. Lett. EDL-1, 38 (1980).

(5) N. C. C. Lu, L. Gerzberg, and C. Y. Lu, and J. D. Meindl, IEEE Electron Dev. Lett. EDL-2, 95 (1981).

(6) A. F. Mayadas and M. Shatzkes, Phys. Rev. B 1382 (1970).

(7) R. M. Eisberg, Fundamentals of Modern Physics (Wiley, New York, 1967).

(8) G. E. Pike and C. H. Seager, J. Appl. Phys. 50, 3414 (1979).

(9) C. H. Seager and G. E. Pike, Appl. Phys. Lett. 35, 709 (1979).

(10) J. Martinez, A. Criado, and J. Piqueras, J. Appl. Phys. 52, 1301 (1981).

(11) D. Redfield, 15th IEEE Photovoltaic Specialists Conf. Record 1981, p. 1179.

E. INTERFACE INTERACTION OF THE Al-nSi SYSTEM*

(C. M. Wu, E. S. Yang)
(JSEP work units 16 and 17, 1979-82)
(Principal Investigator: E. S. Yang (212) 280-3120)

We present a study of the electrical properties of Al-nSi diodes fabricated by thermal annealing in a furnace of 600°C with different heating periods and cooling rates. Since the annealing temperature is above the eutectic, a recrystallized layer is formed in the aluminum-silicon interface. This is in contrast with previous studies where a low-temperature (300-500°C) annealing is employed.[1]-[3] Because the ideality factor is far from unity, the I-V data cannot quantitatively indicate the effects of the recrystallized silicon layer. We consider theoretically the influence of a thin Al-doped silicon on the capacitance characteristics of the diode. Both I-V and C-V measurements are made. The C-V data are used to obtain the effective barrier height.

Aluminum dots with a thickness of 2000 Å are deposited on (111)n/n^+ silicon wafers that have an epitaxial layer with a resistivity of 0.4 Ω cm and a thickness $\omega = 15$ μm. These dots are covered with an e-beam-evaporated silicon film of approximately 300 Å thick. In the backside of the wafer, gold is evaporated to provide a good ohmic contact. The structure of the diode before heat treatment is shown in Fig. 1 Subsequently, the diodes are thermally annealed in a hydrogen environment of 600°C for 1 h. It is important to note that the cap silicon layer and hydrogen gas are employed to prevent the aluminum film from reacting with the environment during the heat treatment. To study the effect of cooling rate, we cool the samples either with a temperature rate 1°C/min (diodes TR1) or quenching by withdrawing the furnace away from the sample (diodes TRQ, the cooling rate is about 100°C/min). A control sample TRO is also

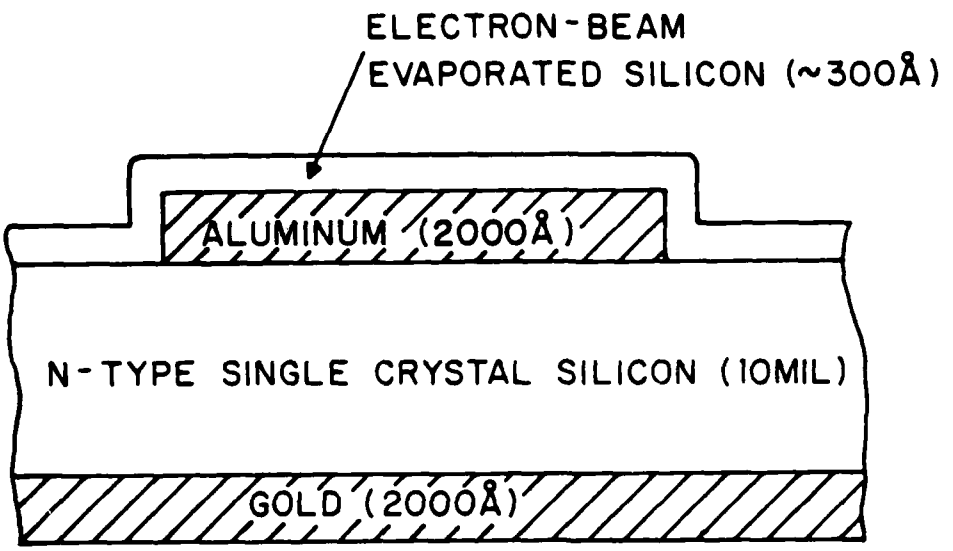

Figure 1. Structure of the Al-nSi diode before heat treatment.

prepared by annealing the specimen for 5 min at 300°C and then turning off the furnace. This cooling process takes 10 h for the specimen to reach room temperature.

Another series of diodes were made to test the dependence of the diode performance on the annealing time. T20, T40, and T60 are diodes prepared, respectively, by 20, 40, and 60 min of thermal annealing on the same structure as shown in Fig. 1 The substrate of these diodes are (100) oriented.

The metal-semiconductor junction with a heavily doped interfacial layer has been studed by Shannon[4] and van der Ziel.[5] The models they proposed are limited to a description of the I-V properties and show the dependence of the ideality factor and the barrier height on the thickness and the doping density of the interfacial layer. However, the measurement of the barrier height using the I-V curve requires the ideality factor to be unity. But the space-charge recombinations current gives rise to a 2-kT-current component. Therefore it is ambiguous to deduce the barrier height only from the I-V

data, since the recrystallized Al-nSi Schottky barriers are nonideal diodes. The space-charge capacitance is derived,[6] and it is used to determine the effective barrier height.

The I-V curves of the diodes T20, T40, T60 are shown in Fig. 2. We find that the diode characteristics do not change significantly with the different annealing times. In addition, the C-V curves yield the same barrier height. We conclude that the p^+ layer is not formed by the diffusion of aluminum into the silicon substrate, otherwise the thickness and doping density would have to be a strongly time-dependent process. Hence, the modulation of the barrier height is more likely to be caused by the recrystallized silicon layer doped with aluminum. In Ref. 7, we showed that the barrier height increases with the thickness of the evaporated aluminum, and it saturates at 0.93 eV when the aluminum layer is thicker than 1500 Å. The saturation is probably due to the limitation of the silicon diffusivity in aluminum, such that the silicon atoms dissolved deep in aluminum are locked in and unable to precipitate out. At the annealing temperature ($600^{\circ}C$), the maximum silicon molar fraction of Al-Si liquid solution is 13.2%.[8] Thus 270 Å of silicon may be dissolved in 1500 Å of aluminum. However, the dissolved silicon is not completely precipitated out of the aluminum after the cooling down, so that the final residue aluminum contains some portion of silicon atoms. The eutectic composition (11.3% of Si) is most likely a molar fraction in aluminum residue, such that only 40 Å of silicon is recrystallized.

Figures 3 and 4 separately show the I-V and C-V charactersitics of the diodes TRO, TR1, and TRQ. As mentioned previously, TRO is a control diode which is fabricated without the silicon recrystallization at the interface. The diode has a barrier height determined by the work function of aluminum and the electron affinity of silicon. The C-V data show that ϕ_{int} is equal to - 0.187 V, such that the barrier height is 0.075 eV. The low barrier

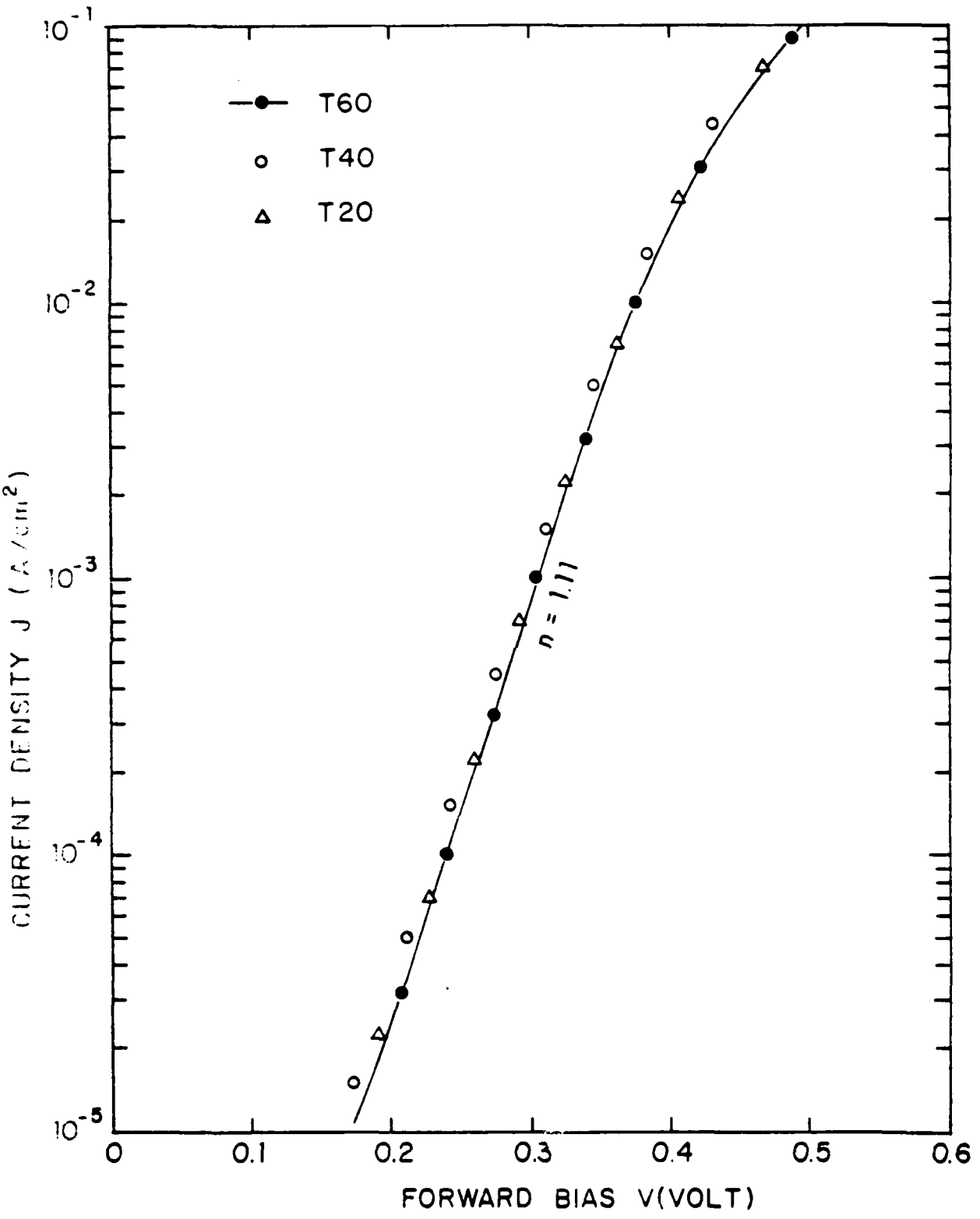

Figure 2. Forward I-V characteristics of T20, T40, and T60.

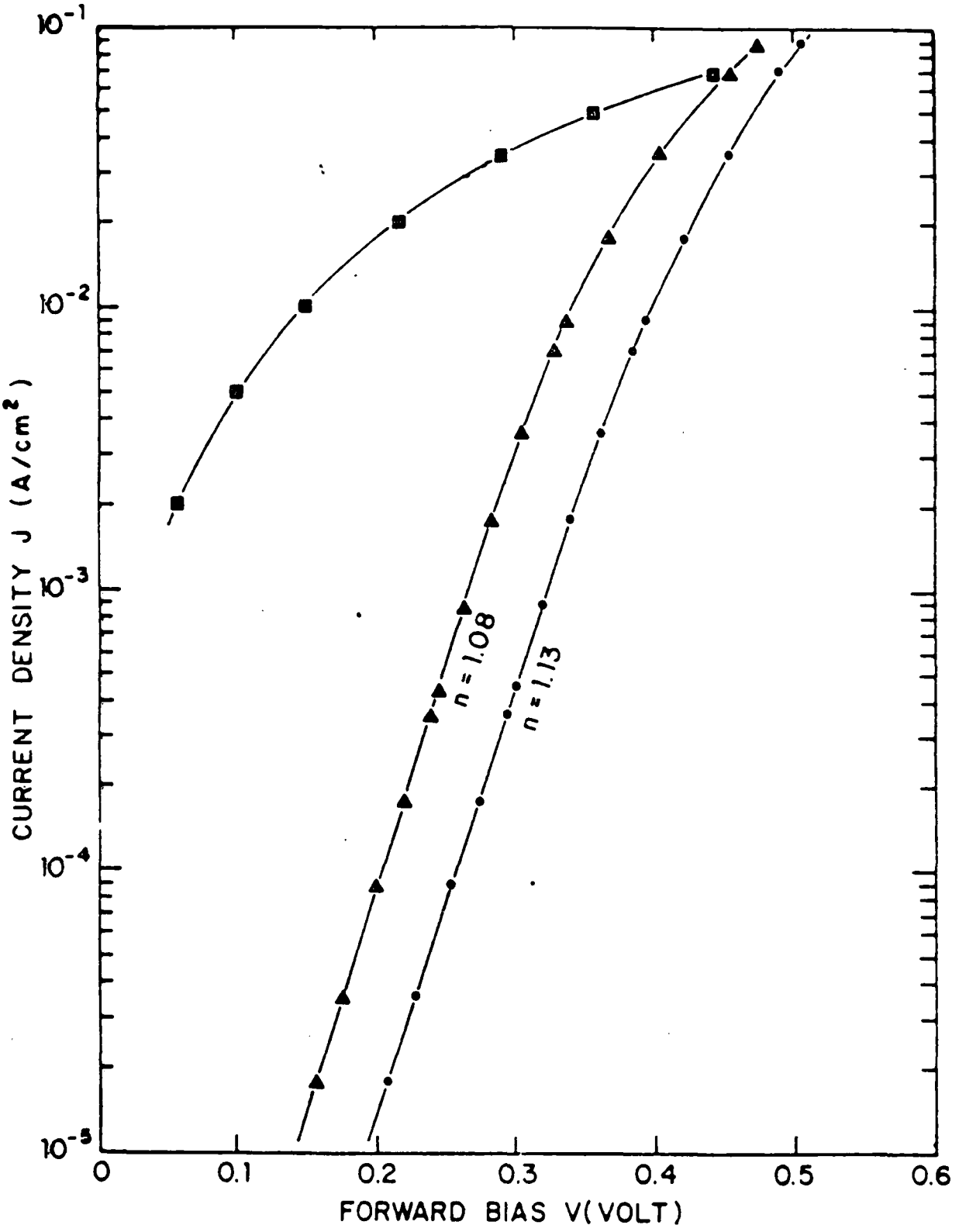

Figure 3. Forward I-V characteristics of TRO, TR1, and TRQ.

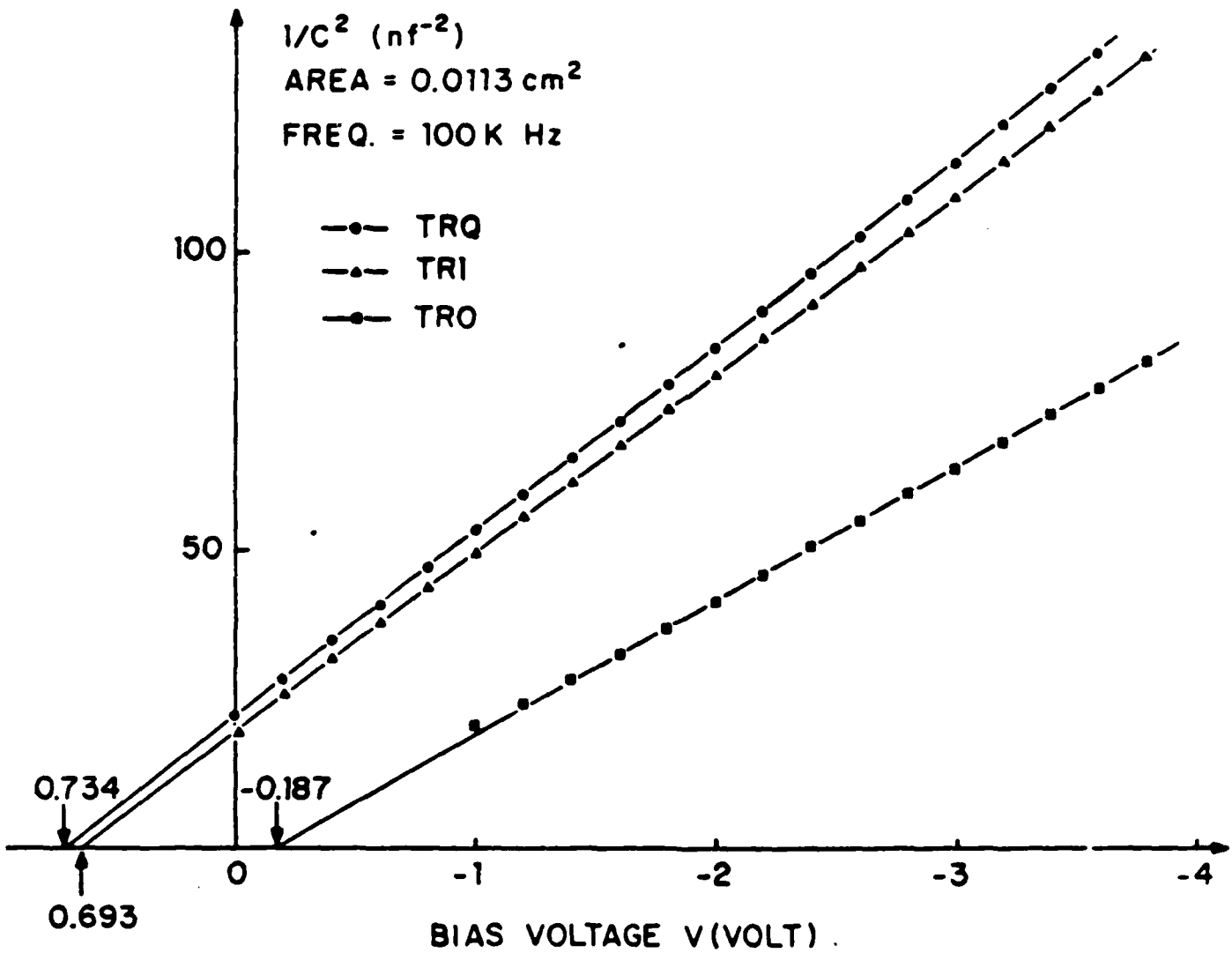

Figure 4. C-V characteristics of TRO, TR1, and TRQ.

height of the diode is correlated to the poor I-V characteristics (Fig. 3). We define the barrier height of TRO to the ϕ_{Bno}, which is assumed to be invariant in the aluminum-silicon contact. From the C-V data, we obtain the intersection voltage ϕ_{int} of TR1 and TRQ to be 0.693 and 0.734 eV. The barrier heights are calculated to be 0.96 and 0.99 eV, respectively. The difference is clearly caused by different cooling rates. The faster cooling gives rise to a higher intersection voltage. It is reasonable to say that more impurities stay in the recrystallized silicon in faster cooling. In this paper, we have qualitatively correlated the cooling rate and the doping density of the recrystallized p^+ layer which modulates the barrier height of Al-nSi diode. In fact, with postannealing at a low temperature ($\sim 300^{o}C$), the oversaturated aluminum in the recrystallized p^+ layer will precipitate out.[3] Although the diode prepared by quenching process has a large barrier height, the diode may not be stable if it operates in a temperature cycling environment.

The thermal annealing of the aluminum-silicon contact yields an Al-nSi diode with a p^+-silicon interfacial layer which increases the barrier height. Cooling from the temperature above the eutectic point ($600^{o}C$), the diode has a barrier height which does not vary with the annealing time, but changes with the cooling rate. To avoid the inaccuracy in determinating the barrier height from the I-V curve, we have used the C-V measurements, which clearly show the effect of the doping density and the thickness of the p^+ layer. It is concluded that the diffusion of aluminum into the silicon is not significant, and a fast cooling process causes a high aluminum concentration in the recrystallized silicon layer.

*This work is also supported by DOE/SERI Contract xz-ϕ-9226.

(1) T. M. Reith and J. D. Schick, Appl. Phys. Lett. 25, 524 (1974).

(2) G. Ottaviani, D. Sigurd, V. Marrello, J. W. Mayer, and J. O. McCaldin, J. Appl. Phys. 45, 1730 (1976).

(3) T. M. Reith, Appl. Phys. Lett. 28, 152 (1976).

(4) J. M. Shannon, Solid-State Electron. 19, 537 (1976).

(5) A. van der Ziel, Solid-State Electron. 20, 269 (1977).

(6) C. M. Wu and E. S. Yang, J. Appl. Phys. 52, 4703 (1982).

(7) C. M. Wu and E. S. Yang, J. Appl. Phys. 51, 5889 (1980).

(8) S. K. Ghandhi, The Theory and Practice of Microelectonics (Wiley, New York, 1968), p. 47.

F. LASER PHOTOCHEMISTRY FOR MICROELECTRONICS*

(R. M. Osgood)
(JSEP work unit 5, 1982-1985)
(Principal Investigator: R. M. Osgood (212) 280-4462)

Introduction

This report covers a new program which was initiated in September, 1981. The objective of the research is 1) to develop an understanding of laser-initiated interface reactions and 2) to apply the results of this research to problems in microelectronic fabrication. Recently it has been shown that laser chemistry at or near surfaces can form the basis of a new direct-write processing technology for microelectronics. In addition, an understanding of laser surface reactions may lead to the realization of photochemical catalysis reactions, for bulk chemical synthesis.

In the first year of this program, we have concentrated on treating theoretically light-induced surface reactions and on setting-up a laboratory which can analyze both the theoretical and applied aspects of laser surface chemistry.

Theoretical

While surface chemistry has been the subject of a vast amount of pure and applied research, there have been only limited studies of photochemistry at fluid-solid interfaces. A solid surface can be expected to modify the usual homogeneous photochemical reactions through changes in the photodissociation dynamics, shifts in the spectral features of adsorbed species, and formation of new chemical species.[1],[2] The surface can enter in a more subtle but equally important manner by modification of the local optical field at the interface. Depending on the surface morphology and its optical properties, the local electric field can be enhanced or diminished considerably with respect to its value in the gas alone.[2]

The enhancement results from the increase in the local optical field in the vicinity of microscopic metal features which exhibit plasma resonances for frequencies close to that of the incident electric field. Recently, related studies of this phenomena for Raman scattering,[3] linear scattering, and linear absorption[4] and luminescence[5] have been reported. For Raman scattering, an increase of 10^6 is seen in the spontaneous Raman cross-section of molecules adsorbed on metal surfaces.[3] Surface-enhanced Raman scattering (SERS) has been observed for photolithographically fabricated artificial surfaces.[6]

We have shown that this increase in the local field can also cause an enhancement by many orders of magnitude in the rate of an interface photochemical reaction. The effect is not only significant for species adsorbed directly on the surface, but it can also be an important factor for heterogeneous reactions which are initiated in the gas phase. The increase in local field is greatest for metal particles with the appropriate shape and material characteristics to exhibit a plasma resonance near the frequency of the optical source. This effect has many similarities with SERS; however, both the UV operating wavelength and the polarization typical of photochemical reactions give rise to different conditions in calculating the enhanced reaction rate. Under typical conditions, reaction enhancements of $\sim$100 are found for adsorbed layers undergoing single-photon photodissociation; multiple-photon reactions exhibit enhancements of $\sim 10^4$. The random size and shape which can be expected on real but artificially prepared surfaces do not significantly alter these ratios.

Surface enhancement of chemical reactions has been recently considered by Brus and Nitzan.[2] They point out that, although it is reasonable to expect an increase in the rate of reactions on surfaces due to the enhancement of the local optical field, radiationless transfer to the solid substrate may be expected to reduce the quantum yield of the bound-free event. However, the nature and degree

of energy transfer to the surface during a photodissociative event is currently not well understood either theoretically or experimentally.[7] Recent experiments[8] indicate, for example, that metal alkyls can be photodissociated readily on metal surfaces. To simplify our treatment of the influence of the local field enhancement, we have not included energy transfer from the adsorbed phase to the surface or the reverse process in our calculation. This simplification does not influence our calculation for the case of enhanced fields in the gas or in upper-multilayer-adsorbed species, where energy transfer is greatly reduced.

Experimental

The experimental facilities necessary for carrying out the work described above should consist of a modern optical laboratory including laser sources and optical spectroscopic techniques, and facilities for fabricating and testing microelectronic devices. During this year we have set up an optical laboratory with cw and pulsed laser sources at both visible and infrared wavelengths. These sources have been used for both direct-writing and pulsed laser experiments. In addition, a computer-controlled UV spectrometer has been equiped with an orgometallic gas handling system and temperature controlled cell. The apparatus permits observation of the UV adsorption spectrum of weakly bound surface films of adsorbed material.

Construction of a clean room for fabrication and testing of microelectronic devices has been started. This facility will be equipped with diffusion furnances, wet and dry clean benches, and other facilities for fabrication of small scale electronic devices.

We anticipate that the room will be completed by the first part of July.

*This research was also supported by the Army Research Office under Grant #DAAG29-82-K-0089 and Air Force Office of Scientific Research/DARPA under Grant F-49620-82-K-0008.

(1) T. F. George, J. Lin, K. Lam, and C. Chang, Opt. Eng. 19, 100 (1980).

(2) A. Nitzan adn L. E. Brus, J. Chem. Phys. 74, 537 (1981).

(3) R. P. van Duyne, Chemical and Biological Applications of Lasers, Vol. 4, Ch. 5; S. L. McCall and P. M. Platzman, and P. A. Wolff, Phys. Lett. 77A, 381 (1980).

(4) R. H. Doremus, J. Chem. Phys. 40, 2389 (1964), 42, 414 (1965). Or more recently R. K. Chang, private communication.

(5) A. M. Glass, P. F. Liao, J. G. Bergman, and D. H. Olsen, Opt. Lett. 5, 368 (1980).

(6) P. F. Liao, J. G. Bergman, D. S. Chemla, A. Wokaun, J. Melngailis, A. M. Hawryluk, N. P. Economou, Chem. Phys. Lett. 82, 355 (1981).

(7) See for example Ph. Avouris and J. Dehmuth, J. Chem. Phys. 75, 4783 (1981) and references cited therein.

(8) D. J. Ehrlich, R. M. Osgood, and T. F. Deutsch, IEEE J. Quantum Electron. QE-16, 1233 (1980).

G. A NEW CAPILLARY NOZZLE ION SOURCE: THE CAPILLARITRON*

(Toomas Allik, George Flynn)
(JSEP work unit 7, 1982-85)
(Principal Investigator: G. W. Flynn (212) 280-4162)

Within the past few years the use of ion beams in the field of microelectronics has become extremely important. Due to great interest in ion beam lithography, ion implantation and ion sputtering, immense technological advances have been achieved in the field of ion sources. For microelectronic devices and circuit processing, the key parameters in determining the supremacy of a given ion source are: brightness, emittance, beam divergence, ion current production, energy distribution and ionization efficiency.[1] While in most cases the construction of ion sources has been tailored to the semiconductor industry, these ion sources can be utilized in other disciplines. For example, ion-molecule reactions and ion spectroscopy are two fields of active research that have benefited tremendously from the discoveries of new ion sources. Our objective is to develop new and improved methods for the production of metastable molecular and atomic ion beams; to characterize the translational, vibrational, rotational and electronic energy distributions and relaxation rates of such beams, and to study the chemical reactions of these metastable ion species with both gases and surfaces.

Since the original reports of a new capillary nozzle ion source called the "Capillaritron",[2],[3] we have concentrated our efforts on characterizing the ion beam. The Capillaritron is a simple device consisting of a metal nozzle and an extractor electrode.[4] The nozzle is electrically isolated by a dielectric from the source gas chamber and is brought to voltage levels on the order of several kilovolts. The extractor electrode is kept at ground potential, and is placed in the plane of the nozzle tip or slightly in front of

(downstream) the nozzle. When gas is fed to the nozzle and a threshold voltage is applied, a plasma is formed at the nozzle tip, which is visible. The theory of operation can be found in References 2 and 3.

The Capillaritron was installed in a differentially pumped molecular beam apparatus so that backing pressures as high as five atmospheres could be applied behind the nozzle. Since the molecular beam contains an extranuclear quadrupole mass spectrometer, a home-made Faraday cup and time of flight chopper, the identity as well as the energy spread of the ions produced can be easily determined.

Various gases have been ionized such as Ar, Ne, Xe, He, O_2 and N_2. A comparison of the overall ionization efficiency of each gas shows that under equivalent conditions (backing pressure, orifice diameter, etc.), the number of ions produced scales inversely as the ionization potential. With regard to flow rates, the threshold for breakdown ionization in all cases decreased as the backing pressure was increased. In addition, as the orifice diameter was increased to as large as 500 microns, ion production increased. Since the supersonic nozzle was placed on a motorized translational stage the nozzle to extractor distance could be varied as much as one inch. When the distance was set to a maximum, the only effect noticed was that a few hundred volts more were required to reach threshold ionization. Mass spectral analysis for Ar produced a majority of the Ar^+ ion, but a significant abundance of the Ar^{+2} and Ar_2^+ species was present. Neon exhibits similar features as is shown in Figure 1. Energy analysis of the ion beam by two techniques: time-of-flight and floating the potentials on the quadrupole rods shows a large energy spread. These results are in good agreement with recent work of Goebel et al.[5] Presumably the large energy spread is due either to charge exchange with slow neutrals in the ion extraction region,[5] or non-uniform acceleration in the ionization

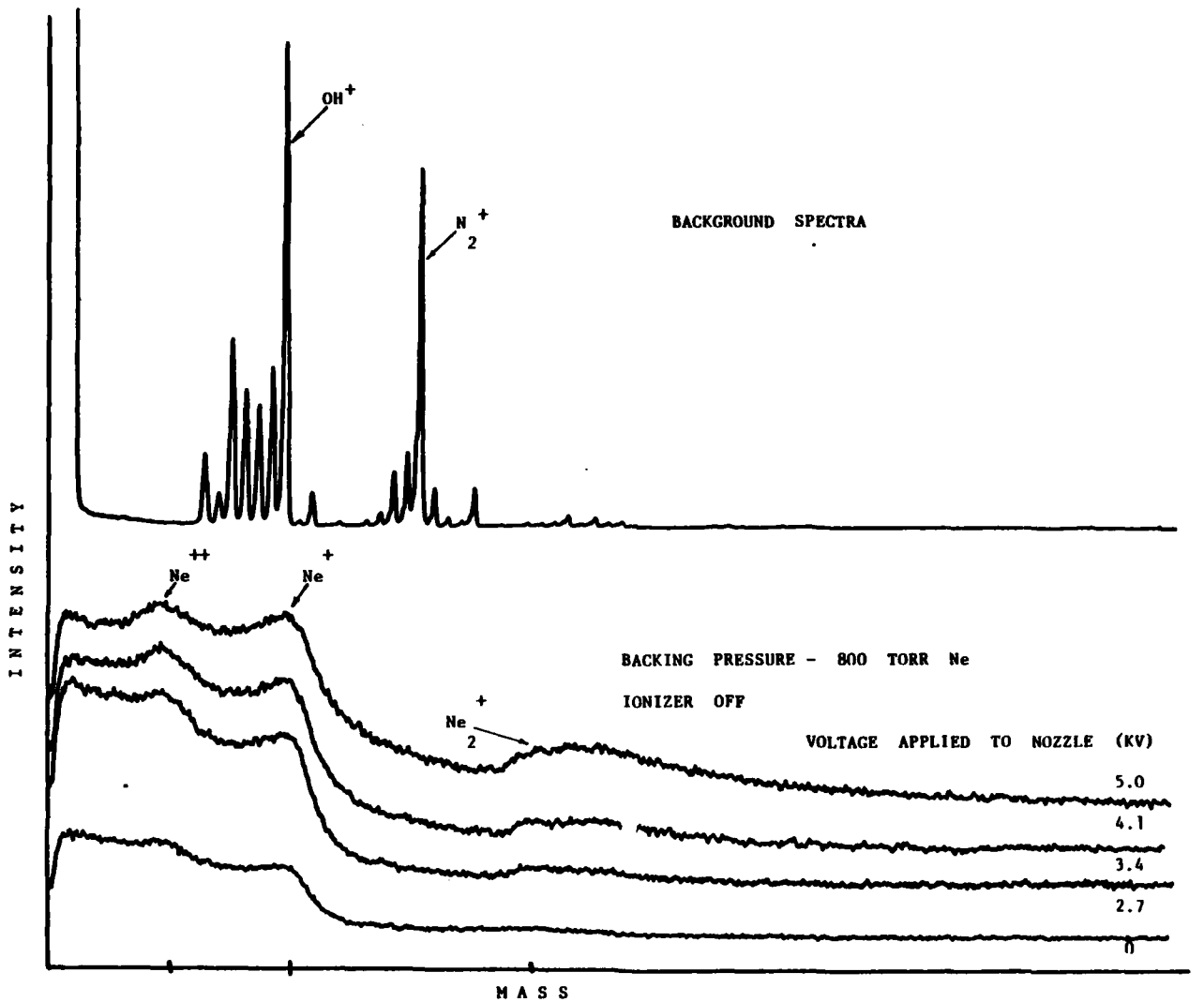
OH+
N2+
BACKGROUND SPECTRA
INTENSITY
++
Ne
+
Ne
BACKING PRESSURE - 800 TORR Ne
IONIZER OFF
Ne2+
VOLTAGE APPLIED TO NOZZLE (KV)
5.0
4.1
3.4
2.7
0
MASS

Figure 1

region. Change transfer collisions of the type:

$$Ar^{+}(fast) + Ar(thermal) \rightarrow Ar(fast) + Ar^{+}(thermal)$$

have been seen since the time-of-flight exhibits a <u>double</u> peak! (see Figure 2). Finally, the Capillaritron has the ability to produce <u>negative</u> ions. When a negative voltage is applied to the nozzle and O_2 is sent through the apparatus, a plasma is visible that is quite different in appearance from that observed with a positive voltage. In addition, no positive ions could be detected with the mass spectrometer. Minor modifications to the Channeltron will make it possibile for us to look at negative ions in the future.

In conclusion, the Capillaritron is a powerful ion source capable of producing large ion currents (> 1 mA) with small beam divergence (2-8 degrees).[5] The only drawback of this source is that it produces beams having a large energy spread. In the future we plan to use several novel techniques to produce reactive ion beams and to characterize the chemical and energy distribution of these beams. Experiments designed to probe the structure and relaxation properties of the ion beams will then be performed. Finally, the chemical reactions of these ions with gaseous neutrals and their surface etching properties will be investigated in an attempt to achieve a fundamental understanding of ion-neutral interactions and the reactive ion etching process.

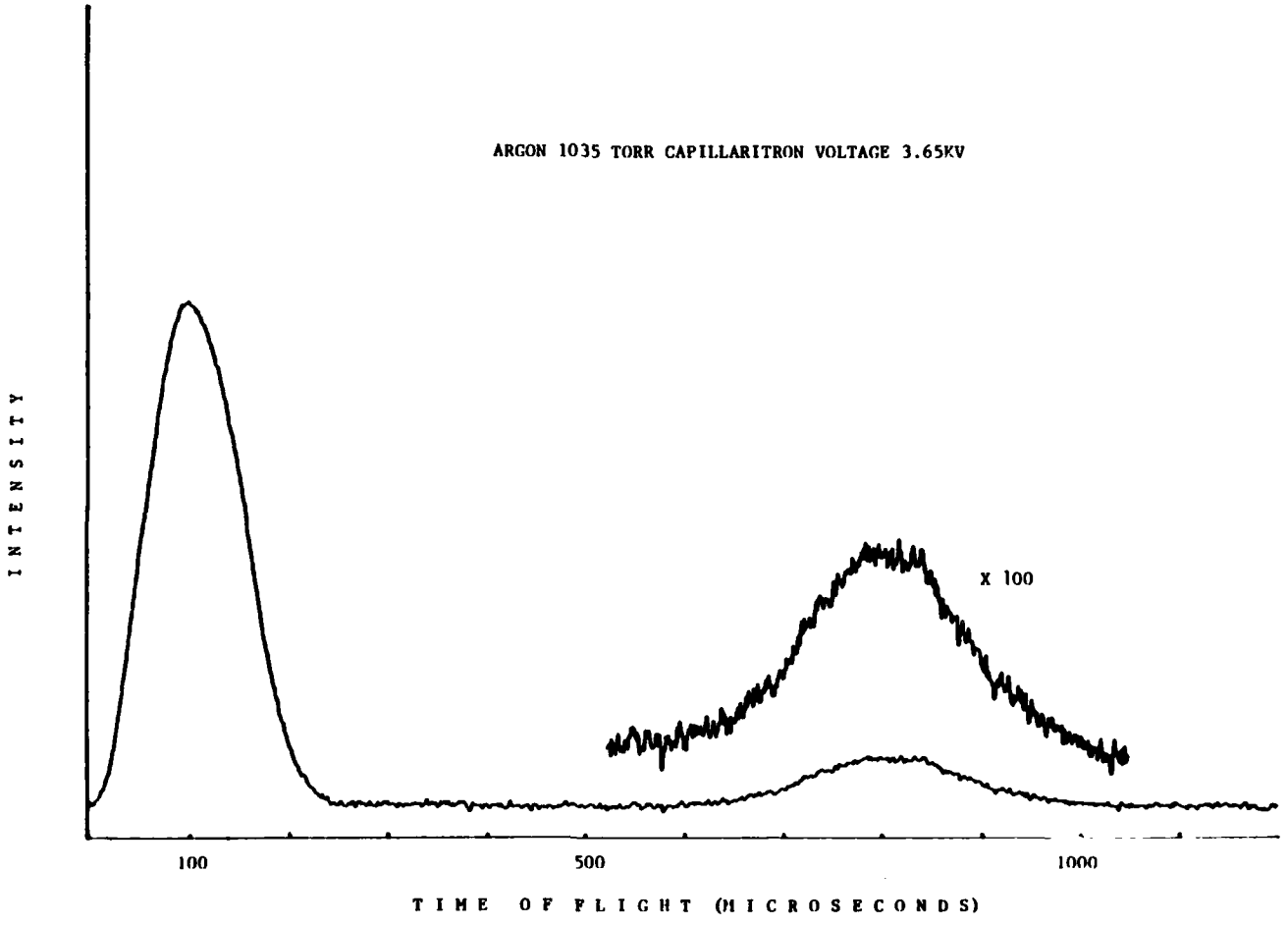

Figure 2. Time of flight of argon utilizing the Farday cup. The distance of travel is approximately 55 cm.

AD-A117 626 COLUMBIA RADIATION LAB NEW YORK F/G 20/3
RESEARCH INVESTIGATION DIRECTED TOWARD EXTENDING THE USEFUL RAN--ETC(U)
MAR 82 G W FLYNN DAAG29-79-C-0079
UNCLASSIFIED NL

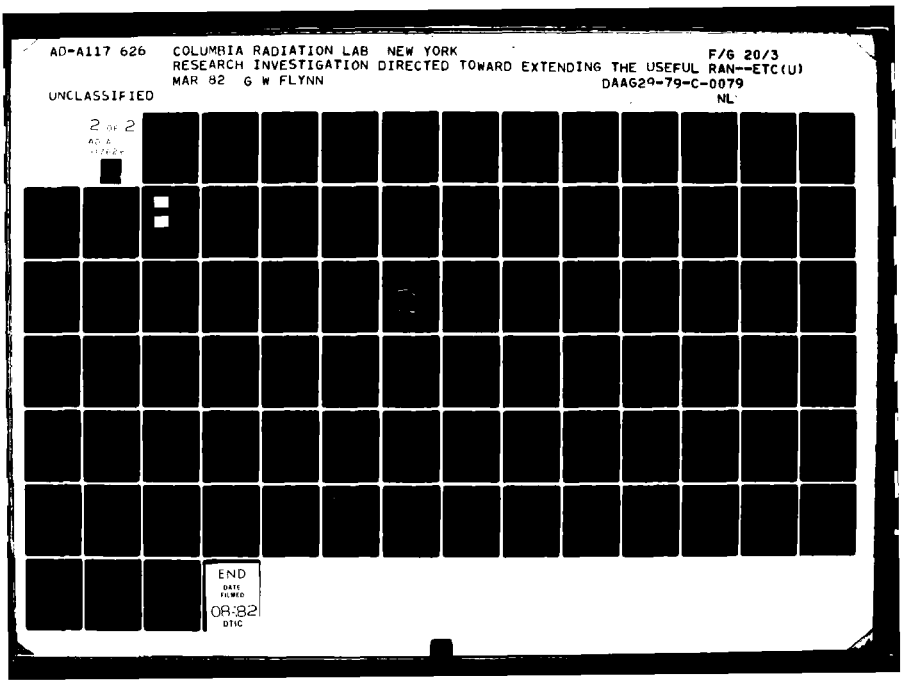

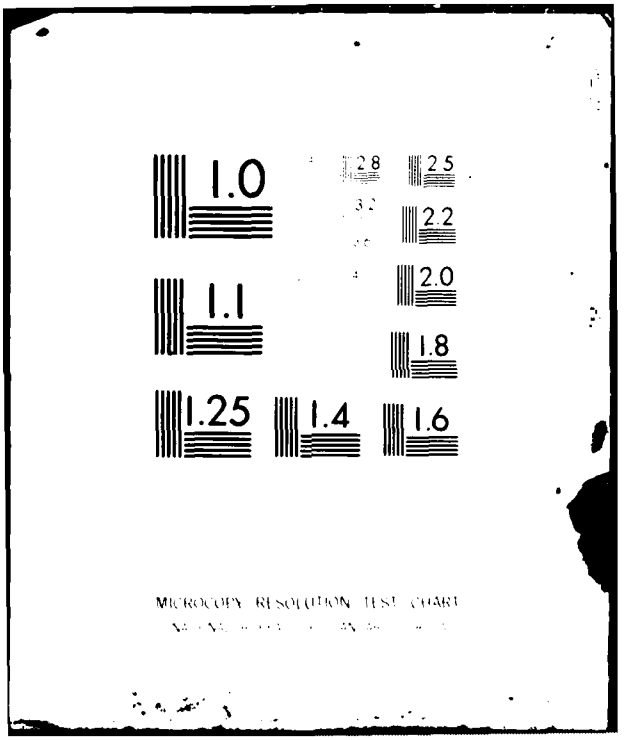
1.0
1.1
1.25
1.4
1.6
2.0
2.2
2.5
1.8
MICROCOPY RESOLUTION TEST CHART

*This research was also supported by the National Science Foundation under Grant NSF-CHE80-23747 and Department of Energy under Contract DE-AS02-78ER04940.

(1) R. G. Wilson and G. R. Brewer, Ion Beams: With Applications to Ion Implantation (Krieger, New York, 1979) p.12.

(2) J. F. Mahoney, J. Perel, and A. T. Forrester, Appl. Phys. Lett. 38, 320 (1981).

(3) J. Perel, J. F. Mahoney, B. E. Kalensher, and A. T. Forrester, "Investigation of the Capillaritron Ion Source For Electric Propulsion", AIAA-81-0747, AIAA 15th International Electric Propulsion Conference, Las Vegas, NV (21-23 April 1981).

(4) Phrasor Scientific, Inc. Manufactors the Capillaritron, price $1,950. Since our molecular beam appratus already included gas and high voltage feedthrus and translational stages, it was cost effective to design our own Capillaritron.

(5) D. M. Goebel, J. Perel, J. F. Mahoney, and A. T. Forrester, "Characteristics of the Capillaritron Ion Source", submitted for publication in the Journal of Applied Physics, April 1982.

III. ENERGY TRANSFER AND RELAXATION IN SMALL POLYATOMIC MOLECULES

A. PHOTOCHEMICAL DYNAMICS OF $^{79}Br_2$ IN Xe MATRICES*

(Paul Beeken, Mary Mandich, George Flynn)
(JSEP work unit 6, 1979-82)
(Principal Investigator: G. W. Flynn (212) 280-4162)

The photochemical dynamics of Br_2 trapped in a Xe matrix have been investigated. Following excitation into either the $B^3\pi(0_u^+)$ or $^1\pi(1u)$ states, emission occurs in the far red and infrared region. Analysis of the emission allows the emitting states to be characterized as $B^3\pi(0_u^+)$ $v'=0 \rightarrow X^1\Sigma_g^+$, and (tentatively) the $A'^3\pi(2u) \rightarrow X^1\Sigma_g^+$. The spectrum of the B → X emission was recorded and exhibited unusually broad vibronic emission lines when compared with Ar spectra. The B → X emission lifetime was measured to be 3.6 ± .5 μsec and is in excellent agreement with the expected value for the radiative lifetime. The risetime of the B signal was found to be limited by the detection system (∿ 15 nsec). The tentatively identified A' → X emission has a lifetime of 4 ± 1 msec. The $A^3\pi(1u) \rightarrow X^1\Sigma_g^+$ emission resolved clearly in Ar and Kr matrices is altogether absent from Br_2 isolated in Xe. Experiments were performed to measure the relative intensities of the B/A' emissions in Xe and compare them with earlier results from Ar matrices. The Xe B/A' ratio was found to be nearly 100 times greater in Xe then in Ar. The observations were found to be independent of temperature from 12K to 60K and independent of concentrations from 1:500 to 1:10000, Br_2 in Xe.

This work has been accepted for publication in the Journal of Chemical Physics. Please refer to the article (June 1982) for a more detailed account.

* This research was also supported by the Department of Energy under Contract DE-AS02-78ER04940 and the National Science Foundation under Grant NSF-CHE80-23747.

B. EMISSION SPECTRA AND RELAXATION DYNAMICS OF EXCITED $^{79}Br_2$ in Ar AND Kr MATRICES*

(Mary Mandich, Paul Beeken, George Flynn)
(JSEP work unit 6, 1979-82)
(Principal Investigator: G. W. Flynn (212) 280-4162)

The photochemical dynamics of Br_2 trapped in Ar and Kr matrices have been studied. Following laser excitation into either the $B^3\Pi(0_u^+)$ or $^1\Pi(1u)$ states, emission occurs in the near infrared spectral region. Analysis of this emission indicates that it consists of three electronic transitions which have been assigned as $B^3\Pi(0_u^+)$ $v' = 0 \rightarrow X^1\Sigma_g^+$ (previously reported), $A^3\Pi(1u)$ $v' = 0 \rightarrow X^1\Sigma_g^+$ and (tentatively) $A'^3\Pi(2u) \rightarrow X^1\Sigma_g^+$. The B → X emission lifetime was measured to be 8.0 ± .5 μsec in Ar matrices (5.3 ± .5 μsec in Kr) and is in good agreement with both earlier determinations in matrices and the gas phase B → X radiative lifetime. The observed A → X emission lifetime of 170 ± 10 μsec in Kr is approximately the same as the measured A → X gas phase radiative lifetime but appears shortened in Ar matrices where the lifetime is 67 ± 4 μsec. The lifetime of the A' → X transition is 11 ± 1 msec in Ar and 6 ± 1 msec in Kr matrices. The spectral and temporal data are consistent with an overall energy transfer mechanism involving both vibrational and electronic relaxation. The intramolecular electronic relaxation is somewhat restricted in that the highest lying $B^3\Pi(0_u^+)$ state is populated only by direct absorption into its bound and continuum levels whereas the two lower states, $A^3\Pi(1u)$ and $A'^3\Pi(2u)$, acquire population after either the $^1\Pi(1u)$ or $B^3\Pi(0_u^+)$ state are initially excited. Both the initial vibrational and electronic relaxation rapidly (< 20 nsec) routes the excited population into the lowest $v' = 0$ levels of the A and B states (and tentatively A') where the subsequent decay occurs on a $10^{-6} - 10^{-2}$ sec timescale. All of the observed emission lifetimes are independent of temperature, laser power and Br_2: matrix dilutions ranging from 1:500 - 1:10,000.

This work has been accepted for publication in the Journal of Chemical Physics. Please refer to the article (July 1982) for a more detailed account.

*This research was also supported by the Department of Energy under Contract DE-AS02-78ER04940 and the National Science Foundation under Grant NSF-CHE80-23747.

C. PHOTOCHEMICAL DYNAMICS OF I_2 IN RARE GAS MATRICES*

(Paul Beeken, George Flynn)
(JSEP work unit 6, 1979-82)
(Principal Investigator: G. W. Flynn (212) 280-4162)

I_2 is a fascinating molecular system which has stirred considerable interest because of the development of the iodine atom laser.[1]-[4] This device has shown promise as a high powered source for laser fusion experiments.[5] One possible drawback to the attainment of a high efficiency I^* chemical laser, however, might be interference from the quenching of excited iodine atoms by I_2. A complete analysis of the intramolecular relaxation pathways for molecular iodine is thus essential for optimizing the I^* laser.

We have just completed a detailed analysis of the spectra and dynamics of Br_2 in rare gas matrices.[6],[7] Other workers have investigated the dynamics of Cl_2 in low temperature solids.[8] The common elements of these studies has led to a generalized picture of halogen molecule relaxation in a rare gas case.[7] The investigations into Br_2 dynamics include characterization of the lower electronic states.[7] In iodine the low lying A and A' electronic states are thought to hinder efficient operation of the I^* laser.[9] Studies of I_2 would not only serve to solidify some of the generalizations proposed for intramolecular halogen relaxation but would also contribute to the development of a laser system.

Experimental

The apparatus has been described elsewhere and will not be presented here.[6],[7] The only change in the experimental setup has been the inclusion of a new Lambda Physik excimer pumped dye laser system.

Results

When a matrix of 1:1000 I_2:Ar was deposited on a CsI substrate and irradiated with 568.2 nm light from a pulsed dye laser two fluorescences were observed. The signals occur in two different spectral regions. One signal (visible to far red region of the spectrum) was found to decay extremely fast (< 200 usec). The range of this signal extends from below 700 nm and extends to just beyond 1100 nm. Using an S1 type phototube and, in another experiment, a more sensitive GaAs phototube, we were unable to resolve this emission into distinct spectral features.

The other fluorescence signal occurs in the IR and was found to have a lifetime of ∿250 μsec. The spectral range of this signal extended from 1.2 μ to 1.6 μ. Work is currently in progress to resolve this emission using a monochromator.

Discussion

The emission spectrum for the $X^1\Sigma_g \rightarrow B^3\Pi(0_u^+)$ transition has been reported for I_2 isolated in a rare gas matrix.[10] The experiment employed a cw Ar^+ ion laser for excitation so no lifetimes were measured. Dimer species were also detected which complicated the otherwise simple emission spectrum. The spectral bands were identified as emissions from the lowest vibrational level of the excited B electronic state. This observation is consistent with what has been observed in matrix isolated Br_2 and Cl_2.[6]-[8]

Measurments of the gas phase lifetime of the B state only allow us to estimate the radiative lifetime since the $v' = 0$ to ground electronic state transition has not been characterized.[11] The value obtained by extrapolation from higher vibronic transitions would be ∿ 800 nsec.[11] If the matrix

index of refraction is used to correct this value then the expected radiative lifetime in Ar would be ∿650 usec.[7],[8] In the gas phase, the rate of predissociation is known to be quite rapid as excitation moves down the B vibrational ladder from v' = 10.[11] Therefore, as was suggested for Br_2 in various rare gas matrices, non-radiative curve crossing could shorten this lifetime considerably.[7]

The IR emission has not been spectrally resolved using a monochromator and an InSb detector yet. But the general spectral features of the emission were determined with a series of narrow band interference filters. The resolution of these filters is, unfortunately, not sufficient to determine the origin of the emitting species by spectroscopic means. A crude estimate of the radiative lifetime for the A state places the expected value in the range of several hundred microseconds.[12] Since the lifetime of the A' state is expected to be much longer than this based on observations of other halogen species, the most likely source for the 250 μsec emission would be the $A^3\Pi(1u)$ electronic stage. Further experiments are required, however, to confirm these conclusions.

*This research was also supported by the National Science Foundation under Grant NSF-CHE80-23747 and the Department of Energy under Contract DE-AS02-78ER04940.

(1) W. E. McDermott, N. R. Pchelkin, D. J. Bernard, and R. R. Bousek, Appl. Phys. Lett. 32, 469 (1978).

(2) D. J. Bernard, W. E. McDermott, N. R. Pchelkin, and R. R. Bousek, App. Phys. Lett. 34, 40 (1979).

(3) R. J. Richardson and C. E. Wiswall, Appl. Phys. Lett. 35, 138 (1979).

(4) R. J. Richardson, J. D. Kelley, and C. E. Wiswall, J. Appl. Phys. 52, 1066 (1981).

(5) To be obtained from Cehm abstracts.

(6) M. L. Mandich, P. B. Beeken, and G. W. Flynn, "Emission Spectra and Relaxation Dynamics of Excited $^{79}Br_2$ Isolated in Ar and Kr Matrices" to be published in J. Chem. Phys. (1982).

(7) P. B. Beeken, M. L. Mandich, and G. W. Flynn, "Relaxation Dynamics of $^{79}Br_2$ Isolated in Xe Matrices" to be published in J. Chem. Phys. (1982).

(8) V. E. Bondybey and C. Fletcher, J. Chem. Phys. 64, 3615 (1976).

(9) J. D. Kelley, Private communication.

(10) B. S. Ault and L. Andrews, J. Mol. Spec. 70, 68 (1978).

(11) L. Brewer and J. Tellinghuisen, J. Chem. Phys. 56, 3929 (1972).

(12) J. A. Coxon, "Molecular Spectroscopy" (The Chemical Society, London, 1973), Vol. 1.

D. LASER EXCITED INFRARED FLUORESCENCE IN OXALYL FLUORIDE: RELAXATION IN THE PRESENCE OF A LOW ENERGY, ONE DIMENSIONAL QUASI-CONTINUUM *

(Toomas Allik, George Flynn)
(JSEP work units 4 and 5, 1979-82)
(Principal Investigator: G. W. Flynn (212) 280-4162)

Work on this project was finished in January of 1982. A paper describing these results is scheduled for publication in the Journal of Physical Chemistry, August 1982. An abstract of the paper is given below:

Fluorescence has been observed from various fundamental and combination states of oxalyl fluoride excited by a Q-switched CO_2 laser. The presence of a low frequency torsional mode in this molecule provides a one dimensional quasicontinuum of vibrational levels at energies above the barrier to rotation about the C-C bond. Intermode vibrational relaxation rates in $(COF)_2$ are extremely rapid (possibly collisionless). The observed temperature dependence of fluorescence intensity and the overall rapid equilibration in $(COF)_2$ suggest a mechanism in which many rovibrational transitions that possess ν_{10} character (e.g. $0 \rightarrow \nu_{10}$, $\nu_{10} \rightarrow 2\nu_{10}$, $\nu_x \rightarrow \nu_x + \nu_{10}$ etc.) are excited by the laser.

*This research was also supported by the Department of Energy under Contract DE-AS02-78ER04940 and the National Science Foundation under Grant NSF-CHE80-23747.

E. INVESTIGATION OF CYCLIC ENERGY TRANSFER PATHWAY IN OCS/He*

(Steven Goates, George Flynn)
(JSEP work units 4 and 5, 1979-82)
(Principal Investigator: G. W. Flynn (212) 280-4162)

Previously in this laboratory the rates of collisional vibrational energy transfer between the ν_1 level of OCS and the ν_2 bending mode as well as the overall vibrational relaxation to the translational/rotational degrees of freedom were measured for mixtures of OCS and the various rare gases.[1] These measurements were made by observing fluorescence from the ν_1 state following absorption of a laser pulse by $2\nu_2$. In the OCS/^{4}He system the equilibration of the ν_1 and ν_2 modes was found to be unexpectedly rapid with respect to the rates for the other OCS/rare gas mixtures. For all mixtures except OCS/^{4}He, the dominant energy transfer pathway connecting the ν_1 and ν_2 modes is

$$OCS(2\nu_2) + M \rightleftharpoons OCS(\nu_1) + M + 188\ cm^{-1} \qquad (1)$$

along with equilibration of ν_2 and $2\nu_2$ via

$$OCS(2\nu_2) + OCS(0) \rightleftharpoons 2\ OCS(\nu_2) + M + 7\ cm^{-1}, \qquad (2)$$

the intramode equilibration (process 2) occurring much more rapidly than the intermode transfer (process 1). It was proposed that in the case of OCS and He a second pathway, namely

$$OCS(\nu_2) + M \rightleftharpoons OCS(\nu_1) + M - 339\ cm^{-1}, \qquad (3)$$

becomes competitive with the first, accounting for the rapidity of the equilibration. It is to be noted that the two pathways together constitute a "cyclic" pathway. Such cyclic routes have been postulated to play an important role in the relaxation of molecules but have been rarely verified experimentally.

If our suspicions are well-founded, that the pathway directly coupling

ν_1 and ν_2 is important for collisions of OCS with the light ^{4}He atom, this route should be further enhanced for the yet lighter collision partner ^{3}He. Accordingly, rise and fall rates of ν_1 fluorescence for OCS/^{3}He mixtures have been measured. While the analysis of these data have not yet been completed, it is clear that the equilibration of ν_1 and ν_2 in this mixture proceeds significantly faster than in OCS/^{4}He. This result is certainly indicative of the proposed cyclic pathway, but does not provide definitive evidence.

An analysis of the kinetics for the cyclic pathway reveals, however, that its presence can be clearly distinguished by observing fluorescence from the ν_2 state at 19.1 μ.[2] Two exponential decays of this fluorescence have been observed in pure OCS and are related to the rates of ν_2/ν_1 equilibration and vibrational to translational/rotational relaxation.[3] The relative amplitudes of these two decay rates can reveal the presence of the cyclic pathway. An attempt to sufficiently accurately determine the amplitudes from the weak 19μ fluorescence for OCS/^{4}He and OCS/^{3}He mixtures awaits the arrival of a detector sensitive to this long wavelength.

*This research w. also supported by the Department of Energy under Contract DE-AS02-78ER04940 and the National Science Foundation under Grant NSF-CHE80-23747.

(1) M. L. Mandich and G. W. Flynn, J. Chem. Phys. 73, 1265 (1980).

(2) M. L. Mandich and P. Beeken, unpublished research.

(3) M. L. Mandich and G. W. Flynn, J. Chem. Phys. 73, 3679 (1980).

F. VIBRATIONAL RELAXATION DYNAMICS IN POLYATOMIC GAS MIXTURES: A STUDY OF COF_2 AND NO*

(J. Subbiah, G. W. Flynn)
(JSEP work units 4 and 5, 1979-1982)
(Principal Investigator: G. W. Flynn (212) 280-4162)

In order to achieve control of energy flow, storage and release in gas phase laser systems, electric discharges, shock waves and gasdynamic flows, it is important to understand the dynamics of energy flow among the internal degrees of freedom of molecules. As of now an empirical study of the experimental data has led to some understanding of qualitative trends. In addition, semi-quantitative theories can explain the experimental data, but accurate a priori predictions are still not feasible. This study of intermolecular vibrational energy transfer between COF_2 and NO is aimed at improving our understanding of relaxation dynamics.

NO is an interesting case because its ground electronic state ($^2\pi$) has an unpaired spin which may result in unusual relaxation behavior. In fact, its vibration-vibration (V-V) relaxation is of the same order of magnitude as CO (which is similar in many respects), while its vibration-translation (V-T) relaxation rate is about five orders of magnitude faster than CO.[1] Most of its other V-V behaviour is normal, but its excitation from laser-excited COF_2 may still hold some surprises.

Fig. 1 shows the relevant energy levels of COF_2 and NO. The energy flow pattern in vibrationally excited neat COF_2 has been studied.[1] There it has been shown that following excitation of the ν_2 mode by different CO_2 laser lines (10.6μ P branch), COF_2 undergoes intra and intermode relaxation as shown below:

Type 1 excitation: $COF_2(0) \xrightarrow{h\nu} COF_2(\nu_2)$ (1)

Type 2 excitation: $COF_2(\nu_2) \xrightarrow{h\nu} COF_2(2\nu_2)$ (2)

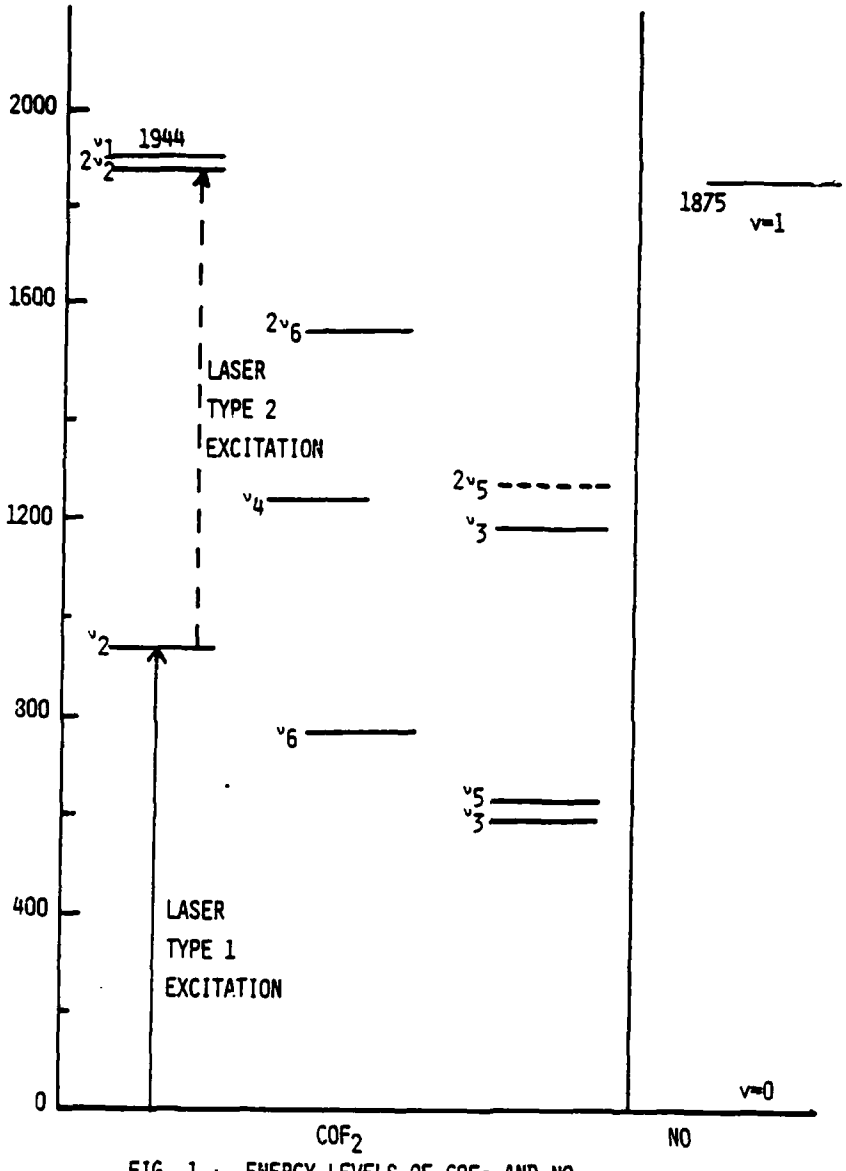

FIG. 1.: ENERGY LEVELS OF COF_2 AND NO.

Ladder Climbing: $COF_2(\nu_2) + COF_2(\nu_2) \underset{k_d}{\overset{k_u}{\rightleftharpoons}} COF_2(0) + COF_2(2\nu_2)$ (3)

Equilibration of Fermi-coupled levels : $COF_2(2\nu_2) + M \rightleftharpoons COF_2(\nu_1) + M$ (4)

Fig. 2 shows typical type 1 and type 2 fluorescence traces in COF_2 alone. (The same eigenvalues appear in both types, but the fastest eigenvalue, which appears in the rise of type 1 turns up in the fall of the type 2 signal.) Subsequently the excitation remains localized in the ν_1, ν_2 manifolds for about 35 μsec at 1 torr before further relaxation sets in.

If NO is added to this system one possible new path would include energy-transfer:

Crossover: $COF_2(\nu_1) + NO \longrightarrow COF_2(0) + NO\ (v = 1)$ (5)

The crossover rate in COF_2-NO mixtures was determined by following the time-dependent population in $COF_2(\nu_1, 2\nu_2)$ via its 5μ fluorescence intensity.

Experimental and Results

A Q-switched CO_2 laser operating on different lines of the 10.6 micron P branch was used to excite the ν_2 mode of COF_2 (C-F stretch). Typical pulse energies were 0.5 to 1 mj/pulse, and typical pulsewidths about 1 microsecond. The laser was run single line to better than 95%. The COF_2 used was taken directly from a high purity Synthatron tank, while the NO was purified by successive trap-to-trap distillation at -160° C. In all cases IR fluorescence was observed through a 4.6 micron long pass filter as well as a 2 mm thick MGF_2 window. This isolates the 5 micron fluorescence of COF_2 corresponding to the ν_1, $2\nu_2$ band (C = O symmetric stretch), as well as the v = 1 fluorescence from NO. This does not complicate the interpretation, however, as the same eigenvalues appear in the NO and COF_2 fluorescences, although with different amplitudes.

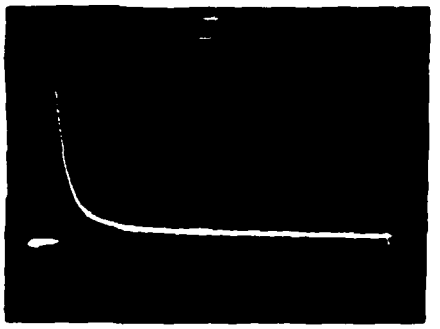

TYPICAL 5μ FLUORESCENCE DECAY OF COF_2 ALONE FOLLOWING TYPE 1 EXCITATION.
COF_2 PRESSURE 1.023 TORR
0.4 MS FULL-SCALE.

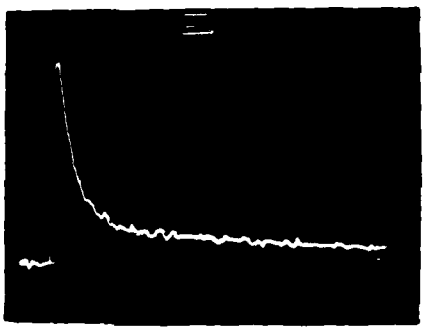

TYPICAL 5μ FLUORESCENCE DECAY OF COF_2 ALONE FOLLOWING TYPE 2 EXCITATION.
COF_2 PRESSURE 1.006 TORR
0.02 MS FULL-SCALE

FIGURE 2: TYPE 1 AND TYPE 2. FLUORESCENCE SIGNALS FROM NEAT COF_2

Fluorescence decay rates of the COF_2 (ν_1, $2\nu_2$) level were studied as a function of pressure at different mole fractions of NO in the COF_2-NO mixtures. The results for both type 1 and type 2 excitation are shown in Figure 3. The two types give eigenvalues that agree within experimental error. Further, in order to see whether NO is merely acting as an inert collision partner, data taken with COF_2-Ar mixtures at identical mole fractions is also tabulated in Table 2.

Fig. 3 shows the simplified kinetic scheme used to model the intermolecular energy transfer. Under the approximations listed, there are two eigenvalues, and one can, in this case, express each eigenvalue in terms of the rate constants. The fast eigenvalue is linear both in the total pressure of the mixture at constant mole fraction as well as in the pressure of NO added to a fixed pressure of COF_2. Although k_f can be obtained from any value of the mole fraction, the low mole fraction runs are not as accurate as the k_f here turns out to be the difference of two large numbers (see Equation (4), Fig. 3). Table 1 lists the calculated eigenvalues based on this scheme while Table 2 includes the experimentally observed rates. As can be seen the rates converge to a value around 170 $ms^{-1}torr^{-1}$ for k_f.

Discussion

The measured k_f (the rate constant for energy transfer, see Equation (5)) corresponds to 50 collisions or a vibrational energy transfer probability per collision of 2×10^{-2} at room temperature, which is a large value. This is about an order of magnitude larger than expected even for exact resonance on the basis of a theory of energy transfer assuming exponentially repulsive interaction potentials.[3] It seems likely, however, that long-range attractive interactions involving dipole-dipole potential (as modelled by Sharman and Brau[4]) should in agreement with the results. Work along these lines is being pursued.

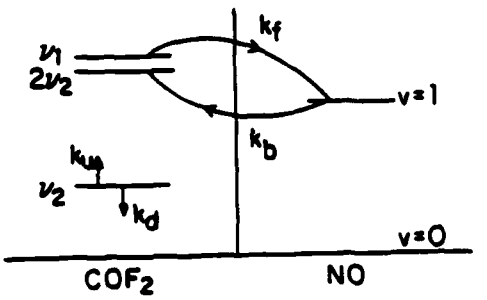

$$COF_2(\nu_2) + COF_2(\nu_2) \underset{k_d}{\overset{k_u}{\rightleftharpoons}} COF_2(2\nu_2) + COF_2(0) + 14cm^{-1} \quad \text{(i)}$$

$$COF_2(\nu_1, 2\nu_2) + NO(\nu=0) \underset{k_b}{\overset{k_f}{\rightleftharpoons}} COF_2(0) + NO(v=1) + 69cm^{-1} \quad \text{(ii)}$$

THE RESULTING RATE MATRIX A IS

$$\begin{bmatrix} \frac{dN}{dt} COF_2(\nu_1, 2\nu_2) \\ \frac{dN}{dt} NO\ (v=1) \end{bmatrix} = \begin{bmatrix} -K_d(1-x) - K_f x - \lambda & K_b(1-x) \\ K_f x & -K_b(1-x) - \lambda \end{bmatrix} \begin{bmatrix} N_{COF_2\ (\nu_1, 2\nu_2)} \\ N_{NO\ (v=1)} \end{bmatrix} \quad \text{(iii)}$$

RESULTS:

$$\frac{\lambda^+}{m} = 0.99\,(k_d + k_b)(1-x) + k_f x \quad \text{(iv)}$$

$$\lambda^+ = k_f P_{NO} + 0.99\, k_b P_{COF_2} + 0.99\, k_d P_{COF_2}$$

$$\lambda^- = \frac{1}{\lambda^+} \left[0.04\, k_f P_{COF_2} P_{NO} + k_b P_{NO}^2\right]$$

P_{COF_2} = PARTIAL PRESSURE OF COF_2

P_{NO} = PARTIAL PRESSURE OF NO

FIG. 3 KINETIC SCHEME FOR COF_2 – NO ENERGY TRANSFER

TABLE 1: Numerical Solution for the Time-dependence of Population in $COF_2(\nu_1, 2\nu_2)$ using the kinetic scheme in Fig. 4.

Following is the calculated time-dependent variation of the population deviation (from thermal equilibrium) of $COF_2(\nu_1, 2\nu_2)$ in a mixture of CO_2 and NO at an NO mole fraction of 0.9.

The guess values for the bimolecular rate constants used are: (in units of $ms^{-1}\ torr^{-1}$)

$k_u = 620$ $\qquad$ $k_d = 620$

$k_f = 170$

$k_{20} = 30$ $\qquad$ $k'_{20} = 4.5$

$k_{10} = 2.5$ $\qquad$ $k'_{10} = 2.0$

$$COF_2(\nu_1, 2\nu_2)\ (t) = A_1\ e^{-\lambda_1 t} + A_2\ e^{-\lambda_2 t} + A_3\ e^{-\lambda_3 t} + B$$

$A_1 = 0.93$ $\qquad$ $\lambda_1 = 242\ ms^{-1}$

$A_2 = 0.04$ $\qquad$ $\lambda_2 = 13.1\ ms^{-1}$

$A_3 = 0.01$ $\qquad$ $\lambda_3 = 5.4$

TABLE 2: Results of Type 1 and Type 2 excitation of COF_2-NO mixtures

Type 2 Excitation

Slope of λ_{fast} (ms^{-1}) versus pressure of added NO: 154 ms^{-1} $torr^{-1}$

Gases Mix COF_2-M	Mole fraction of M	λ_{fast} (experimental) (ms^{-1})	k_f* ms^{-1} $torr^{-1}$	k_f** ms^{-1} $torr^{-1}$
COF_2-NO	0.986	164	171 to 137	155
COF_2-NO	0.9	240	195 to 136	170
COF_2-NO	0.7	317	161 to 71	150
COF_2-Ar	0.9	95	46 to 16	

Type 1 excitation

The slope of λ_{fast} (ms^{-1}) versus pressure of added NO: 170 ms^{-1} $torr^{-1}$

*The range of k_f got using the experimental λ_{fast} and eqn. iv of Fig. 3.

**The guess value of k_f which when used in numerical solution using this kinetic scheme results in the best agreement with λ_{fast}.

The expected additional rate process following addition of NO to COF_2 is not experimentally observed, but this is understandable in view of the small amplitude expected for it based on our kinetic model (the rate processes included are indicated in Fig. 4 and the results shown in Table 1). The rates with argon are found to be non-zero but still much smaller than the rates observed with NO.

Table 3 lists the known transfer probabilities from NO to other molecules. It is seen that the NO to D_2S probability is very large, as might be expected for its small energy defect. The NO to NO_2 is also large and one possible explanation has been a possible reactive channel:

$$NO + NO_2 \longrightarrow N_2O_3 + 9.7 \text{ Kcal/mole}$$

There is the possibility that a similar channel may be available for the COF_2-NO system as well. The C atom in COF_2, flanked by two highly electronegative F atoms, as well as the polarizable cloud connected to the electronegative O atom, is likely to be an electron deficient center. NO, on the other hand, has an odd electron, and its attack on the nucleophilic C atom seems plausible. In the case of the HF-COF_2 and DF-CO_2 systems, where similar strong intermolecular forces operate, it was found that agreement with experiment could be improved by invoking the possiblity of 'orbiting' collisions.[6] That is, when the kinetic energy is less than 0.8 times the well depth, for certain values of the impact parameter the trajectory can no longer be described by a straight line path, but executes multiple revolutions (i.e. scattering angle greater than 2π). Inclusion of such trajectories in the case of the HF-CO_2 system resulted in increasing the calculated V-V probability by a factor of 2.5. Another system that's probably reactive is CO_2-H_2O,[7] with a probability of energy transfer of 5×10^{-2}.

A mixture of COF_2 and NO in a stainless steel cell develops a new IR absorption band which grows as a function of time. The pressure dependence

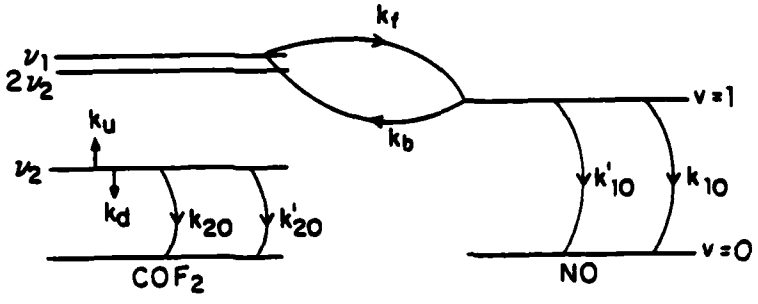

$$COF_2(\nu_2) + COF_2(\nu_2) \underset{k_d}{\overset{k_u}{\rightleftharpoons}} COF\ (2\nu_2) + COF_2(0)$$

$$COF_2(\nu_1) + NO(0) \underset{k_b}{\overset{k_f}{\rightleftharpoons}} COF_2(0) + NO\ (v=1)$$

$$COF_2(\nu_2) + NO \xrightarrow{k'_{20}} COF_2(0) + NO$$

$$COF_2(\nu_2) + COF_2 \xrightarrow{k_{20}} COF_2(0) + COF_2$$

$$NO(v=1) + NO \xrightarrow{k_{10}} NO\ (0) + NO$$

$$NO\ (v=1) + COF_2 \xrightarrow{k'_{10}} NO\ (0) + COF_2$$

THIS RESULTS IN A SYSTEM OF THREE INDEPENDENT LINEAR FIRST ORDER COUPLED DIFFERENTIAL EQUATIONS.

FIG. 4 DETAILED KINETIC SCHEME FOR THE COF_2-NC SYSTEM INCLUDING V-T RELAXATION

TABLE 3: Intermolecular Vibrational Energy Transfer Probabilities.

(Largely taken from Ref. 5a)

From M_1	To M_2	ΔE^* cm^{-1}		Z^+
NO	CO	267	10^{-4}	10,000
NO	N_2	455	6×10^{-6}	166,667
NO	CO_2	491	1.7×10^{-4}	5,882
NO	D_2S	-16	1.1×10^{-2}	91
NO	H_2O	281	6×10^{-3}	167
NO	H_2S	586	3.2×10^{-3}	313
NO	D_2O	697	10^{-3}	1,000
NO	CH_4	343	9×10^{-4}	1,111
NO	COF_2	-68	2×10^{-2}	50
HF	$CO_2(00°1)$	1612	8.5×10^{-3}	118
DF	$CO_2(00°1)$	557	3×10^{-2}	33
CO_2	H_2O	55	5×10^{-2}	20

+Z (collision number) = $\frac{\sigma_{gk}}{\sigma_{vv}}$ where σ_{gk} is the gas-kinetic collision cross-section, and σ_{vv} is the vib energy transfer cross section.

*Energy defect ΔE: $M_1(v=1) + M_2 \rightarrow M_1(0) + M_2(v=1) + \Delta E$

**Probability of vibrational energy transfer per collision.

of the intensity of this band suggests a 1:1 complex formation or reaction. However the reaction appears to be slow enough that on the timescale of a fluorescence measurement the fraction of molecules that have reacted is not large. It would be interesting to study the temperature dependence of the intensity of the 1800 cm^{-1} band. It would be expected that in the case of complex formation the equilibrium would be shifted in the direction of the complex at low temperature. Once that is known the temperture dependence of the crossover probability may yield information about the role of the complex in the excitation transfer.

Ultimately the most definitive evidence for energy transfer would be to directly monitor the population of NO in v = 1. This however, is hard to do by IR fluorescence, both because of the relatively low intensity of the NO fundamental, and because its rotational envelope overlaps that of COF_2. One alternative would be to directly excite NO by a CO or doubled CO_2 laser, and monitor COF_2 5 micron fluorescence.

This system is interesting in the context of using CO_2 as an energy storage medium or sensitizing agent. For example, the relaxation time of the population in NO (v = 1) in the gas mixture is about 77 μsec at 1 torr total pressure (NO mole fraction = 0.9). It may now be possible to use this metastable population to study the vibrational enhancement of the chemical reactivity of NO with, say, Cl_2. In addition, this is an example where a population of vibrationally excited molecules can be prepared even when no coincidence with a convenient laser can be found.

The intermolecular vibrational relaxation probability from COF_2 to NO has been measured to be 2×10^{-2}. This can be understood in terms of long-range attractive interactions and possibly reactive scattering. This system has interesting applications involving sensitization and energy storage.

*This research was also supported by the National Science Foundation under Grant NSF-CHE80-23747 and the Department of Energy under Contract DE-AS02-78ER04940.

(1) J. C. Stephenson, J. Chem. Phys. 59, 1523 (1973).

(2) K. Castleton and G. W. Flynn, J. Chem. Phys. 67, 3133 (1977).

(3) R. N. Schwartz, Z. N. Slawsky, and K. F. Herzfeld, J. Chem. Phys. 20, 1951 (1952).

(4) R. D. Sharma and C. A. Brau, Phys. Rev. Lett. 19, 1273 (1967); R. D. Sharma and C. A. Brau, J. Chem. Phys. 50, 294 (1969).

(5) a) C. B. Moore, Adv. Chem. Phys. 23, 41 (1973).
b) E. Weitz and G W. Flynn, Annu. Rev. Phys. Chem. 25, 275 (1974).

(6) T. A. Dillon and J. C. Stephenson, J. Chem. Phys. 60, 4286 (1974).

(7) Original references can be obtained from.R. L. Taylor and S. Bitterman, Modern Physics 41, 1960 (1973).

G. OBSERVATION OF VIBRATIONAL EXCITATION IN PHOTOFRAGMENTS OF S-TRIAZINE*

(Steven Goates, Jack Chu, George Flynn)
(JSEP work unit 7, 1979-82)
(Principal Investigator: G. W. Flynn (212) 280-4162)

Last year's progress report contained very preliminary results of an experiment which seeks to determine excess energy in the vibrations of HCN molecules produced in the photodissociation of s-triazine, $(HCN)_3$. Work on this project has recently been advanced.

s-Triazine is a benzene-like molecule which has elicited much attention in recent years becuase of the importance of Jahn-Teller distortion of its excited states.[1] Molecular beam experiments have demonstrated that triazine is cleanly dissociated into three HCN fragments when exposed to 193 nm radiation.[2] The distribution of excess energy among the degrees of freedom of the HCN fragments is expected to provide information about the dissociating states of the triazine molecule and the dissociation process. Considering the different geometries of the HCN units in triazine and free HCN molecules (bent versus linear) a high degree of vibrational excitation in the HCN products is not unexpected.

We have used the pulsed 193 nm output (ArF) from a rare gas-halide excimer laser to irradiate a flowing sample of triazine in a glass cell and viewed infrared fluorescence following each pulse at a right angle to the UV beam path. Combinations of filters were employed to select particular wavelength regions and the infrared fluorescence was detected with either a HgCdTe or InSb detector; temporal response of the detectors was recorded with a transient signal digitizer/averager combination. We have made crude measurements of the absorption coefficient of triazine at 193 nm (~ 0.025 torr^{-1}cm^{-1}) and calculated that less than a few hundredths of a percent of the triazine

s in the beam path are dissociated with each pulse of the laser at the fluences ($\sim$ 20 mJ/cm^2) employed. Confirmation of the low dissociation provided by the very small increase in pressure observed after irradiaziazine vapor in a closed cell.

espite the low dissociation yields we have been able to observe infrared ence from many vibrational transitions in HCN (ν_2, $2\nu_2$, $3\nu_2$ and ν_1, ν_3, $\nu_1 + \nu_3$, $2\nu_3$), and the HCN fragments appear to be highly vibrationally

The rise of fluorescence from all HCN states is essentially instanand preliminary analysis indicates that excess vibrational energy y evenly distributed among all the modes. Time-of-flight measurements olecular beam study of reference 2 revealed that very little of the cess energy resides in the translational motion of the fragments. Rise fluorescence which we have observed from undissociated triazine, excited sions with the HCN fragments, seem to match the molecular beam results. to quantitatively determine the amount of energy residing in each mode ation of HCN immediately after triazine dissociation by employing the s-filter technique[3] for determining vibrational temperatures. The of rotational excitation cannot be established from our present meats; experiments with a circularly variable filter are planned to probe ational envelope of the observed transitions.

Our results for 193 nm dissociation of s-triazine contrast sharply to om a study of dissociation of a similar molecule, s-tetrazine, where vibrational excitation of the fragments (2 HCN + N_2) was found.[4] These suggest a much different dissociation mechanism for these two molecules their structural similarity. Molecular beam work cited above indicates, that a much different distribution of excess energy occurs in the ation fragments of triazine when it is irradiated with 248 nm rather

than 193 nm.[2] We will extend our studies to 248 nm dissociation in the coming months.

*This research was also supported by the Department of Energy under Contract DE-AS02-78ER04940 and the National Science Foundation under Grant NSF-CHE80-23747.

(1) See for example, J. D. Webb, K. M. Swift, and E. R. Bernstein, J. Chem. Phys. 73, 4891 (1980); and G. Fischer and G. J. Small, J. Chem. Phys. 56, 5934 (1972).

(2) R. Bersohn, G. Ondrey, S. Kanfer, P. Brewer, and S. Yang, J. Photochem. 17, 257 (1981).

(3) R. E. McNair, S. F. Fulghum, G. W. Flynn, M. S. Feld, and B. J. Feldman, Chem. Phys. Lett. 48, 241 (1977).

(4) D. Coulter, D. Dows, H. Reisler, and C. Wittig, Chem. Phys. 32, 429 (1978).

H. VIBRATIONAL EXCITATION OF CARBON MONOXIDE BY COLLISIONS WITH TRANSLATIONALLY "HOT" H ATOMS PRODUCED VIA LASER PHOTOFRAGMENTATION*

(C. F. Wood, G. W. Flynn)
(JSEP work unit 7, 1979-82)
(Principal Investigator: G. W. Flynn (212) 280-4162)

Although the theory of translational to vibrational energy transfer processes is quite well developed in the literature,[1] direct experimental confirmation of these theories is not easily obtainable. The reason for this paucity of experimental information has been largely due to the small excitation cross sections for T → V processes at easily obtainable energies. Associated with this problem is the additional difficulty resolving state-to-state cross sections at collisional energies large enough to vibrationally excite a polyatomic molecule; at translational temperatures high enough to cause collisional excitation, the higher vibrational levels of a molecule are also likely to be populated causing difficulties in interpreting data.

Recently a bulb technique has been developed that overcomes the problem of producing translationally energetic atoms in the presence of thermally populated vibrational and rotational states of molecules.[2] An excimer laser is used to photolyze simple molecules, producing translationally fast photofragments. The subsequent energetic collisions of the fast atoms with other polyatomics present causes IR emission from the polyatomic. The emission can be both wavelength and time resolved. Since most of the theories of T → V processes best describe an atom colliding with a diatomic molecule it is of particular interest to study such a system. We have begun a study of the vibrational and rotational excitation of carbon monoxide caused by collisions with fast hydrogen atoms produced in the photolysis of HBr.

$$HBr \xrightarrow{193nm} H^* (20{,}000\ cm^{-1}) + Br\ (^2P_{3/2} \sim 85\%,\ ^2P_{112} \sim 15\%)$$

$$H^* + CO(v=0) \rightarrow CO(v=n) \qquad n = 1,2,\ldots$$

$$CO(v=n) \rightarrow CO(v=n-1) + h\nu \quad h\nu = 4.6\mu$$

A pulsed Lumonics TE-860S laser was used to produce the 193 nm UV light needed to dissociate the HBr. The laser was pulsed at low repetition rates (∿1 Hz) and at low energies (∿ 10 mJ/p). Infrared emission from the system was monitored using an InSb photovoltaic infrared detector (77°K). The emission was wavelength resolved using either narrow band pass filters (∿ 120 cm^{-1} B.P.) or a circular variable filter (30 cm^{-1} B.P.). The signal from the detector is amplified, digitized with a Biomation model 8100 transient recorder, summed in a signal averager (Nicolet 1170 or Northern 575 A), stored in a PDP 11/34 or VAX 11/780 for analysis. A flowing stainless steel vacuum line was used in order to reduce buildup of fragmentation products in the cell.

We have observed T → V energy transfer in this system up to CO (v = 2) and perhaps higher. The emission profiles from the R branch (4.5 μ) and from the P branch (4.8 μ) are quite different. (See Figure 1.) The R branch profile is dominated by a fast "spike" that decays at nearly a gas kinetic rate ($6x10^6$ sec^{-1} $torr^{-1}$), followed by a slower rise and then a very slow decay. The spike may be caused by "hot" rotational levels rapidly relaxing to lower levels. The "spike" is unattenuated by passing through a 2 cm long cold gas filter containing up to 4 torr CO. (See Figure 2.) The intensity of the spike as a function of wavelength was studied using the 30 cm^{-1} band pass circular variable filter. This study indicates that the H atom projectiles are initially exciting the CO (v=1) up to at least J = 20. The spike occurs as the high J states rapidly relax to what is probably a Boltzmann rotational distribution. The final rotational temperature has not been determined and, due

IR EMISSION FROM HBR/CO MIXTURES

LAMBDA DISSO = 193 NM

PTOT = .5 TORR HBR/CO=1/5

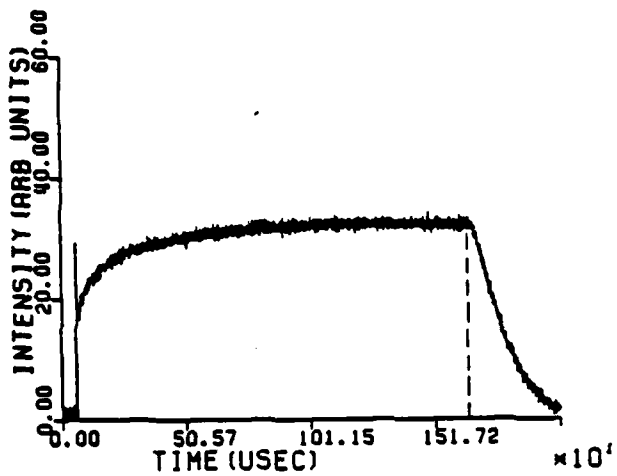

R BRANCH
4.5 UM

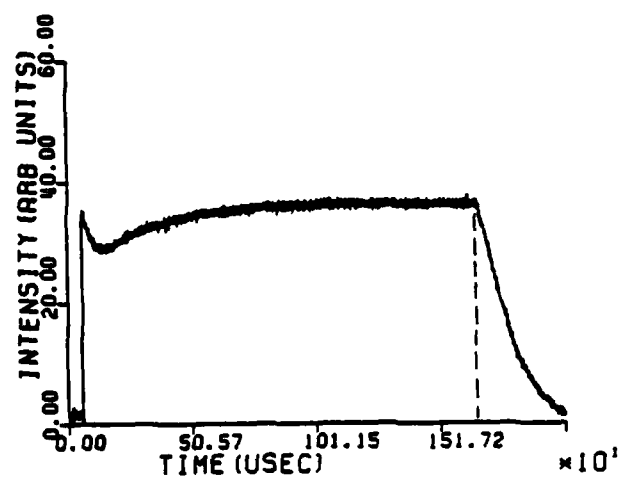

P BRANCH
4.8 UM

FIGURE 1

IR EMISSION FROM HBR/CO MIXTURES

LAMBDA DISSO = 193 NM

PTOT = .5 TORR HBR/CO=1/5

4.0-5.0 UM FILTER

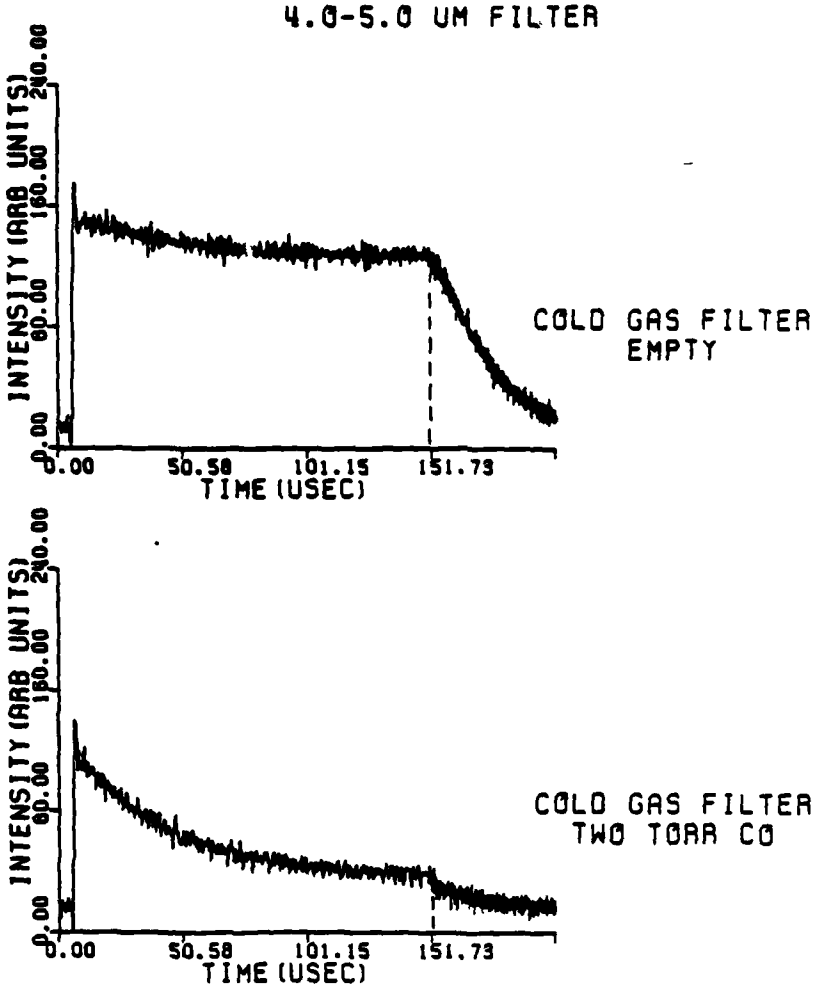

FIGURE 2

to the overlap of the higher vibrational levels with the R branch CO (v = 1) transitions, cannot easily be measured.

The initial fast fall in the P branch profile decays with a rate corresponding to the process $CO(v=0) + CO(v=2) \rightarrow CO(v=1) + CO(v=1)$. The second slower rise in the R branch rises at this same rate. Cold gas filter studies were performed using a 4.0 to 5.0 μ filter. The results indicate that about 70% of the excited carbon monoxide is in v = 2 or higher levels. (See Figure 3.)

In order to study the efficiency of energy transfer as a function of mass, some isotope studies have been performed. ^{13}CO was studied under the same conditions as ^{12}CO. Use of the spectator model[3] to calculate the efficiency of energy transfer shows that the difference in energy transfer probability would be on the order of 1% greater for $H^* + {}^{12}CO$ than $H^* + {}^{13}CO$. No significant differences in the data were observed. DBr was also used as a source of hot atom excitation. The same energy transfer calculation[3] indicates that the D atoms can transfer up to 30% of their energy per collision as opposed to the 16% calculated for H atoms from HBr. Cold gas filter studies comparing CO excitation with both D atoms and H atoms do not show appreciable differences in the per cent excitation in the v = 2 or higher vibrational levels. However, since it is impossible to distinguish the extent of excitation into v = 2 versus higher levels with cold gas filter studies, the possibility remains that the hot D atoms might be exciting CO into the v > 2 levels more efficiently than the hot H atoms.

IR EMISSION FROM HBR/CO MIXTURES

LAMBDA DISSO = 193 NM

PTOT = .5 TORR HBR/CO=1/5

4.5 UM FILTER

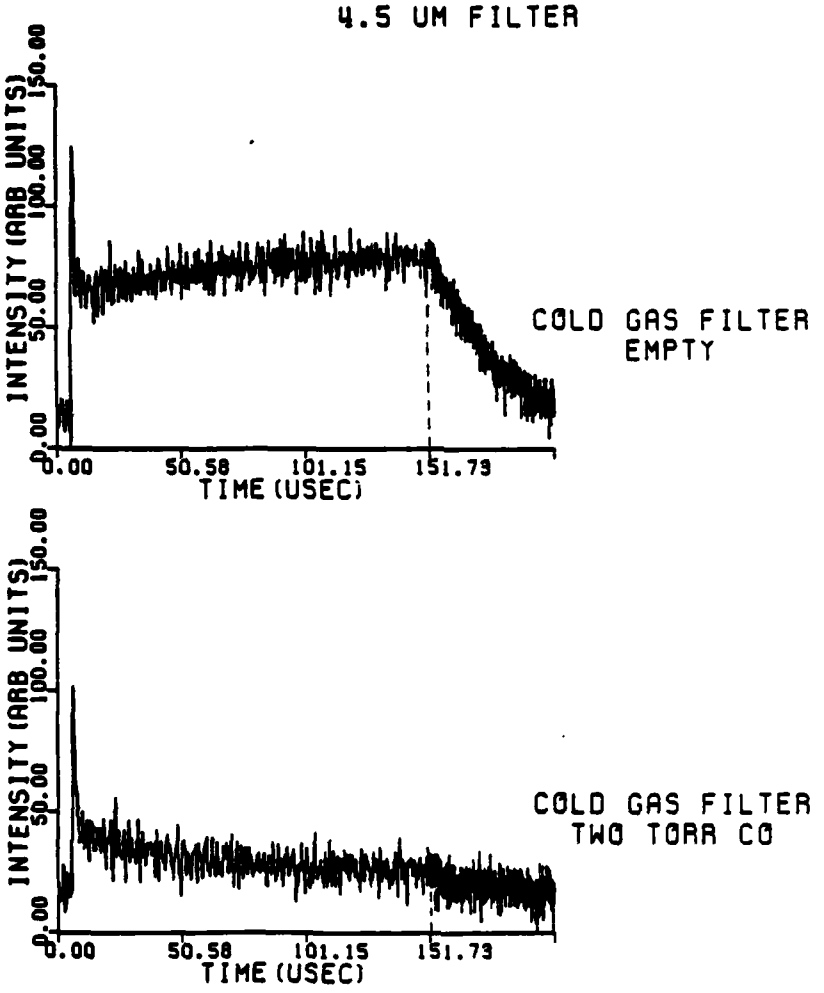

FIGURE 3

*This research was also supported by the Department of Energy under Contract DE-AS02-78ER04940 and the National Science Foundation under Grant NSF-CHE80-23747.

(1) D. Rapp, T. Kassel, Chem. Rev. 69, 61 (1969).

(2) C. R. Quick, R. E. Weston, and G. W. Flynn, Chem. Phys. Letters 83, 15 (1981). F. Magnorta, D. J. Nesbitt, and S. R. Leone, Chem. Phys. Letters 83, 21 (1981).

(3) R. D. Levine and R. B. Bernstein, Molecular Reaction Dyuamics (Oxford Univ. Press, London, 1974) p 135.

I. TRANSLATIONAL-TO-VIBRATIONAL (T-V) EXCITATION OF CO_2 BY COLLISIONS WITH "HOT" HYDROGEN ATOMS PRODUCED FROM LASER PHOTOLYSIS*

(J. O. Chu, G. W. Flynn)
(JSEP work unit 7, 1979-82)
(Principal Investigator: G. W. Flynn (212) 28-4162)

Energy transfer in the collisional excitation or relaxation of the internal states of a molecule is a topic of fundamental importance which plays a significant role in the study of chemical reactions.[1] Such processes involve the simplest type of energy transfer collision event, namely the energy exchange between the translational and the internal vibrational and rotational degrees of freedom of a molecule. However, in contrast to the numerous investigations of the collisional vibrational relaxation of neutral molecules,[2] there have been very few studies of the reverse process of collisional excitation. This can in part be attributed to the expected small excitation cross section for such energy exchange events involving particles with velocities near those at room temperature. Relatively difficult molecular beam techniques must be employed in order to obtain collisional energies above the endothermic threshold. Furthermore, beam scattering experiments involving neutral collision partners suffer from difficulties associated with resolving individual vibration-rotation transitions. Only one report of a molecular beam scattering experiment has been made in which a single vibrationally excited state has been resolved under single-collision conditions.[3]

A new technique has recently been developed for studying the process of translation to vibration (T-V) energy transfer and translationally enhanced reactive events. The method involves excimer laser photolysis of bound molecules to produce translationally "hot" (superthermal) atoms (or radical fragments) in a gas sample, followed by direct time-resolved detection of infrared fluorescence from vibrationally excited product species. This technique essentially provides

a sensitive and direct probe of the translation-to-vibration, rotation (T-V/R) energy transfer dynamics that occur during each highly energetic collision event. Furthermore, infrared luminescence detection of T-V excited products can readily be made wavelength state specific, and subsequent vibrational (and possibly rotational) distributions can be obtained from the direct wavelength resolved emission profile. In cases where "hot", highly reactive radical fragments are generated, dynamical competition between T-V energy transfer and reactive exchange reactions can be studied in detail.

In a general application of this technique to the study of "hot-atom" excitation, initial results focussing on the collisional T-V excitation of the molecules HCl, DCl, HBr, DBr, CO_2, and N_2O by hot H and D atoms produced by ArF laser photolysis of HCl/DCl, HBr/DBr or H_2S have been reported.[4],[5] The present study extends this work, in particular, to wavelength resolution of the 4-5 μm IR emission observed from CO_2 excited by translation-to-vibration (T-V) energy transfer collisions with hot H atoms produced by the ArF laser photolysis of HBr.

The output of a pulsed Lumonics TE-860S excimer laser operated at 193 nm (ArF, pulse width 10 ns FWHM) was used to irradiate a cyclindrical Pyrex sample cell, which was fitted with Suprasil windows. A conventional stainless steel vacuum flow system was used to flow, from a pre-mixed sample in a glass bulb, fresh gas samples through the fluorescence cell to prevent gas depletion and the build up of reaction products. Typically all experiments were performed at low fluences in order to avoid multiple photon events. Infrared emission was detected through a NaCl window at right angles to the laser beam with a Judson Infrared InSb detector (1 μs risetime, $77^{o}K$). Either broadband interference filters or a narrowband OCLI circular variable filter (≈ 30 cm^{-1}, FWHM) were used to view only the desired wavelength regions. When working with the

circular variable filter (CVF), a KCl or CaF_2 lens was employed to focus the IR emission through the narrow entrance slit (.125") of the CVF housing and onto the detector. FTIR spectral analysis was used to provide an absolute calibration of the wavelength and resolution function of the circular variable filter. CO_2 hot band emission was detected by cold gas filtering techniques whereby a gas filter cell (3.5 cm optical length, filled with CO_2) was placed between the detector and the cell window to remove emission from the $00^0 1 - 00^0 0$ and $01^1 1 - 01^1 0$ transitions.

Wavelength resolved emission from vibrationally excited CO_2 molecules produced via collisional (T-V) energy exchange with "hot" hydrogen atoms have been observed for the first time. The relative rovibrational populations of the excited CO_2 product were estimated from the amplitudes of the initial fast rise component of fluorescence (see Fig. 1a). Figure 2 shows the CVF (bandwidth, $\approx$30 cm^{-1} FWHM) spectrum of the amplitude of the fast rise emission associated with excited CO_2 product superimposed over a FTIR (IBM 85, 0.5 cm^{-1} resolution) absorption spectrum of room temperature CO_2. The amplitudes for the fast rise emission process were determined by fitting decay times and amplitudes to latter portions of the fluorescence signals and then extrapolating these amplitudes to zero time to give an amplitude for the initial fast rise component. The CVF emission profile does show coarse rotational structures which are noticeably red shifted from the ν_3 ($00^0 1 - 00^0 0$) fundamental transition indicating considerable hot band emission.

Cold gas filtering (CGF) techniques were used as a probe to study and identify the state and nature of the highly excited CO_2 product. A typical fluorescence observed through an empty filter cell exhibits three characteristic exponential components in its emission profile as shown in Fig. 1a. To isolate the emission from highly excited CO_2 states, the cold gas filter is used to effectively remove all emission terminating on the $00^0 0$ and $01^1 0$ levels

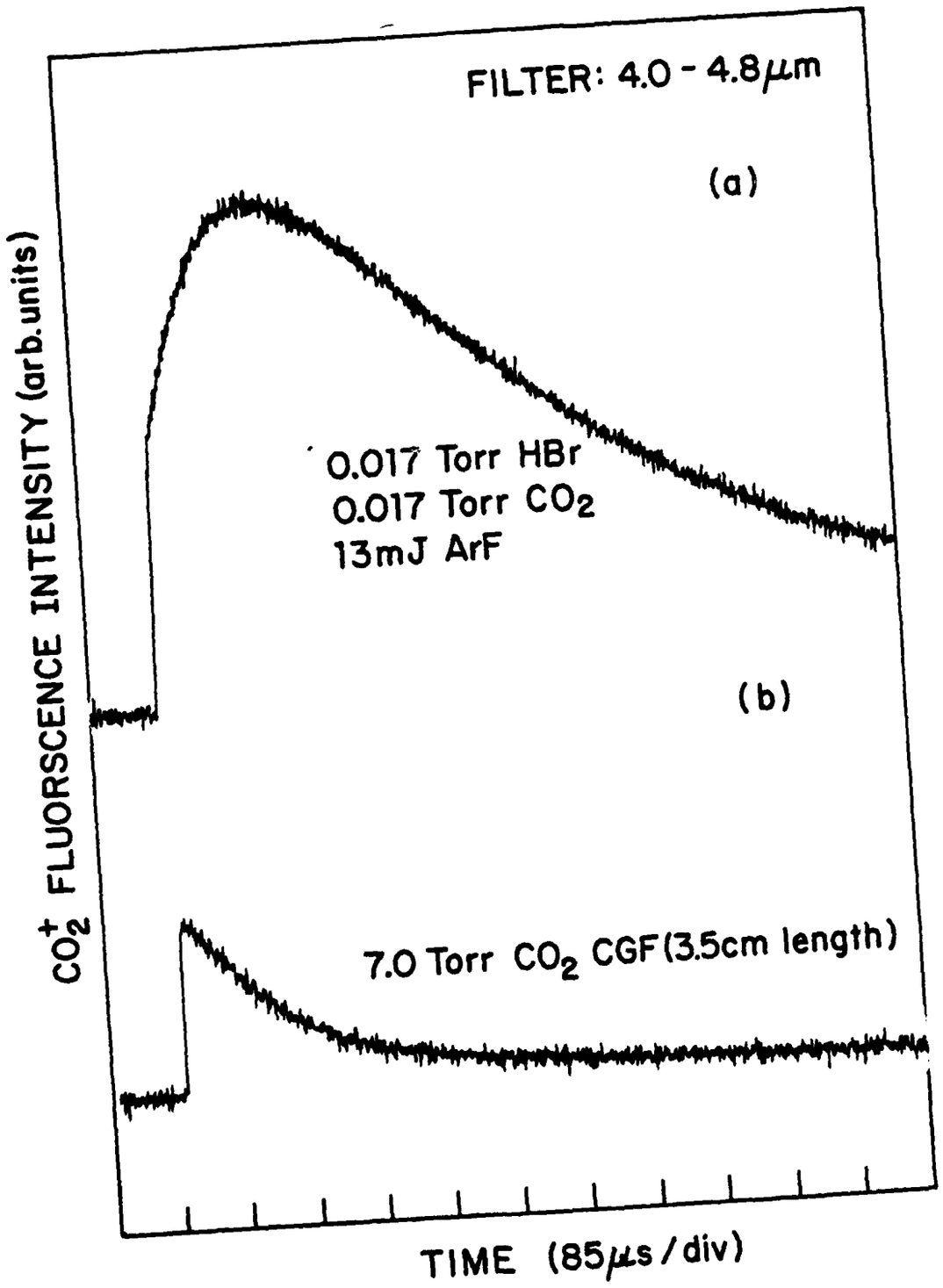
FILTER: 4.0 - 4.8μm
(a)
0.017 Torr HBr
0.017 Torr CO2
13mJ ArF
(b)
7.0 Torr CO2 CGF (3.5cm length)
CO2+ FLUORSCENCE INTENSITY (arb.units)
TIME (85μs / div)

Figure 1

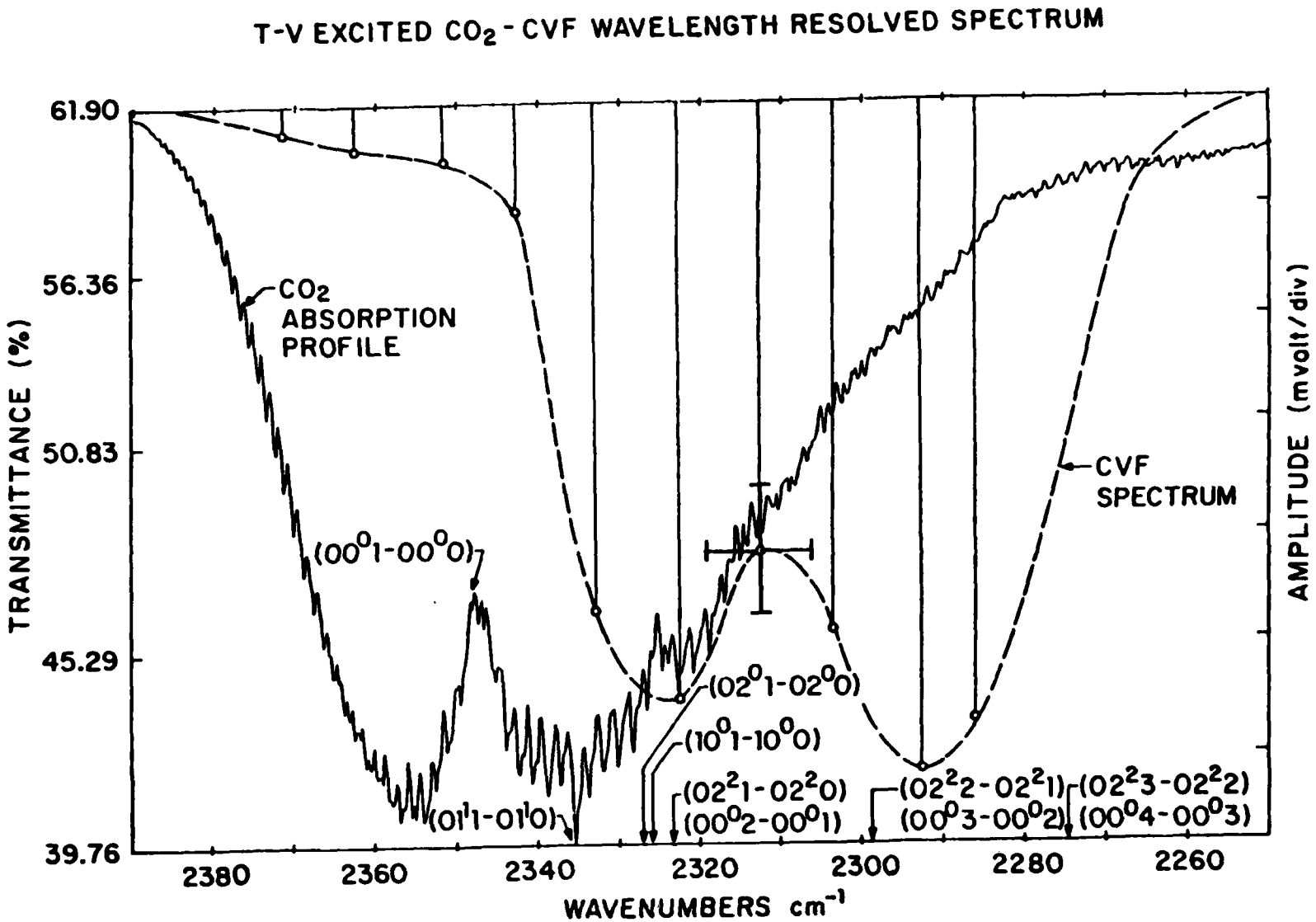
T-V EXCITED CO_2 - CVF WAVELENGTH RESOLVED SPECTRUM
61.90
56.36
50.83
45.29
39.76
TRANSMITTANCE (%)
AMPLITUDE (mvolt/div)
CO_2 ABSORPTION PROFILE
CVF SPECTRUM
(00^01-00^00)
(01^11-01^10)
(02^01-02^00)
(10^01-10^00)
(02^21-02^20)
(00^02-00^01)
(02^22-02^21)
(00^03-00^02)
(02^23-02^22)
(00^04-00^03)
2380
2360
2340
2320
2300
2280
2260
WAVENUMBERS cm^{-1}

Figure 2

filter pressure 7 torr, length 3.5 cm). The results obtained using gas filter (Fig. 1b) show a small attenuation of the initial fast onent whereas the slowly rising component is completely absorbed by r cell. This implies, in agreement with the circular variable filter data, that the fast component has contributions largely from hot band ns and possibly, from highly excited rotational states. Subsequent and R-branch filter results indicate that this emission is not due to cited J states but rather to vibrational states higher in energy than e decay rate of the 4.3 μm CO_2 fluorescence observed through the filled filter cell (see Fig. 1b) was also measured. Figure 3 shows a Stern- lot of the decay rate versus pressure which yields a relaxation rate 12 $msec^{-1}$ per torr of CO_2. Similarly at a constant CO_2 pressure, ate of approximately 20 $msec^{-1}$ per torr of HBr was observed. Without ilter cell, rates of 127 ± 16 $msec^{-1}$ per torr of CO_2 and 144 ± 11 $msec^{-1}$ Br were also obtained for the slowly rising portion of the fluorescence

large red shift in the wavelength resolved CVF spectrum of the col- y excited CO_2 molecule is strong evidence that the majority of the fluorescence emission is not due directly to the fundamental vibra- ansition of the antisymmetric stretch $00^0 1 - 00^0 0$ of CO_2 centered at Rather the emission corresponds to hot band transitions $nm^P\ell - nm^P(\ell-1)$ In particular, this suggests that during collisional excitation, the rgy transfer which produces CO_2 molecules having at least one quantum ferentially excites combination or overtone levels in the target . An estimate of the collisional excitation to the ν_3 mode was pre- ade and considered for the case with H-atoms. Bass[6] has derived expressions for the collisional vibrational excitation of the ν_3

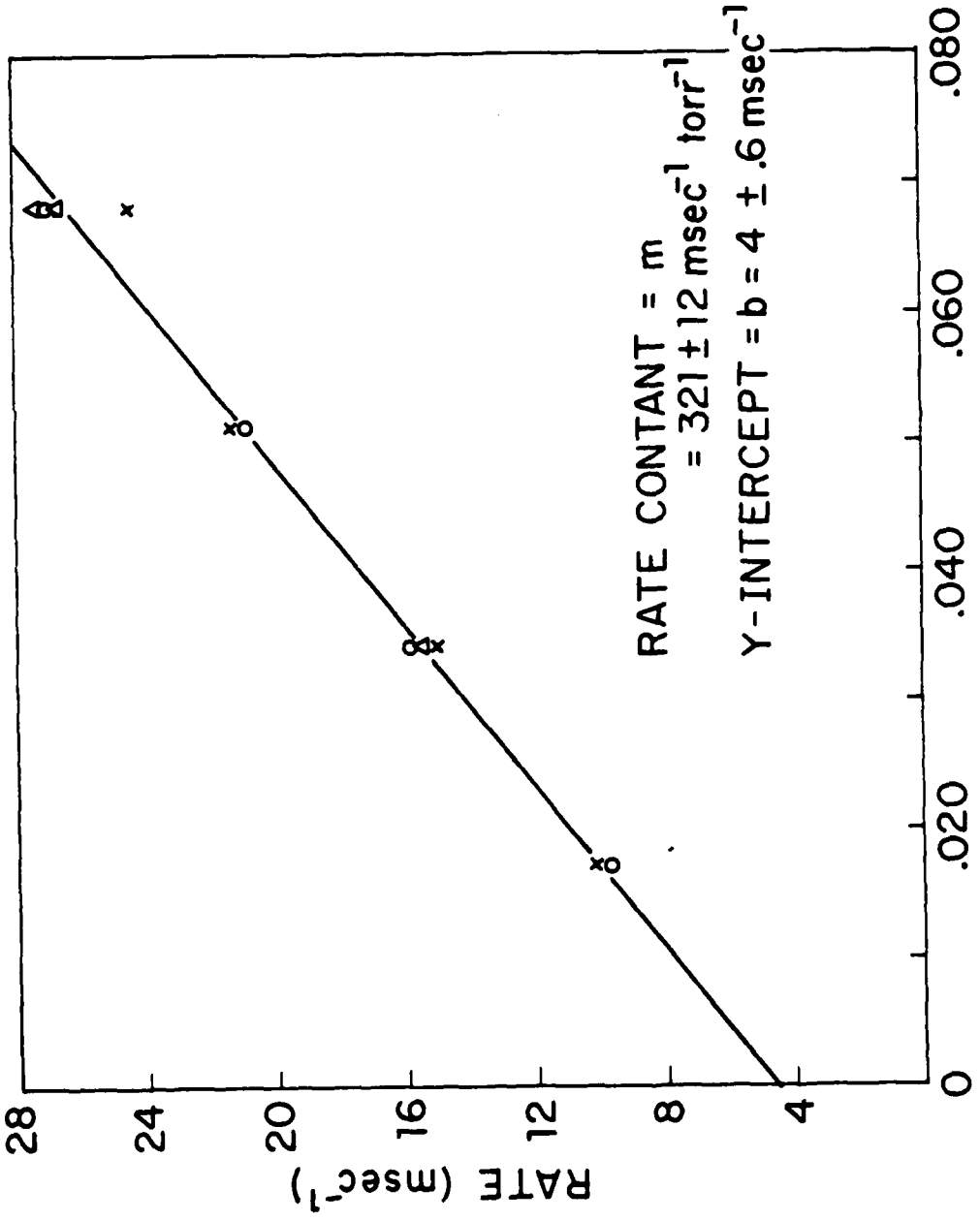
RATE CONTANT = m
= 321 ± 12 msec^{-1} torr^{-1}
Y-INTERCEPT = b = 4 ± .6 msec^{-1}
RATE (msec^{-1})
28
24
20
16
12
8
4
0
.020
.040
.060
.080
CO_2 PRESSURE (Torr)

Figure 3

mode of CO_2 which indicate that from the available center of mass translational energy the maximum vibrational energy available for the CO_2 molecule is 4290 cm^{-1}. This suggests that single collisions cannot excite levels higher than v = 1 in the ν_3 manifold (i.e. nm^p1), and the minimum translational energy necessary for pure ν_3 excitation (i.e. 00^o1) is 11186 cm^{-1}. Moreover, the combination states or hot band transitions of CO_2 which have energies less than 4290 cm^{-1} can be collisionally excited.

Vibrational energy transfer in CO_2 molecules has been studied extensively and a number of resonant vibration-vibration energy transfer ates have either been well established or recently measured. Weitz et. al.[7] have studied the equilibration of the (10^o0) and (02^o0) lower laser states in CO_2 and concluded that the coupling rate between these states is very rapid, $\geq$ 1100 $msec^{-1}torr^{-1}$. In addition ,these Fermi mixed levels are also coupled to the bending modes of CO_2,

$$CO_2(02^o0/02^20/10^o0) + CO_2(00^o0) \rightleftharpoons CO_2(01^10) + CO_2(01^10)$$

at a slower forward rate of 389 $\pm$ 75 $msec^{-1}torr^{-1}$. By comparison with the present cold gas filter results, this (V-V) transfer rate is also observed as a relaxation process following T-V excitation. This suggests that the states emitting through the cold gas filter are tightly coupled by collisions to the bending manifold. Moreover, in consideration of the estimated maximum 4290 cm^{-1} excitation at the available collisional energies, the possible excited CO_2 "hot band" transitions are $(10^o1 - 10^o0)$, $(02^o1 - 02^o0)$ and $(02^21 - 02^20)$. Under the present conditions, we are unable to resolve emission from these closely coupled Fermi mixed or degenerate combination states of CO_2.

The studies we plan to pursue to monitor the product vibrational state populations of CO_2 involves time resolved absorption spectroscopy of the target

molecules. This method employs a tunable narrowband IR diode laser to monitor and discriminate the absorption of a specific v, J → v+1, J ± 1 transition during and immediately following the T-V excitation process. In addition, time dependent absorption changes resulting from collisional process will provide information about some of the energy rearrangement and relaxation events which cannot be determined with interference filters. We have also obtained considerable data in the study of energy variation effects (i.e. mass and velocity dependence of projectiles) on the (T-V) energy transfer dynamics that occur during the collisional excitation events. These studies involve laser photolysis at 193 nm (ArF) and 248 nm (KrF) of DBr, H_2S, HCl and Cl_2 molecules as sources of light and heavy "hot" atoms to determine the effect of mass and electronics structure on the excitation of CO_2. Further energy variation is also available by using a doubled excimer pumped dye laser pulse in the region of 250-300 nm for photolysis.

*This research was also supported by the Department of Energy under Contract DE-AS02-78ER04940 and the National Science Foundation under Grant NSF-CHE80-23747.

(1) J. P. Toennies, Ann. Rev. Phys. Chem. 27, 225 (1976).

(2) E. Weitz and G. W. Flynn, Ann. Rev. Phys. Chem. 25, 275 (1974).

(3) P. J. Dagdigan, Chem. Phys. 52, 279 (1980).

(4) C. R. Quick, Jr. R. E. Weston, Jr. and G. W. Flynn, Chem. Phys. Lett. 83, 15 (1981).

(5) F. Magnotta, D. J. Nesbitt, and S. R. Leone, Chem. Phys. Lett. 83, 21 (1981).

(6) J. N. Bass, J. Chem. Phys. 60, 2913 (1974).

(7) R. K. Huddleston and E. Weitz, Chem. Phys. Lett. 83, 174 (1981).

IV. PICOSECOND ENERGY TRANSFER AND PHOTOFRAGMENTATION SPECTROSCOPY

A. GENERATION OF SINGLET OXYGEN, $^1O_2$, FROM LASER INDUCED PHOTOREACTIONS

(S. Y. Hou, C. G. Dupuy, M. J. McAuliffe, K. B. Eisenthal)
(JSEP work units 8 and 9, 1979-82)

(Principal Investigator: K. B. Eisenthal (212) 280-3175)

Singlet oxygen is significantly involved in chemical, physical, biological, atmospheric, and in recent years medical phenomena. Its spectroscopy, its novel chemistry, its role in energy and materials degradation, have made this field an extremely important and fertile one.[1] We have been engaged in using picosecond lasers to study the photodissociation pathways of molecules which yield $^1O_2$ as one of the photofragments. These processes are an important class of excited state adiabatic photoreactions[2] as well as providing a convenient photochemical source for producing $^1O_2$ and studying its photophysics and chemistry.

We have recently discovered[3] that one of the paths in the photodissociation of an anthracene endoperoxide produces not only $^1O_2$ but also an excited aromatic fragment; this represents one of the few cases of a photodissociation producing two electronically excited fragments.

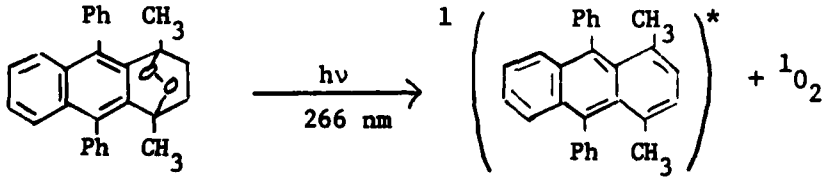

The importance of this pathway, relative to other decay routes, has a direct bearing on, and can be used to test correlation diagram predictions of the photodissociation of the endoperoxides as well as the reaction of $^1O_2$ with the

organic moiety.

An important aspect of this photodissociative route is the particular state in which the oxygen is formed. By considering the energetics of the reaction we have been able to determine the particular excited state in which $^1O_2$ is produced. From Fig. 1 we can see that it is only the $^1\Delta_g$ state which is populated in this photoreaction; the $^1\Sigma_g^+$ state being too high in energy to be reached. This finding represents the first time that the state of $^1O_2$ resulting from a photodissociation has been established.

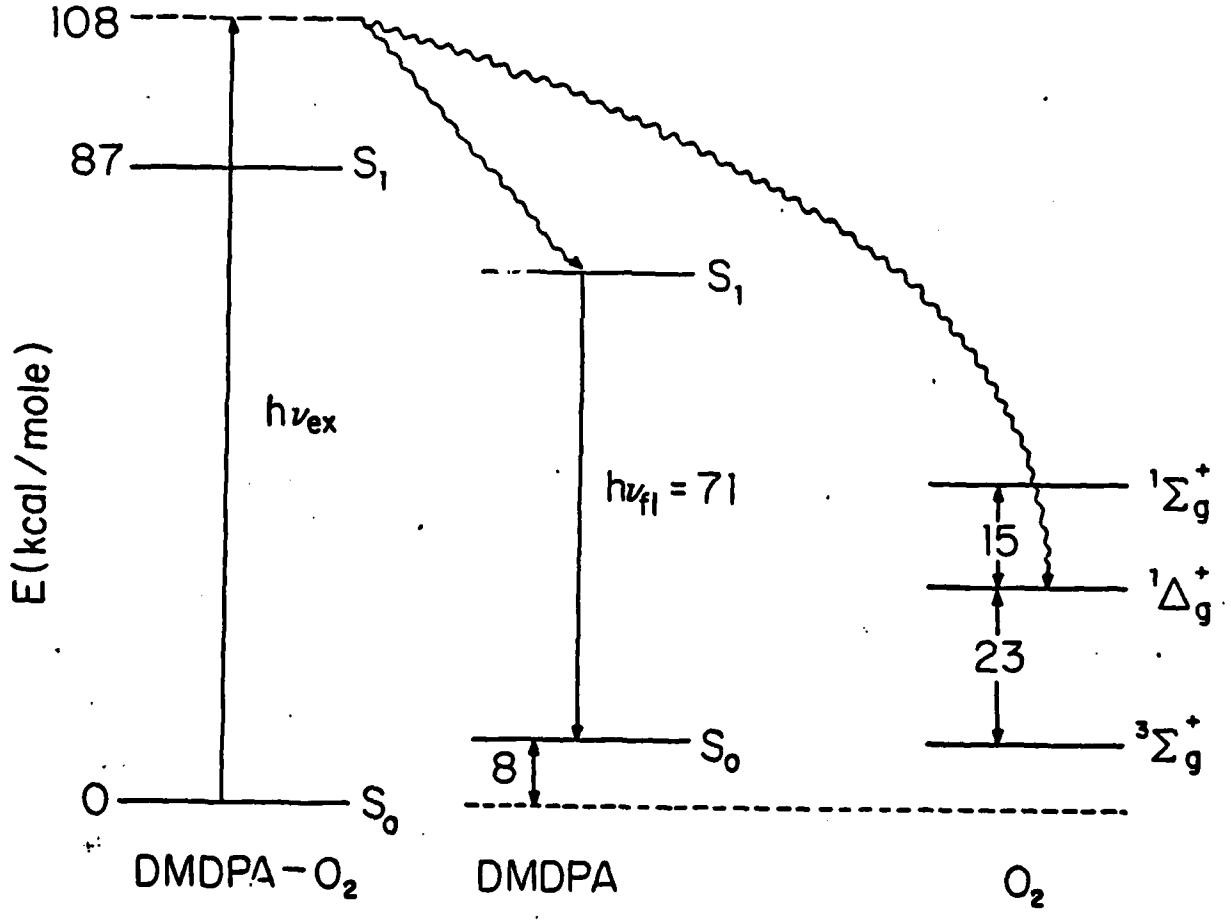

Figure 1. Energetics of endoperoxide photodissociation, λ_{ex} = 266 nm.

*This work is also supported by the Air Force Office of Scientific Research under Grant AFOSR-81-0009-A and the National Science Foundation under Grant NSF-CHE81-21945.

(1) For a theoretical and experimental discussion of $^1O_2$, its spectroscopy, and reactions, see: Wasserman, H.H.; Murray, R. W., Eds. "Singlet Oxygen", Academic Press: New York, 1979.

(2) Förster, Th. Pure Appl. Chem. 34, 225 (1973).

(3) S. Y. Hou, C. G. Dupuy, M. J. McAuliffe, D. A. Hrovat, and K. B. Eisenthal, "Picosecond Laser Study of the Adiabatic Photodissociation of an Endoperoxide". Jounral of the American Chemical Society, 103, 6982 (1981).

B. INTRAMOLECULAR CHARGE REDISTRIBUTION AND ANOMALOUS FLUORESCENCE

(Ying Wang, K. B. Eisenthal)

(JSEP work units 8 and 9, 1979-82)

(Principal Investigator: K. B. Eisenthal (212) 280-3175)

Photoexcitation can lead to significant charge separation in a molecule thereby producing a large molecular dipole.[1]-[7] The phenomenon of photo-induced charge separation is one of the most important primary processes in photochemistry and photobiology. For the molecule p-(dimethylamino) benzonitrile, DMABN,

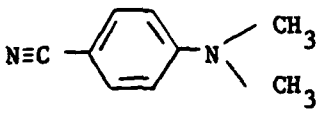

DMABN

this charge redistribution process leads to the appearance of an anomalous dual fluorescence in polar media.[1]-[7] A bond twisting event between the amino group and the benzene ring and solvation of the excited molecule are involved in the charge rearrangement.

In our picosecond laser studies[8] we have addressed the key issues of (1) the relationship between the two fluorescences, one in the ultraviolet at 350 nm and the other in the visible at 480 nm, (2) the nature of the short wavelength emission at 350 nm and (3) the role of the solvent on the dynamics of the charge transfer process.

Our results definitively show that an equilibrium is rapidly established between the short wavelength emission from S* and the visible emission from CT*, (Figs. 1 and 2), and can be depicted as follows

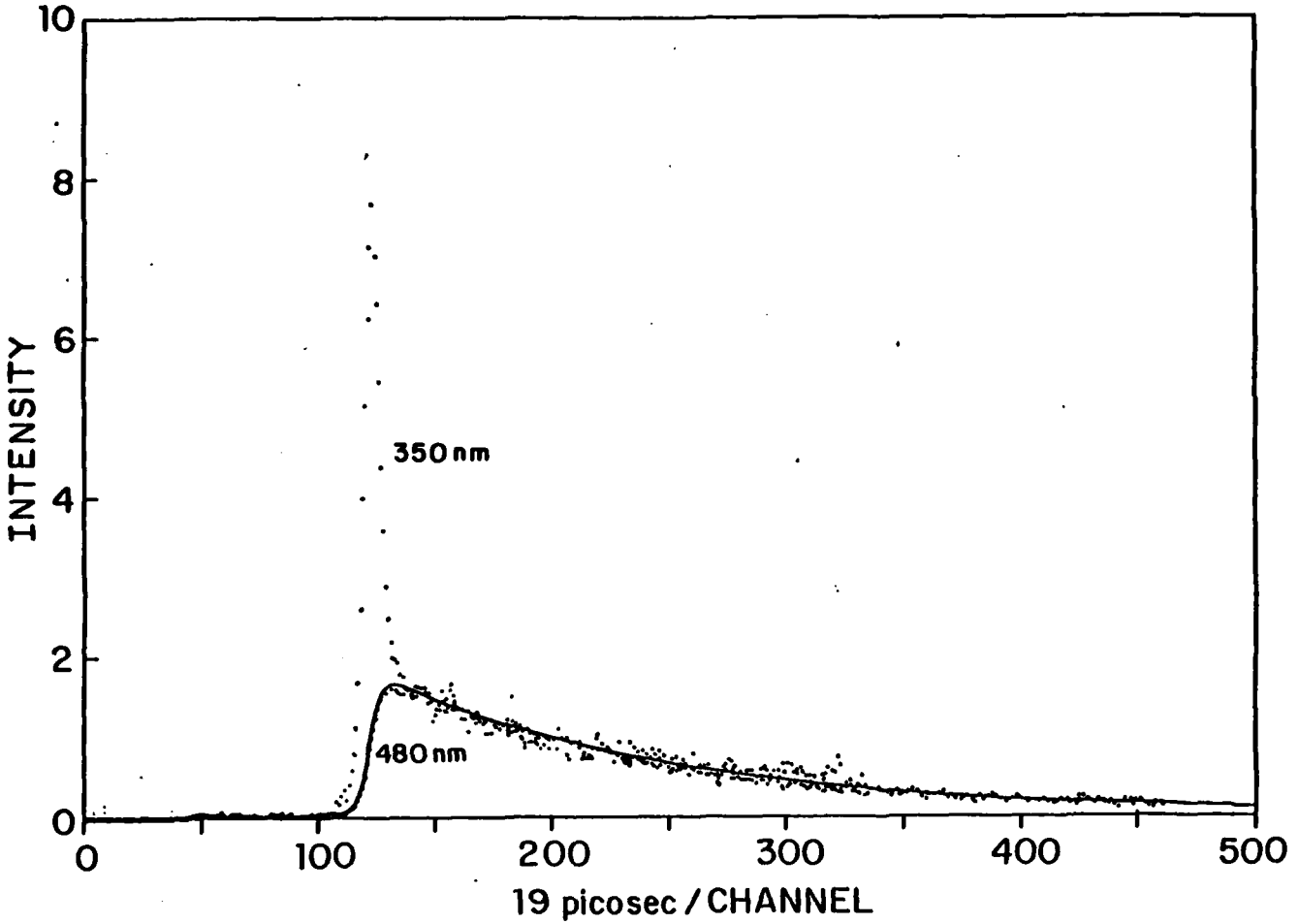

Figure 2. The DMABN fluorescence signals at 350 nm and 480 nm at slow streak speed. The solid curve is the theoretical calculation and the points are experimental data.

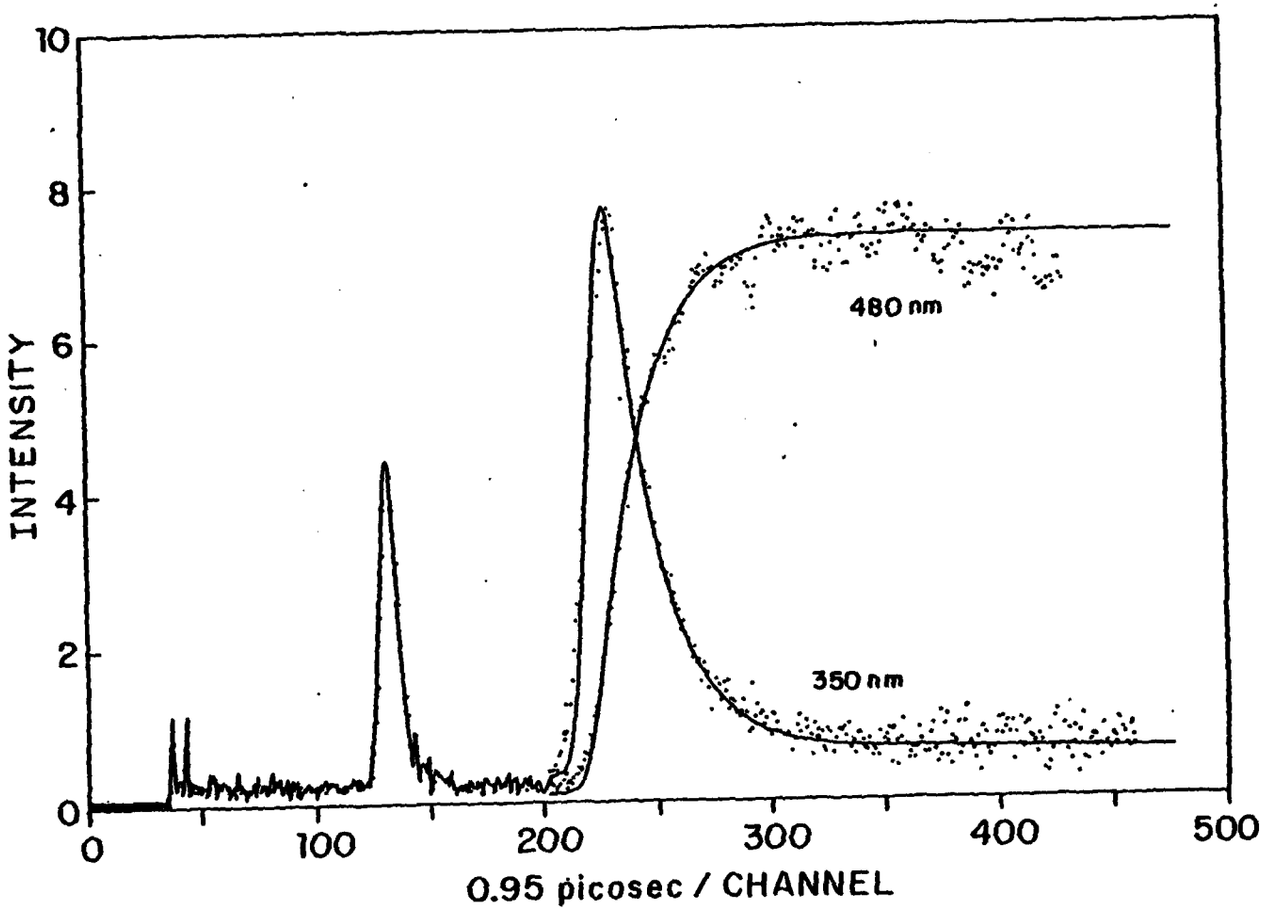

Figure 1. The DMABN fluorescence decay at 350 nm and the rise at 480 nm at fast streak speed. The solid curve is the theoretical calculation and the points are experimental data. The prepulse appearing at channel 140 is a time marker.

The emitting state S* we conclude is due to the excited singlet state S_1 which borrows intensity from S_2 by vibronic coupling. The measured time of 20 ps obtained from the reaction rates is interpreted as the time required for the molecule to relax conformationally to the twisted charge transfer geometry as shown below.

*This work is also supported by the Air Force Office of Scientific Research under Grant AFOSR-81-0009-A and the National Science Foundation under Grant NSF-CHE81-21945.

(1) E. Lippert, W. Lüder, and H. Boos, Advan. Mol. Spectrosc. 443 (1962).

(2) O. S. Khalil, J. L. Meeks, and S. P. McGlynn, Chem. Phys. Lett. 39, 457 (1976).

(3) H. Dodiuk and E. M. Kosower, Chem. Phys. Lett. 34, 253 (1975).

(4) E. A. Chandross in "The Exciplex", M. Gordon and W. R. Ware, Ed., Academic Press, New York, 1975, p. 187.

(5) K. Rotkiewicz, K. H. Grellmann, and Z. R. Grabowski, Chem. Phys. Lett. 19, 315 (1973).

(6) E. Kirko-Kaminska, K. Rotkiewicz, and A. Grabowska, Chem. Phys. Lett. 58, 379 (1978).

(7) Z. R. Grabowski, K. Rotkiewicz, A. Siemiarczuk, D. J. Cowley, and W. Baumann, Nouv. J. Chim. 3, 443 (1979).

(8) Ying Wang, M. McAuliffe, F. Novak, and K. B. Eisenthal, "Picosecond Dynamics of Twisted Internal Charge-Transfer Phenomena", The Journal of Physical Cehmistry, 85, 3736 (1981).

C. SMALL CHAIN RELAXATION OBSERVED BY INTRAMOLECULAR EXCITED STATE CHARGE TRANSFER

(Ying Wang, M. Crawford, K. B. Eisenthal)
(JSEP work units 8 and 9, 1979-82)
(Principal Investigation: K. B. Eisenthal (212) 280-3175)

The nature of rapid internal rotational motions can be obtained by determining the dynamics of reaction of the end groups on the opposite sides of the chain.[1]-[10] In our earlier studies[8],[9] we determined that exciplex (excited charge transfer complex) formation in the small chain system,

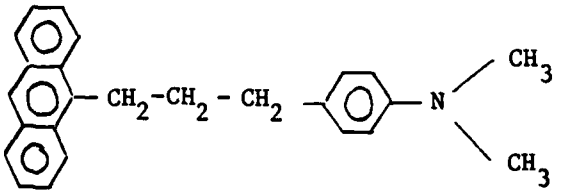

requires a favorable geometry in nonpolar solvents, most likely a sandwich type structure.

We have used picosecond laser excitation and streak camera-optical multichannel detection of exciplex fluorescence at different emission wavelengths and as a function of solvent viscosity to characterize the dynamics of the chain motions.

For the model compound we have studied we conclude that:

(1) The dynamics of exciplex formation are influenced by the starting ground state conformations. For the model compound studied, it was found that exciplexes with different emission energies were formed independently from two distinct groups of ground state conformers at different rates, *Table 1*. The structures of these conformers are not known but possibly differ in the relative orientation of the anthracene and the dimethylaniline chromophores.

(2) The observed viscosity dependence we find, Fig. 1, combined with literature values[11]-[14] for other three chain systems, points to the methylene chain motions as the key factor in determining the viscosity dependence of

Table 1

Time constants for intramolecular exciplex formation in various solvents. Uncertainty in lifetimes is ± 10%.

SOLVENT	Isopentane	Hexane	Decane	Tetradecane
Viscosity (cp)	0.22	0.33	0.92	2.18
Dielectric Constant	1.84	1.89	1.99	
Anthracene Moiety decay at 410 nm (ns)	1.4	1.9	2.8	3.8
CT Formation at 480 and 520 nm (ns)	1.4	1.9	2.9	4.1
CT Formation at 570 and 600 nm (ns)	2.0	2.6	3.8	5.5

$A-(CH_2)_3-D$

Decay of anthracene moiety and CT formation in nonpolar media. Uncertainty in lifetimes is ± 10%.

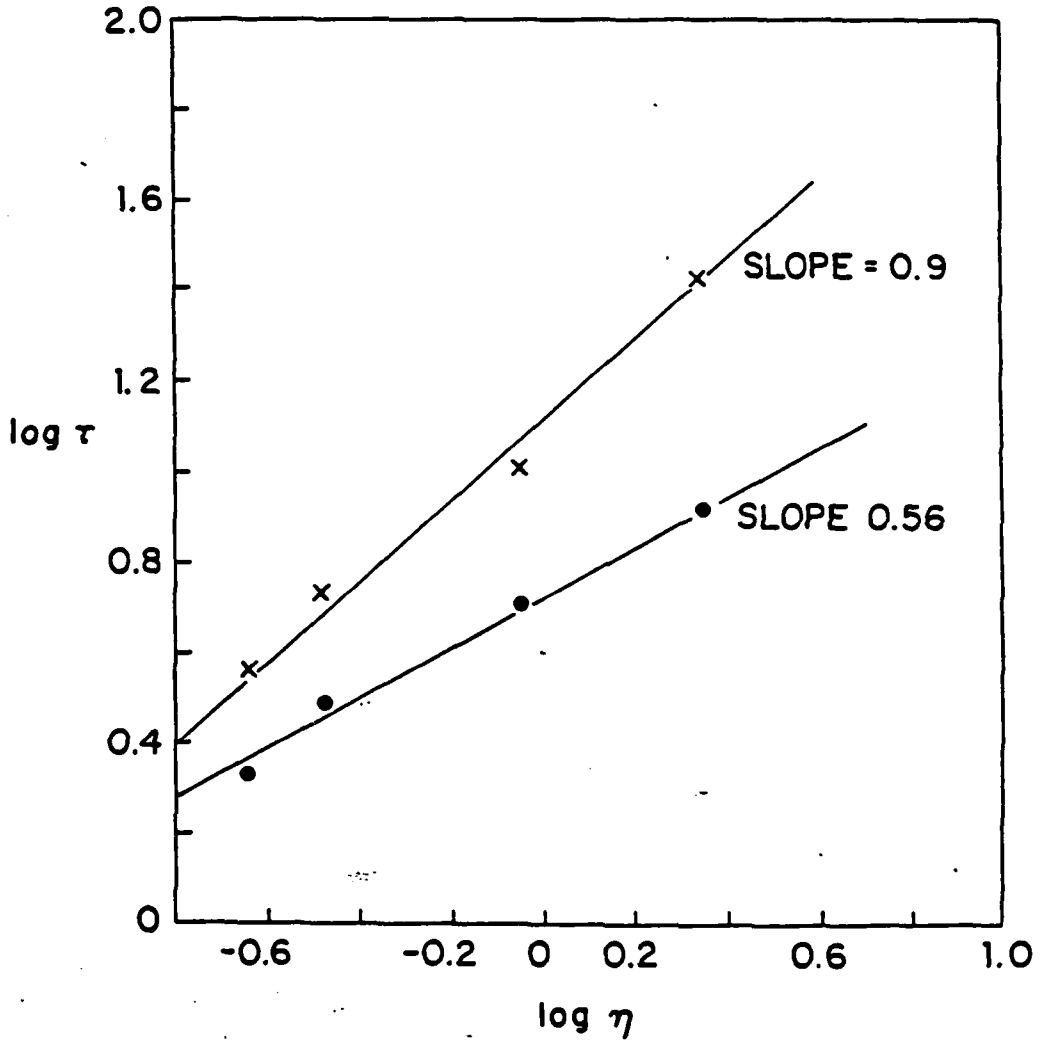

Figure 1. Plot of log of rotational relaxation time vs. log of solvent viscosity for two conformers of anthracene-$(CH_2)_3$-DMA in isopentane, hexane, decane and detradecane.

. The attached end groups alter the formation rates but not the dependence of the rates for most of the cases considered. We observe diverse cases that the lifetime of chain relaxation scales as $y)^{1/2}$.

experimentally observed exponential rise for intramolecular exciplex suggest that a single chain relaxation mode, perhaps the large scale d relaxation mode, is dominant, at least in the picosecond to nano- me regime we have examined.

t is also supported by the Air Force Office of Scientific Research it AFOSR-81-0009-A and the National Science Foundation under Grant -21945.

. Chandross and H. T. Thomas, Chem. Phys. Lett. 9, 393 (1971).

. Chuang, R. J. Cox, and K. B. Eisenthal, J. Amer. Chem. Soc. 96, (1974).

. Davidson and V. R. Tretheway, J. Chem. Soc., Chem. Comm. 827 6).

ie, Y. Sakata, and S. Misumi, J. Chem. Soc., Chem. Comm., 1009 2).

tada, T. Fujita, M. Kubota, S. Masaki, N. Mataga, R. Ide, Y. Sakata, 3. Misumi, Chem. Phys. Lett. 14, 563 (1972).

, Borkent, A. W. J. De Jong, J. W. Verhoeven, and Th. J. De Boer, Phys. Lett. 57, 530 (1978).

agst, H. J. Hamann, K. Teuchner, and S. Daehne, J. of Luminescence 25 (1978).

ng, M. K. Crawford, and K. B. Eisenthal, J. Phys. Chem. 84, 2696).

Crawford, Y. Wang, and K. B. Eisenthal, Chem. Phys. Lett. 79, 1981).

M. A. Winnik, Acc. Chem. Res. 10, 173 (1977).
M. A. Winnik, Chem. Rev. 81, 491 (1981)

Johnson, J. Chem. Phys. 63, 4047 (1975).

Yang, S. B. Neoh, T. Naito, J. K. Ng, D. A. Chernoff, and McDonald, J. Am. Chem. Soc. 102, 2806 (1980).

(13) P. Avouris, J. Kordas, and M. A. El-Bayoumi, Chem. Phys. Lett. 26, 373 (1974).

(14) K. A. Zachariasse, W. Kühnle, and A. Weller, Chem. Phys. Lett. 59, 375 (1978).

V. GENERATION AND CONTROL OF RADIATION

A. OPTICAL COHERENT TRANSIENT SPECTROSCOPY

(R. Beach, E. Whittaker, E. Xu, R. Kichinski, M. Glick, S. Hartmann)
(JSEP work units 10 and 11, 1979-82)
(Principal Investigator: S. R. Hartmann (212) 280-3272)

During the last year, our laboratory has undergone a major overhaul. We acquired a second Quanta Ray YAG laser which motivated us to develop a centralized laser facility in which a pair of YAG lasers could be used simultaneously in several different laboratories. Stable beam steering optics had to be developed to separately image each YAG into the several laboratories. Currently, the two YAGs are located next to each other with ~30% of their output split off for use in the room in which they are housed and the other 70% steered into a duct suspended just below the ceiling so as to be out of the way of traffic within the rooms. The duct work containing the laser beams passes into two other laboratories each of which uses half of the remaining 70% of the laser light. We are now in the process of extending the laser beam line into a fourth laboratory.

The YAG lasers pump tunable dye lasers in the different labs. Here again we revamped our system by building a set of ten new dye lasers and amplifiers of the Littman design as improved by Frank Tompkins of Argonne Laboratories. These new lasers are easy to use, stable, have a narrow linewidth of the order of 1 GHz, and are a significant improvement over our previous Hänsch design. There is also an advantage in several workers using identical lasers as expertise, new approaches, good ideas, etc. are readily transferred and adapted. The feasibility of the system was proven when we saw stable photon echoes in the laboratory furthest removed from the YAG lasers. In fact, no retuning or refocusing were necessary to generate echoes when the system was turned back on a week later. This observation was quite conforting as it tested the stability

not only of the YAG beam transport system but of the dye lasers and the echo generating set-up as well. Since the echoes were generated by using two different dye lasers to provide the excitation pulse pairs, rather than an optical delay line with a single dye laser, the test was quite demanding. The very narrow pulsed dye laser linewidth is achieved by pumping the dye lasers lightly, so laser amplifiers are necessary to attain sufficient laser pulse power. These also have been totally successful, as demonstrated by the above-mentioned echo experiment. We now routinely and simultaneously achieve pairs of 100 kW 1 GHz-wide laser pulses in each of three laboratories. Before our change over, all pumping was done by separate homemade N_2 lasers, each of which put out no more than 100 to 200 kW of pump power when and if they worked. Our dye lasers now provide as much power as our pump lasers previously provided and the reliability and stability have been significantly increased.

The great advantage of having two YAG lasers is that we can create and control a continuously variable time separation between them - with remote electronics - and thereby do experiments to directly study echo modulation and relaxation. Implementation of the electronic system to achieve this control was itself a major accomplishment. Finally, the problem of a residual one or two nanosecond jitter in pulse separation is circumvented by a detection scheme which directly measures the pulse separation to within a few hundred picoseconds and labels the corresponding data accordingly.

At the tail end of the laboratory overhaul we are replacing our obsolete PDP8 computer system with a multi-user LSI 11/23. Separate stations will be placed in the individual laboratories to allow for a more efficient operation than was possible when our one PDP8 had to be physically wheeled from lab to lab as demand required.

During the laboratory overhaul research progress proceeded as manifested in the Billiard Ball Echo model.[1] Photon echoes in gaseous media have up

to now been treated in a rather formal manner. This is unfortunate particularly because photon echo phenomena display a wide variety of forms. Aside from the two pulse photon echo and the three pulse stimulated photon echo there are Raman echoes, tri-level echoes, grating echoes, two photon echoes, etc. Each echo has its particular application and a simple uniform treatment would facilitate the proper general understanding and application of the echo technique. Such a treatment is now available with the Billiard Ball Echo model.[1]

The Billiard Ball Echo model takes an unconvential view of nonlinear optics. The key is atomic recoil. When an atom is excited to a higher atomic state by absorbing light it must recoil with the momentum of the absorbed photon. An atom which has been subjected to irradiation by a light pulse thus finds itself in a linear superposition of its ground and excited states with its excited state recoiling away from its ground state. A $\pi/2$ light pulse has a 50% probability of putting an atom into its excited state so the atom has equal probabilities of being left alone and not recoiling or being excited and recoiling with the momentum of the absorbed photon. Since the coherently excited atoms are in a linear superposition of these states they effectively split apart. But the atom's ability to radiate coherently proportional to its radiative dipole moment $\langle pe^{i\vec{k}\cdot\vec{r}} \rangle$ (where p is the dipole moment operator and $\vec{k}$ is the photon wave vector) which depends on the overlap of these ground and excited states. Thus as the "atom" splits apart the coherent radiation it emits diminishes.

The universal trick to generate photon echoes of whatever type is to irradiate the atoms with a such a series of pulses as to split its component parts apart and then to bring them back together again. The analysis is just a simple matter of mechanics. Each laser pulse resonant with an optical transition splits the atom apart, its component parts recoiling as the laser pulse stimulates the atom to emit or absorb a photon. We need only keep track

of atomic recoil to determine when and if an echo will occur. Since all atoms recoil in identical manner we need only consider one atom. We illustrate this idea with the well known, basic, two-pulse case. In Figure 1 we display the atomic recoil for the simple case where the two excitation pulses are collinear. The ground state trajectory is represented by a solid line and the excited state trajectory by a dashed line. The atom is initially in its ground state and since it is therefore not recoiling its trajectory is horizontal as indicated. At $t = 0$ a $\pi/2$ laser pulse excites the atom into a linear superposition of its ground and excited states so the trajectory behaves as shown in Fig. 1. Only the excited state trajectory indicates recoil as only the excited state has absorbed a photon. The trajectory slope is given as $\hbar k/m$ where m is the atomic mass to represent the recoil velocity. The short wiggly line at the vertex at $t = 0$ indicates the absorption of a photon. The atom proceeds to separate at a uniform rate until $t = \tau$ when a second collinear excitation pulse arrives. This pulse is adjusted to have area π so its effect is as shown. The ground state atom component has 100% probability of absorbing a π pulse (the definition of a π pulse) and so it is transformed entirely into an excited state component with a recoil trajectory of slope $\hbar k/m$. The excited state component, on the other hand, is stimulated with 100% probability to emit a photon of momentum $\hbar k$. It thus recoils backward and since it was originally created by the absorption of an identical photon, it stops in its tracks. We thus have the situation of the newly created ground state component standing motionless while the newly created excited state component approaches it with velocity $\hbar k/m$. When overlap reoccurs the radiative moment reforms and a burst of radiation is emitted. This is the photon echo. The short wiggly lines in the diagram indicate the absorption or emission of radiaton due to the action of the laser excitation pulses, or emission from the renewed overlap of the component parts of the atoms.

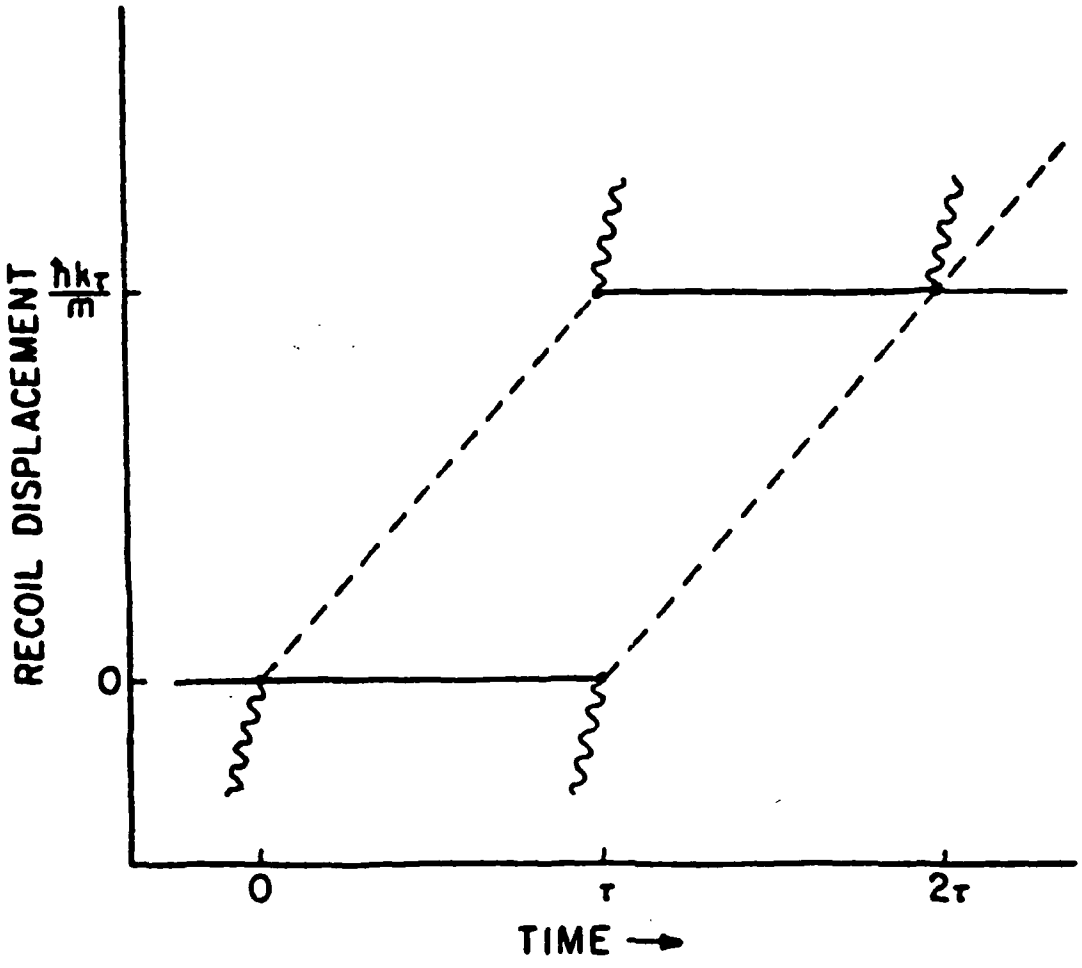

Figure 1. Recoil diagram for a two pulse photon echo formed by applying a $\pi/2$ pulse at $t = 0$ followed by a π pulse at $t = \tau$. The echo forms at $t = 2\tau$. The ground and excited state trajectories are indicated by solid and dashed lines respectively. The short wiggly lines at the vertices represent photons that are either absorbed or emitted.

The above analysis requires no formulas or complicated mathematical analysis - no Schrödinger's equation! Nevertheless, the analysis is readily extended to much more complicated scenarios where noncollinear laser pulses separately resonant to different optical transitions are applied.

This analysis is rather unconventional and experts in the field of nonlinear optics have been uncomfortable with it at first since it doesn't immediately seem to corollate with well-known phenomena. Consider for example the free radiation decay from a gas of atoms excited by a single resonant laser pulse. In its simplest form a $\pi/2$ pulse coherently excites the atoms in a gaseous sample into a linear superposition of their ground and excited atomic states and the atoms then proceed to radiate coherently. The convential view is that since the atoms of a gas are moving, they radiate at Doppler shifted frequencies. The atoms are in a Maxwell Boltzmann distribution for the given gas temperature T, so the coherent radiation disappears due to Doppler dephasing in a time depending on T.

The dephasing time is the time it takes atoms to move away from each other by some critical distance. When atoms initially excited in phase separate by the order of an optical wavelength they destructively interfere. Writing $v_{Doppler}$ to represent the Doppler velocity spread, the dephasing time $\tau_{dephasing}$ is determined from

$$v_{Doppler}\tau_{dephasing} = \lambda_{optical}$$

where $\lambda_{optical}$ is the optical wavelength of the radiative transition excited. This can be cast in a more obvious form by writing $v_{Doppler}$ in terms of a de Broglie wavelength $\lambda_{thermal}$ of the atom, $mv_{Doppler} = \hbar/\lambda_{thermal}$. The dephasing time is then expressed as

$$\tau_{dephasing} = (m/h)\lambda_{optical}\lambda_{thermal}$$

The thermal wavelength $\lambda_{thermal}$ can be seen as the size of a wave packet constructed from the Maxwellian distribution of momentum states which describe the gas at temperature T. In the context of the Billiard Ball model it is what we might consider the size of the atom. Thus the time $\tau_{splitting}$ for the atom to split apart is given by

$$v_{recoil}\,\tau_{splitting} = \lambda_{thermal}$$

where v_{recoil} is the atomic recoil velocity. This recoil velocity is obtained by equating atomic recoil momentum to photon momentum,

$$mv_{recoil} = \hbar k$$

so

$$mv_{recoil} = \hbar/\lambda_{optical}$$

and $\tau_{splitting}$ becomes

$$\tau_{splitting} = (m/h)\lambda_{optical}\lambda_{thermal}$$

which is identical to the expression for $\tau_{dephasing}$.

$$\tau_{splitting} = \tau_{dephasing}$$

and the unconventional point of view taken by the Billiard Ball model leads to conclusions in accord with previous experience. A thorough discussion of the Billiard Ball Echo model appears in Ref. 1.

Until now photon echoes have been confined to those cases where the laser excitation is within a wave numbers of exact resonance. We now report preliminary experiments which lift this restriction. Using a laser working at 6854 Å we have succeeded in generating second harmonic radiation (SHG) by applying a transverse magnetic field. The second harmonic of 6854 Å is at 3427 Å the frequency of the 3D-3S transition in Na; the intermediate 3P state at 5890 Å is far removed from the 6854 Å laser frequency. At a number density of order $10^{16} cm^{-3}$ and in a magnetic field of $\sim$100 gauss we obtain a harmonic generation efficiency of 2×10^{-5}. Our analysis suggests that much higher efficiencies are possible at higher values of the transverse magnetic field.

The detection of SHG means that the atoms have been excited in a linear superposition of the 3S and the 3D states by radiation of half the transition frequency. We plan next to generate a two-photon echo directly on the 3S-3D transition using laser excitation at half the transition frequency and detecting the echo at the full transition frequency.

This experiment has not been done but we have tried another experiment which suggests that the direct two-photon echo is feasible. The experiment is to irradiate Na atoms with two laser pulses, one at 5890 Å and one at 6854 Å. We observe an echo at 8200 Å. This is an entirely new kind of two pulse photon echo experiment. It is readily analysed by means of the Billiard Ball Echo model. Let the 5890 Å pulse be applied at $t = 0$. This excites the 3P state which recoils as indicated in Fig. 2. The 6854 Å pulse then excites the 3D state at $t = \tau$, each atom absorbing two 6854 Å photons and recoiling as indicated in Fig. 2. Following the recoil trajectories in Fig. 2 we note that component parts of the atoms corresponding to the 3P and the 3D states should cross at

$$\tau_e = \frac{5890\ \text{Å}}{5890\ \text{Å} - \frac{1}{2}\ 6854\ \text{Å}}\ \tau = 2.39\ \tau\ .$$

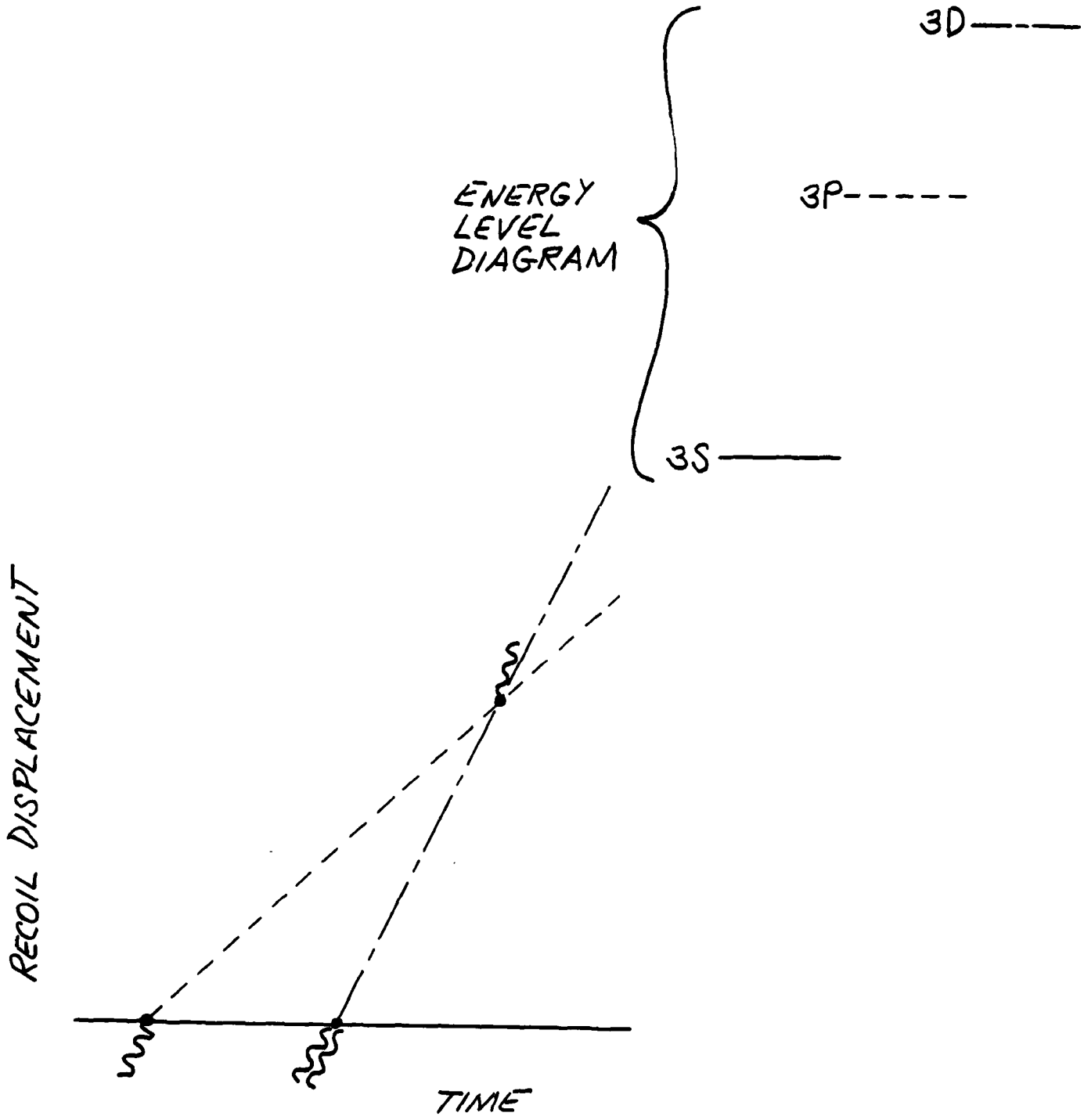

Figure 2. Recoil diagram for a two-pulse - two-photon trilevel echo. A $\pi/2$ pulse exciting a single photon transitions is followed by a $\pi/2$ pulse exciting a two-photon transition. The echo is emitted when the recoiling excited states overlap.

In our experiment when τ = 20 nsec we see an echo at τ_e = 47.8 nsec. This experiment demonstrates the viability of the basic two photon technique.

From the two photon echo experiment on the 3S-3D transition we will be able to determine the relevant collision cross-section. In our previous study of 3S-nD collisional relaxation by the tri-level echo technique we went from principle quantum number n = 4 to n = 40.[2] The tri-level echo for n = 3 was not accessible because the technique depends on the energy separation of the 3S-3P transition being less than the 3P-nD which is not true for n = 3.

Another interesting preliminary experiment in Na vapor involves the generation of what we must now call ordinary two-pulse photon echoes excited on the 3S-4P transition. This is the first time two-pulse ground state echoes have been observed on other than the 3S-3P transition. This was accomplished by frequency-doubling a laser excitation pulse to coincide with the 3302 Å, 3S-4P transtiion. This transition is interesting because its lifetime is about seven times longer than the 3S-3P lifetime. It is therefore an interesting candidate for study of the effect of velocity changing collisions in Na vapor, to complement our recent work in Li vapor.[3]

In the process of generating the 3S-4P echo we observed cascade superradiance from the 4P to 4S to 3P and the 4P to 3D to 3P levels. This has also been seen by other workers;[4] what is new is that we also saw coherent radiation in the 3P-3S transition. Whereas the superradiant bursts seen by others could be seen at both the input and output parts of the Na sample cell the 3P-3S radiation was observed only at the output end. Here we have a true four-photon process. Our present set-up limits us to excitation pulses no shorter than 6 nsec. By shortening the excitation pulse to 1 nsec we hope to observe the coherent 3S-3P radiation after the excitation pulse is gone, thereby demonstrating a superradiant state phase transfer.

In another experimental set-up we have been improving on the basic echo measurement technique. The idea is to use non-parallel excitation pulses to permit non-electronic preliminary separation of the exciting beams. It is well known that an echo is radiated with a polarization density whose k vector is given by $\vec{k} = 2\vec{k}_2 - \vec{k}_1$, where $\vec{k}_1$ and $\vec{k}_2$ are the wavevectors of the first and second excitation pulses. With high intensity lasers broad sample areas can be irradiated, so that it is possible to switch an unattenuated echo far out of the beam divergence of initial laser pulses. For a beam of diameter D the diffraction limited beam divergence θ is given by $\theta = 1.22\ \lambda/D$ where λ is the wavelength of the coherent light. For a sample of length L, on the other hand, it is necessary that at least $\Delta kL < \pi/4$ for the polarization density to contribute uniformly throughout the sample without destructive interference. If $\vec{k}_2$ makes an angle Θ with $\vec{k}_1$ then as long as $\Theta << 1$ it is correct to write $\Delta k - \Theta^2 k$. Thus, choosing $\Delta kL = \pi/4$, we find

$$\Theta/\theta = D/\sqrt{8\pi\ \lambda L}$$

which is generally much larger than one.

Our present angled beam system achieves enough rejection of the excitation pulses to allow echo detection 100 nsec after the first excitation pulse. For a sample gas of lithium this corresponds to about four lifetimes. Further excitation pulse rejection is achieved by using an acoustic-optic modulator switch. Overall excitation pulse rejection already exceeds 10^7 and we expect to be able to improve that considerably. One last trick is to apodize the initial laser beam, taking advantage of the fact that in the focal plane of a lens placed in the laser beam the light field is the Fourier transform of the light field before the lens. Apodizing in a Gaussian manner achieves a Gaussian profile which decreases beam intensity outside the beam divergence. This particular apparatus will be very valuable for all echo techniques, but

especially those involving sub-Doppler linewidth measurements. We already, for example, are able to "beat" the uncertainty principle by observing echoes in Li vapor 15 lifetimes after the exicted state population has died away - the "life after death" effect.

We have also completed a theoretical analysis of the effects of velocity changing collisions in optical experiments.[5] To further aid in our study of velocity changing collisions we have set-up a cw dye laser to burn holes in the Doppler line. With this we will be able to modify the effective Doppler profile and thus achieve more experimental control.

Further measurements and analysis of photon echo modulation in the $^1D_2$ - $^3H_4$ optical transition in Pr^{3+}:LaF_3 have resulted in a more precise evaluation of the spectroscopic and relaxation characteristics of this system. Fourier transformation of the modulation yields the hyperfine splitting frequencies and the related linewidths.

The resonance widths of Pr^{3+}:LaF_3 reflect the total (inhomogeneous and homogeneous) nuclear linewidths of the various hyperfine transitions. Previous measurements[6],[7] have shown the ground state widths to be about 200 kHz. This width is mostly inhomogeneous and arises from the interaction of the enhanced ground state ^{141}Pr nuclear moment of 11.5 kHz/G with the surrounding distribution of static ^{19}F nuclear moments. Macfarlane and Shelby[7] have measured the g-tensor for the $^1D_2$ state and found the enhancement to be roughly one-fifth as much as in the ground state. This would lead one to expect a much narrower linewidth for the nuclear transitions in the $^1D_2$ state and our measurement, while very nearly resolution-limited by the overall echo decay envelope, establishes a new upper limit of 30 kHz [FWHM] for the hyperfine line at 8.51 Mhz, consistent with this expectation. The linewidths of the hyperfine at 3.72 and 4.79 Mhz are somewhat larger, being 70 kHz and 60 kHz respectively. The results for the $^1D_2$ excited state parameters are summarized in Table 1.

Table 1

Resonance	Frequency	Full width at half max
ω_1^e	3.72 ± 0.02 MHz	70 ± 20 kHz
ω_2^e	4.79 ± 0.02 MHz	60 ± 20 kHz
ω_{12}^e	8.51 ± 0.02 MHz	30 ± 30 kHz

able 1: Values for the $^1D_2$ excited state hyperfine frequencies
id nuclear linewidths obtained from the Fourier transform of the
ita. The linewidths have been corrected for the effect
f the finite truncation interval.

The effective hyperfine Hamiltonian is given by

$$H_{g(e)} = P_{g(e)} \left[I^2_{z(Z)} + \frac{\eta_{g(e)}}{3} \left(I^2_{x(X)} - I^2_{y(Y)} \right) \right] \qquad (1)$$

where $P_{g(e)}$ and $\eta_{g(e)}$ are interaction constants. The upper and lower case subscripts emphasize that the ground (g) and excited (e) state principal axes need not be the same, although Neumann's principle requires that they have at least one common axis parallel to the local C_2 symmetry axis. This constraint significantly reduces the number of possible orientations and we may represent these possibilities on a two-dimensional map.[3] The coordinates of such a map give the particular choice of common axis, and the angle θ through which one set of axes is rotated with respect to the other set about the common axis. Since the Hamiltonian in Eq. 1 is insensitive to the sign of the coordinates an orientation of, say, $\hat{x} \parallel \hat{X}$ is equivalent to $\hat{x} \parallel -\hat{X}$. We have calculated the echo modulation in increments of five degrees in the rotation angle θ. In the map presented in Fig. 3, for each orientation coordinate a box is drawn whose width is proportional to the minimum mean square deviation between our data and the calculated modulation. Only the first microsecond of data were used in the fitting procedure for Figure 3. Beyond one μsec. the data are dominated by the excited state hyperfine splittings, due to the relative linewidths of ground and excited state levels, and including these data in the fit considerably reduces the selectivity of the map.

Figure 4 shows in expanded scale the first three μsec of the data, and Figure 5 shows the theoretical curve that was calculated using the orientation coordinate giving the best fit to the data (as indicated by an arrow in the lower left of Figure 3).

The map in Figure 3 shows a high degree of symmetry and concommitant lack of selectivity for determining the orientation parameter. To explore the

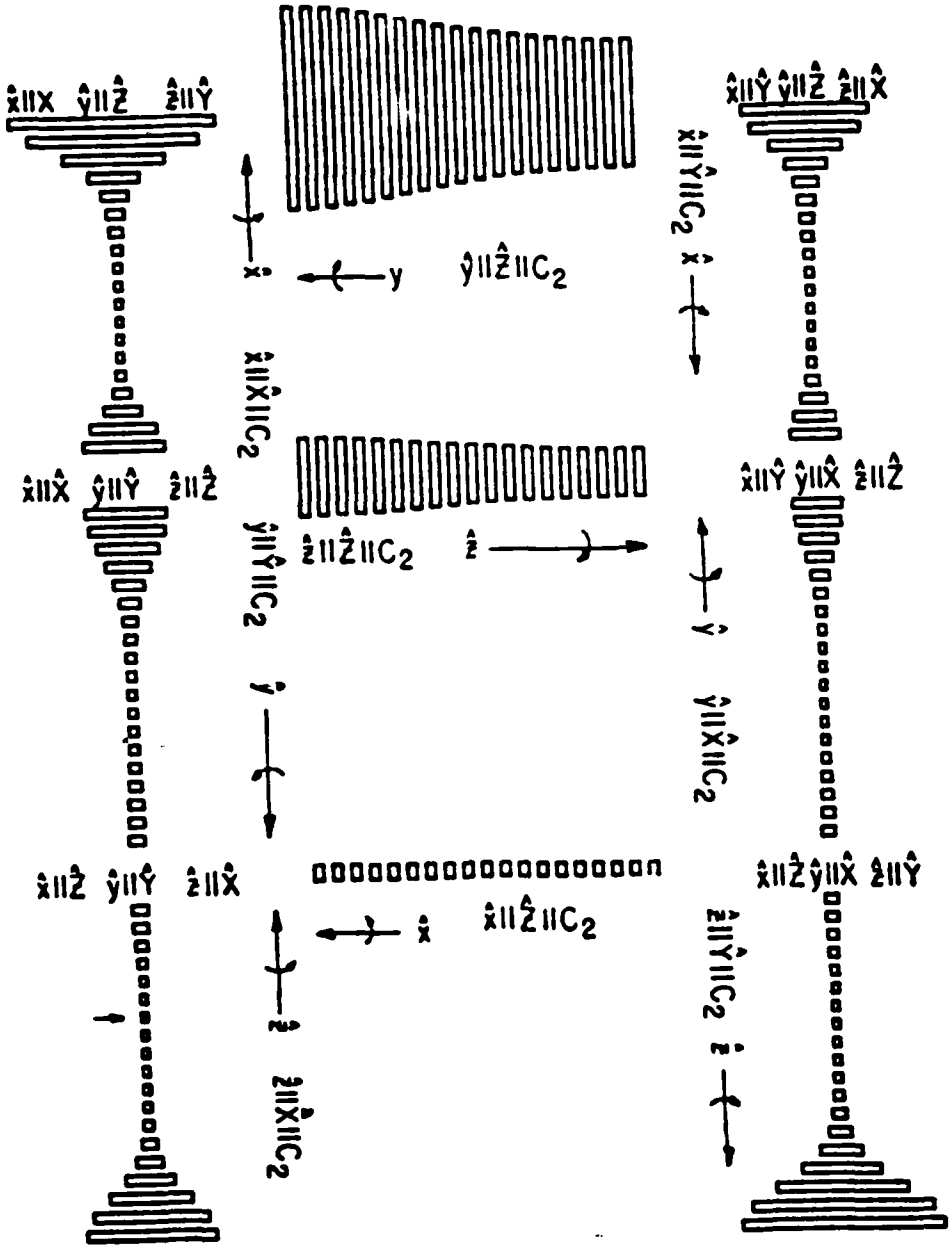

Figure 3.

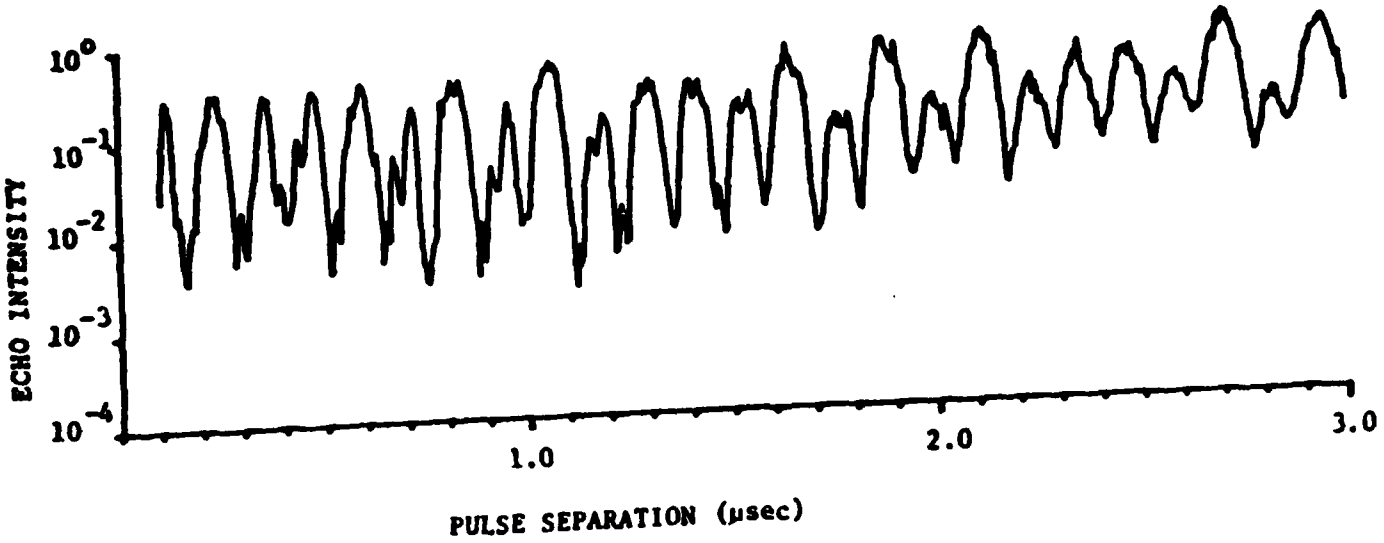

Figure 4. Echo intensities for pulse separations up to 3 μsec.

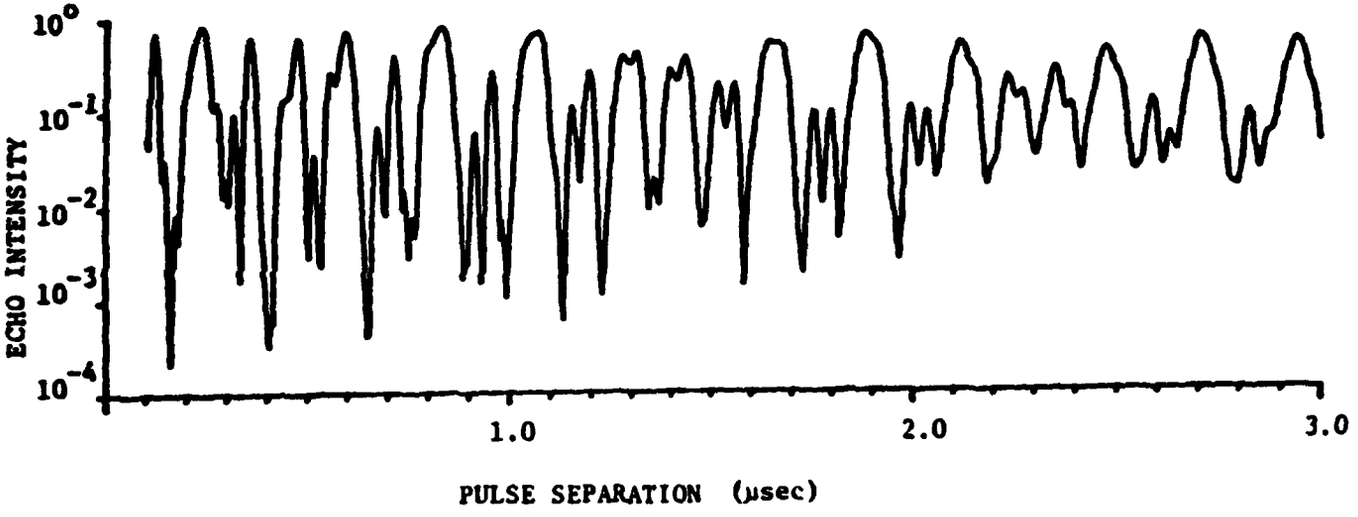

Figure 5. Theoretical dependence at echo intensity on pulse separation for the orientation coordinate giving the best fit to the data (as indicated by the arrow in Fig. 3).

extent to which this symmetry is intrinsic, we have substituted for the data used to calculate the map of Figure 3 the values of the theoretical modulation corresponding to Figure 5, producing the map shown in Figure 6. The scale in Figure 6 was chosen to make the box corresponding to the coordinate with the worst fit in Figure 6 approximately the same size as the box with the worst fit in Figure 4. It is apparent that the high degree of symmetry persists. To estimate the extent to which our signal-to-noise would have to improve to allow us to select one orientation with certainty, we replotted Figure 6 with the box width scale expanded by a factor of ten, as shown in Figure 7. It appears that an improvement in signal-to-noise by a factor of ten or twenty would have made possible a more definitive statement about the orientation. This improvement will probably come from the use of frequency and amplitude stabilized dye lasers. Frequency jitter in particular causes considerable fluctuation in echo intensity, presently averaged by the data-taking system, and such averaging tends to wash out some of the fine details of the modulation pattern. Despite the high symmetry, we can draw a number of conclusions about the relative orientation. All configurations with all axes parallel are ruled out, as are those with the excited state Z-axis parallel to C_2. These conclusions are similar to the measurement of Chen et al.,[6] on the relative orientation of the $^3H_4$ and $^3P_0$ states. Since the g-tensor is nearly isotropic in the $^1D_2$ state[7] and absent completely in the $^3P_0$ state the relative orientation parameter must be primarily determined by the relative orientation of the pure quadrupole tensor with respect to the ground state hyperfine tensor.

*This research was also supported by the National Science Foundation and the Army Research Office under Grant NSF-DMR80-06966 and the U. S. Office of Naval Research under Contract No. N00014-78-C-0517.

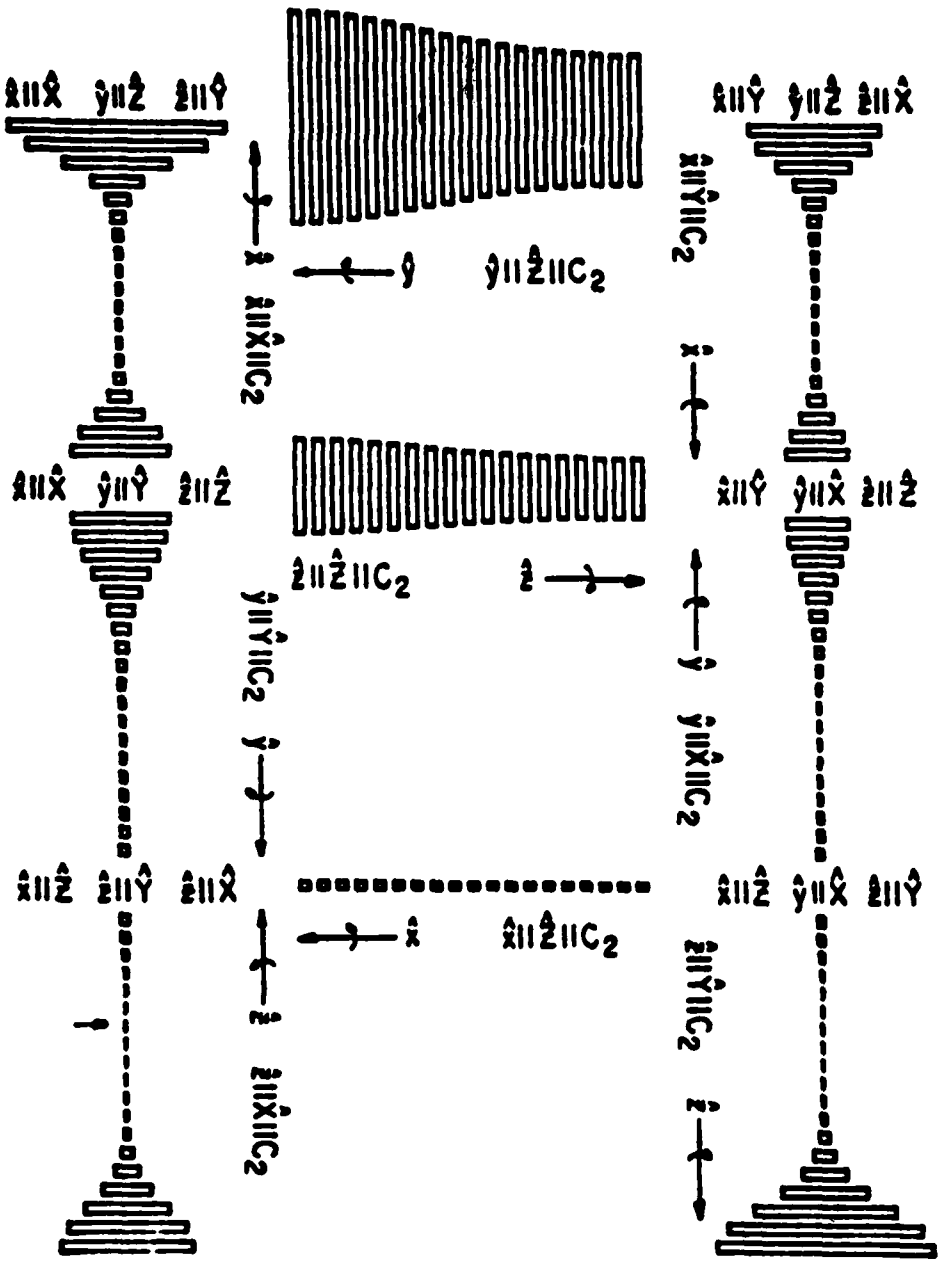

Figure 6. Map of mean square deviation between the theoretically calculated data of Figure 5 and the theoretical curve of Equation 1. Notice the similarity to Figure 3.

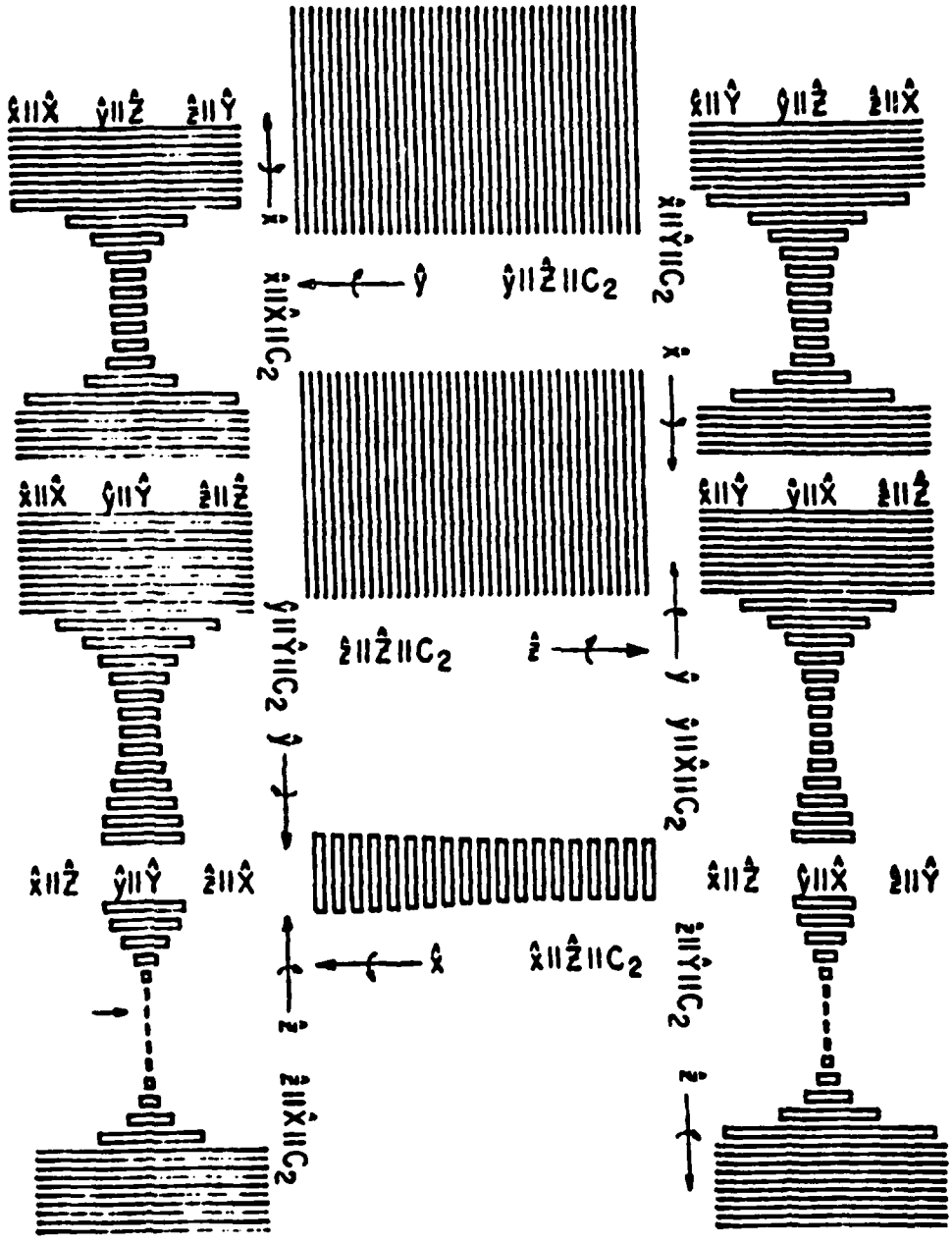

Figure 7. Map of Figure 6 with the scale for the box width expanded by a factor of ten.

(1) R. Beach, S. R. Hartmann, and R. Friedberg, Phys. Rev. A 25, 2658 (1982); Proceeding of Laser 81 Conference, New Orleans, LA (1981).

(2) R. Kachru, T. W. Mossberg, and S. R. Hartmann, Phys. Rev. A 21, 1124 (1980).

(3) R. Kachru, T. J. Chen, S. R. Hartmann, and P. R. Berman, Phys. Rev. Lett. 47, 902 (1981).

(4) M. Gross, C. Fabre, P. Pillet, and S. Haroche, Phys. Rev. Lett. 36, 1035 (1976).

(5) P. R. Berman, T. W. Mossberg, and S. R. Hartmann, "Collision Kernels and Laser Spectroscopy," to be published in Phys. Rev. A (1982).

(6) Y. C. Chen, K. Chiang, and S. R. Hartmann, Phys. Rev. B 21, 40 (1980).

(7) R. M. Macfarlane and R. M. Shelby, Opt. Lett. 6, 96 (1981).

SIGNIFICANT ACCOMPLISHMENTS AND TECHNOLOGY TRANSITION REPORT

Significant Accomplishments

I. Quantum Detection and Sensing of Radiation

Luminescence radiation has been characterized, for the first time, in terms of the underlying physical processes giving rise to it. This formulation shows how differently luminescence radiation behaves from thermal light.

A new method has been developed for incorporating dynamics into particle, photon, and pulse multiplication processes.

A new technique for characterizing fiber-optic system performance and for designing single-threshold fiber-optic receivers has been developed.

II. Physical Properties and Effects in Electronic Materials

A technique for enhancing photochemical reactions through use of photolithographically prepared substrates has been developed. This approach has potential application to the development of new chemical processes through the use of catalyzed photochemical reactions. In addition, such surface chemical reactions can be used to produce novel microstructures for microelectronics devices.

A physical theory has been developed using a charge scattering model to describe the grain boundary transport in polycrystalline semiconductors. The calculated result explains the reduction of majority carrier current in agreement with experimental data. It provides a theoretical basis for use of polycrystalline semiconductors in VLSI interconnects and solar cells.

III. Energy Transfer and Relaxation in Small Polyatomic Molecules

Relaxation processes involving the electronically excited states of the I_2 molecule have been discovered which may shed light on the operation of the iodine chemical laser.

A laser photofragmentation technique has been applied to the study of fast hydrogen atom interactions with molecules. These studies are of potential importance in plasma research, chemical reaction diagnostics, and infrared laser development.

IV. Picosecond Energy Transfer and Photofragmentation Spectroscopy

We have discovered that one of the paths in the photodissociation of an anthracene endoperoxide produces not only $^1O_2$ but also an excited aromatic fragment. This represents one of the few cases of a photodissociation producing both fragments in excited electronic states and furthermore is the first time that the state of $^1O_2$ resulting from a photodissociation has been established. The relative importance of competing dissociative channels for generating $^1O_2$ is determined and the role of a short-lived (45 ps) chemical intermediate in the process is proposed.

V. Generation and Control of Radiation

A simple theoretical model explaining photon echo formation is Gaseous media has been developed. It is called the Billiard Ball Echo Model and works equally well with two-pulse, three-pulse, two-photon, Raman, Grating, standing-wave, etc., photon echoes. The key is atomic recoil. Echo generation can now be understood without recourse to lengthy mathematical analysis thereby facilitating the use of echoes to solve problems in science.

Technology Transition Reports

1. A new nonlinear signal processing scheme to selectively provide improved signal-to-noise ratios for systems including multiplication noise has been conceived. This may be used as part of the optical guidance system in the NASA/JPL Gallileo orbital mission scheduled to orbit Jupiter in 1988.

2. A frequency-shift keyed fiber optic data link that may be used in conjunction with wavelength division multiplexing for high-capacity multi-user data networks has been demonstrated.

3. Although too numerous to mention, there are many examples of laser applications to defense, industrial, and research uses. One of the most potentially interesting is the use of lasers in photochemical direct writing of microcircuits. The original research leading to the development of the laser was begun under the JSEP program at Columbia in 1951 when work on the maser started under the direction of Professor Townes.

PERSONNEL

Faculty

K. Eisenthal, Professor of Chemistry

G. W. Flynn, Professor of Chemistry, Director

S. R. Hartmann, Professor of Physics

W. Hwang, Assistant Professor of Electrical Engineering

R. Osgood, Associate Professor of Electrical Engineering

P. Prucnal, Assistant Professor of Electrical Engineering

I. I. Rabi, University Professor Emeritus

M. C. Teich, Professor of Engineering Science

P. Thaddeus, Adjunct Professor of Physics

E. Yang, Professor of Electrical Engineering

Research Associates and Physicists

Dr. S. Goates

Dr. A. Kerr

Dr. B. Saleh

Dr. M. Wu

Graduate Research Assistants

J. Ahl

T. Allik

L. Barbales

R. Beach

P. Beeken

C. Chen

D. Chen

T. Chen

K. Chiang

J. Chu

M. Crawford

C. Dupuy

H. Evans

R. Kachru

R. Kichinski

M. Lester

K. Leung

M. Mandich

K. Matsuo

F. Novack

E. Poon

J. Rosenberg

P. Siegel

J. Subbiah

E. Whittaker

C. Wood

Administration

Ms. I. Moon

Ms. S. Larchuk

Ms. V. Zell

Technician

D. Rivera

F DEFENSE

urity Agency
. Burdge, R-57
3. Meade, MD 20755

ical Information Center
DA
ion
VA 22314

iced Research Proj. Agency
. Reynolds
Boulevard
A 22209

E
e Deputy Under Secretary
for Research and
g (R&AT)

DC 20301

F THE ARMY

rmament R&D Command
-TSS # 59
801

allistics Research Lab.
-BL
ring Ground
21005

mmunications Command
S-PM
A, AZ 85613

issile Command
ntific Inf. Center
-RPRD (Documents)
nal, AL 35809

tellite Comm. Agency
A, NJ 07703

mospheric Sciences Lab.
-AD-DM (Tech Wrtg)
Missile Range, NM 88002

(K. Lape')
A, NJ 07703

retary, TCC/JSEP
search Office
11
ngle Park, NC 27709

Laboratories
ical Inf. Branch
Hill Road
20783

HQDA
Washington, DC 20310

Director
U. S. Army Electronics Technology
and Devices Laboratory
ATTN: DELET-E (Dr. Jack A. Kohn)
Fort Monmouth, NJ 07703

Commander
U. S. Army Comm. R&D Command
ATTN: DRSEL-TES-CR (Mr. David Haratz)
Fort Monmouth, NJ 07703

Director
U. S. Army Electronics Technology
and Devices Laboratory
ATTN: DELET-M (Mr. V. Gelnovatch)
Fort Monmouth, NJ 07703

Commander
U. S. Army Electronics R&D Command
ATTN: DRDEL-SA (Dr. W. S. McAfee)
Fort Monmouth, NJ 07703

U. S. Army Research, Development
and Standardization Group - CA
National Defense Headquarters
Ottawa, Ontario
CANADA KIA OK2

Commander
U. S. Army Comm. Electronics Command
ATTN: DRSEL-COM-RM-4 (Dr. F. Schwering
Fort Monmouth, NJ 07703

Director
U. S. Army Electronics Technology
and Devices Laboratory
ATTN: DELET-I (Mr. Harold Borkan)
Fort Monmouth, NJ 07703

Director
U. S. Army Electronics R&D Command
Night Vision and Electro-Optics Labs
ATTN: Dr. Randy Longshore, DELNV-IT
Fort Belvoir, VA 22060

Commander
U. S. Army Research Office
ATTN: DRXRO-EL (Dr. James Mink)
P. O. Box 12211
Research Triangle Park, NC 27709

Commander
Harry Diamond Laboratories
ATTN: DELHD-RT-A (Mr. J. Salerno)
2800 Powder Mill Road
Adelphi, MD 20783

Director
U. S. Army Electronics R&D Command
Night Vision and Electro-Optics Labs
ATTN: DELNV-IRTD (Dr. John Pollard)
Fort Belvoir, VA 22060

Commander
U. S. Army Research Office
ATTN: DRXRO-EL (Dr. William A. Sander)
P. O. Box 12211
Research Triangle Park, NC 27709

Director
U. S. Army Electronics Technology
and Devices Laboratory
ATTN: DELET-ES (Dr. A. Tauber)
Fort Monmouth, NJ 07703

Director
Division of Neuropsychiatry
Walter Reed Army Inst. of Research
Washington, DC 20012

Commander
USA ARRADCOM
ATTN: DRDAR-SCF-IO (Dr. J. Zavada)
Dover, NJ 07801

Director
U. S. Army Signals Warfare Lab
ATTN: DELSW-D-OS
Vint Hill Farms Station
Warrenton, VA 22186

Director
U. S. Army Electronics Technology
and Devices Laboratory
ATTN: DELET-ED (Dr. E. H. Poindexter)
Fort Monmouth, NJ 07703

Commander
U. S. Army Research & Standardization
Group (Europe)
ATTN: (Dr. F. Rothwarf)
Box 65
FPO NY 09510

U. S. Army Research Office
ATTN: Library
P. O. Box 12211
Research Triangle Park, NC 27709

Commander
U. S. Army Communications Command
ATTN: DRSEL-COM-RF (Dr. T. Klein)
Fort Monmouth, NJ 07703

Mr. Jerry Brookshire
Guidance and Control Directorate
U. S. Army Missile Command
ATTN: DRSMI-RGG, Bldg. 4381
Redstone Arsenal, AL 35898

Dr. Michael Fahey
Advanced Sensors Directorate
U. S. Army Missile Command
ATTN: DRDMI-RER
Redstone Arsenal, AL 35898

Dr. Charles Bowden
U. S. Army Missile Command
Research Directorate
ATTN: DRSMI-RRD
Redstone Arsenal, AL 35898

Dr. Arthur R. Sindoris
Harry Diamond Laboratories
ATTN: DELHD-PO-P
2800 Powder Mill Road
Adelphi, MD 20783

Dr. Horst R. Wittmann
U. S. Army Research Office
P. O. Box 12211
Research Triangle Park, NC 27709

Dr. Jimmie R. Suttle
U. S. Army Research Office
P. O. Box 12211
Research Triangle Park, NC 27709

Mr. Charles Graff
U. S. Army Comm. - Electronics Command
ATTN: DRSEL-COM-RF-Z
Fort Monmouth, NJ 07703

Mr. Edward Herr
U. S. Army Comm. - Electronics Command
ATTN: DRSEL-COM-RX-4
Fort Monmouth, NJ 07703

Mr. Roland Wright
Night Vision & Electro-Optics Labs
Fort Belvoir, VA 22060

Dr. Robert Rohde
Night Vision & Electro-Optics Labs
Fort Belvoir, VA 22060

Dr. Donn V. Campbell
U. S. Army Comm. - Electronics Command
ATTN: DRSEL-COM-RN-4
Fort Monmouth, NJ 07703

Dr. Nick Karayianis
Harry Diamond Laboratories
ATTN: DELHD-RT-CA
2800 Powder Mill Road
Adelphi, MD 20783

Dr. T. N. Chin
U. S. Army ARRADCOM
ATTN: DRDAR-SCF-10
Dover, NJ 07801

Dr. John Malamus
Night Vision & Electro-Optics Labs
Fort Belvoir, VA 22060

Dr. Rudolf G. Buser
Night Vision & Electro-Optics Labs
ATTN: DELNL-L
Fort Belvoir, NJ 22060

Dr. W. Ealy
Night Vision & Electro-Optics Labs
ATTN: DELNV-AC
Fort Monmouth, NJ 22060

Dr. J. Hall
Night Vision & Electro-Optics Labs
ATTN: DELNV-AC
Fort Belvoir, NJ 22060

Dr. J. Burgess
Night Vision & Electro-Optics Labs
ATTN: DELNV-RM-RA
Fort Belvoir, NJ 22060

DEPARMENT OF THE AIR FORCE

Dr. E. Champagne
AFWAL/AADD-I
Wright-Patterson AFB, OH 45433

Mr. W. Edwards, Chief
AFWAL/AAD
Wright-Patterson AFB, OH 45433

Professor R. E. Fontana
Head, Department of Electrical Engineering
AFIT/ENG
Wright-Patterson AFB, OH 45433

Dr. Alan Garscadden
AFWAL/POOC-3
Air Force Aeronautical Labs
Wright-Patterson AFB, OH 45433

Mr. Alan R. Barnum (CO)
Rome Air Development Center
Griffiss AFB, NY 13441

Chief, Electronic Research Branch
AFWAL/AADR
Wright-Patterson AFB, OH 45433

Mr. John Mott-Smith (ESD/ECE)
HQ ESD (AFSC), Stop 36
Hanscom AFB, MA 01731

Dr. J. Ryles
Chief Scientist
AFWAL/AS
Wright-Patterson AFB, OH 45433

Dr. Allan Schell
RADC/EE
Hanscom AFB, MA 01731

Dr. Howard Schlossberg
Air Force Office of Scientific Research
AFOSR/NP
Bolling AFB, DC 20332

Dr. J. Bram
AFSOR/NM
Bolling AFB, DC 20332

LTC Clarence Gardner
Air Force Office of Scientific Research
AFOSR/NE
Bolling AFB,DC 20332

Dr. David W. Fox
AFOSR/NM
Bolling AFB, DC 20332

Dr. J. Neff
AFOSR/NE
Bolling AFB, DC 20332

Dr. H. M. DeAngelis
RADC/ESR
Hanscom AFB, MA 01731

Mr. Allan Barnum
RADC/IS
Griffiss AFB, NY 13411

Dr. Tom Walsh
AFOSR/NE
Bolling AFB, DC 20332

Dr. Edward Altshuler
RADC/EEP
Hanscom AFB, MA 01731

DEPARTMENT OF THE NAVY

Naval Surface Weapons Center
ATTN: Technical Library
Code DX-21
Dahlgren, VA 22448

Dr. Gernot M. R. Winkler
Director, Time Service
U. S. Naval Observatory
Massachusetts Avenue at 34th Street, NW
Washington, DC 20390

G. C. Dilworth, Jr.
Technical Director
Naval Coastal Systems Center
Panama City, FL 32407

Naval Air Development Center
ATTN: Code - 301 A. Witt
Technical Library
Warminster, PA 18974

R. S. Allgaier, R-45
Naval Surface Weapons Center
Silver Spring, MD 20910

Office of Naval Research
800 North Quincy Street
ATTN: Code 250
Arlington, VA 22217

Office of Naval Research
800 North Quincy Street
ATTN: Code 414
Arlington, VA 22217

Office of Naval Research
800 North Quincy Street
ATTN: Code 411MA
(Dr. Stuart L. Brodsky)
Arlington, VA 22217

Commanding Officer
Naval Research Laboratory
ATTN: Dr. S. Teitler, Code 1450
Washington, DC 20375

Commanding Officer
Naval Research Laboratory
ATTN: Mrs. D. Folen, Code 2627
Washington, DC 20375

Commanding Officer
Naval Research Laboratory
ATTN: Mr. A. Brodzinsky, Code 5200
Washington, DC 20375

Commanding Officer
Naval Research Laboratory
ATTN: Mr. J. E. Davey, Code 6810
Washington, DC 20375

Commanding Officer
Naval Research Laboratory
ATTN: Mr. B. D. McCombe, Code 6800
Washington, DC 20375

Commanding Officer
Naval Research Laboratory
ATTN: Mr. W. L. Faust, Code 6504
Washington, DC 20375

Technical Director
Naval Underwater Systems Center
New London, CT 06320

Naval Research Laboratory
Underwater Sound Reference Detachment
Technical Library
P. O. Box 8337
Orlando, FL 32856

Naval Ocean Systems Center
ATTN: Dr. P. C. Fletcher, Code 92
San Diego, CA 92152

Naval Ocean Systems Center
ATTN: Mr. W. J. Dejka, Code 8302
San Diego, CA 92152

Naval Ocean Systems Center
ATTN: Dr. Alfred K. Nedoluha,
Code 922
San Diego, CA 92152

Naval Weapons Center
ATTN: Dr. G. H. Winkler, Code 381
China Lake, CA 93555

Dr. Donald E. Kirk (62)
Professor and Chairman, Electrical
Engineering
SP-304
Naval Postgraduate School
Monterey, CA 93940

Dr. D. F. Dence
Naval Underwater Systems Center
New London Laboratory
ATTN: Code 34
New London, CT 06320

Director, Technology Assessment
Division (OP-987)
Office of the Chief of Naval Oper.
Navy Department
Washington, DC 20350

Mr. J. W. Willis
Naval Air Systems Command
AIR-310
Washington, DC 20361

Naval Electronics Systems Command
NC #1
ATTN: Code 61R
2511 Jefferson Davis Highway
Arlington, VA 20360

Department of the Navy
Naval Sea Systems Command
ATTN: W. W. Blaine (SEA-62R)
Washington, DC 20362

David Taylor Naval Ship Research
and Development Center
ATTN: Mr. G. H. Gleissner, Code 18
Bethesda, MD 20084

Mr. Martin Mandelberg
Coast Guard R&D Center
Avery Point
Groton, CT 06340

Naval Underwater Systems Center
New London Laboratory
ATTN: 101E (Dr. Edward S. Eby)
New London, CT 06320

Mr. Thomas J. Manuccia, Head
Chemistry and Application Section
Code 6543
Naval Research Laboratory
Washington, DC 20375

Dr. Stephen G. Bishop, Head
Semiconductor Branch
Code 6870
Naval Research Laboratory
Washington, DC 20375

Dr. William F. Gabriel
Antenna Systems Staff
Code 5342
Naval Research Laboratory
Washington, DC 20375

Dr. John W. Rockway
Comm. Technology Prog. Off.
Code 8105
Naval Ocean Systems Center
San Diego, CA 92152

Dr. Barry P. Shay
Systems Integration and
Instrumentation Branch
Code 7522
Naval Research Laboratory
Washington, DC 20375

Dr. Sydney R. Parker
Professor, Electrical Engineering
Code 62PX
Naval Postgraduate School
Monterey, CA 93940

Dr. George B. Wright
Office of Naval Research
Code 427
Arlington, VA 22217

OTHER GOVERNMENT AGENCIES

Dr. Ronald E. Kagarise
Director
Division of Materials Research
National Science Foundation
1800 G Street
Washington, DC 20550

Director
Division of Electrical, Computer
and Systems Engineering
National Science Foundation
Washington, DC 20550

Dr. Dean L. Mitchell
Section Head
Condensed Matter Sciences Section
Division of Materials Research
National Science Foundation
1800 G Street, N. W.
Washington, DC 20550

Judson C. French, Director
Center for Electronics and Electrical
Engineering
B 358 Metrology Building
National Bureau of Standards
Washington, DC 20234

NON-GOVERNMENT AGENCIES

Director
Columbia Radiation Laboratory
Columbia University
538 West 120th Street
New York, NY 10027

Director
Coordinated Science Laboratory
University of Illinois
Urbana, IL 61801

Associate Director pf Materials
and Electronics Research
Division of Applied Sciences
McKay Laboratory 107
Harvard University
Cambridge, MA 02138

Director
Electronics Research Center
University of Texas
P. O. Box 7728
Austin, TX 78712

Director
Electronics Research Laboratory
University of California
Berkeley, CA 94720

Director
Electronics Sciences Laboratory
University of Southern California
Los Angeles, CA 90007

Director
Microwave Research Institute
Polytechnic Institute of New York
333 Jay Street
Brooklyn, NY 11201

Director
Research Laboratory of Electronics
Massachusetts Institute of Technology
Cambridge, MA 02139

Director
Stanford Electronics Laboratory
Stanford University
Stanford, CA 94305

Director
Edward L. Ginzton Laboratory
Stanford University
Stanford, CA 94305

Dr. Lester Eastmen
School of Electrical Engineering
Cornell University
316 Phillips Hall
Ithaca, NY 14850

Dr. Carlton Walter
Electro Science Laboratory
The Ohio State University
1320 Kinnear Road
Columbus, OH 43212

Dr. Richard Saeks
Dept. of Electrical Engineering
Texas Tech University
Lubbock, TX 79409

Director
School of Electrical Engineering
Georgia Institute of Technology
Atlanta, GA 30332

Dr. John F. Walkup
Dept. of Electrical Engineering
Texas Tech University
Lubbock, TX 79409

Mrs. Renate D'Arcangelo
Editorial Office
130 Pierce Hall
Division of Applied Sciences
31 Oxford Street
Cambridge, MA 02138


DATE
ILME